

Distribution Agreement

In presenting this thesis as a partial fulfillment of the requirements for a degree from Emory University, I hereby grant to Emory University and its agents the non-exclusive license to archive, make accessible, and display my thesis in whole or in part in all forms of media, now or hereafter now, including display on the World Wide Web. I understand that I may select some access restrictions as part of the online submission of this thesis. I retain all ownership rights to the copyright of the thesis. I also retain the right to use in future works (such as articles or books) all or part of this thesis.

William John Nobuo Dougherty

April 10, 2024

Understanding the Reactivity of Planar Chiral Naphthindenyl Rhodium(III) Catalysts

By

William John Nobuo Dougherty

Simon B. Blakey, Ph.D.

Adviser

Department of Chemistry

Simon B. Blakey, Ph.D.

Adviser

Austin Scharf, Ph.D.

Committee Member

Skye Comstra, Ph.D.

Committee Member

Richard Himes, Ph.D.

Committee Member

2024

Understanding the Reactivity of Planar Chiral Naphthindenyl Rhodium(III) Catalysts

By

William John Nobuo Dougherty

Simon B. Blakey, Ph.D.
Adviser

An abstract of
a thesis submitted to the Faculty of Emory College of Arts and Sciences
of Emory University in partial fulfillment
of the requirements of the degree of
Bachelor of Science with Honors

Department of Chemistry

2024

Abstract

Understanding the Reactivity of Planar Chiral Naphthindenyl Rhodium(III) Catalysts By William John Nobuo Dougherty

In our study, we aimed to explore the impact of extending the aromatic backbone of the indenyl ligand, coupled with modifications to substituents around the Cp moiety, on the reactivity of planar chiral rhodium(III) catalysts. This exploration was geared towards unlocking new possibilities in asymmetric C-H functionalization and catalysis. We hypothesized that introducing a naphthalene backbone in linear and bent configurations would influence the hapticity of the Cp moiety and preference for ring slip due to preferred resonance structures. Despite encountering challenges in synthesizing the naphthindanone precursors to naphthindenes, we successfully synthesized naphthindenyl rhodium(I)-COD and naphthindenyl rhodium(I)-carbonyl species. While we managed to synthesize and purify one rhodium(III) complex, purification challenges remain. We utilized three methods to investigate hapticity, which we correlated with ring slippage. The methods included Tolman electronic parameter analysis, NMR studies, and solid-state structure analysis, which together show a spectrum of hapticities that we correlate with variable levels of ring slippage as a result of the different naphthalene aromatic backbone orientations. Our future work involves completing the rhodium(III) species scope and assessing their reaction rates to understand how the orientation of the naphthalene backbone affects reactivity. We plan to compare the behavior of these catalysts in reactions we have previously developed, aiming to elucidate the effect of modifications in steric profile and electronic asymmetry on reactivity. Additionally, we intend to correlate the various data sets we have accrued with each other and additional data to better characterize hapticity and ring slippage.

Understanding the Reactivity of Planar Chiral Naphthindenyl Rhodium(III) Catalysts

By

William John Nobuo Dougherty

Simon B. Blakey, Ph.D.

Adviser

A thesis submitted to the Faculty of Emory College of Arts and Sciences
of Emory University in partial fulfillment
of the requirements of the degree of
Bachelor of Science with Honors

Department of Chemistry

2024

Acknowledgments

First and foremost, I would like to thank Dr. Blakey and my committee, Dr. Scharf, Dr. Comstra, and Dr. Himes. Dr. Blakey- I am extremely grateful that you allowed me to conduct research in your lab, and for your constant support over these past two years. It has been an amazing learning experience that has both rewarded and challenged me in many, many ways. Dr. Scharf- you have been an incredible mentor who has provided me with numerous opportunities that have defined my time at Emory. My passion for chemistry would not have become what it is today without your help. Dr. Comstra- I never expected to become interested in biology to the extent that I have now, and I know it was a direct result of your class at Oxford. You are also an extremely authentic and honest person, which makes every conversation with you enjoyable. Dr. Himes- you never fail to lighten up my day with your jokes. I really appreciated your willingness to let me experiment to my heart's desire in analytical lab, even if it led to me nearly destroying the 205 lab UV-vis spectrometer. Also, special thanks to Dr. Patrick Gross and Ethan Heyboer for their guidance over this project.

Next, thank you to all of the amazing individuals I have met over the past four years. To the friends I've met at Oxford and Atlanta, who I've worked alongside in Dr. Blakey and Dr. Scharf's lab, who I've met in residence life, who I've played frisbee with, who I've volunteered with, and much more: it has been amazing to get to know you all, and I am incredibly thankful for all the interactions we have had. You are all extremely talented, intelligent individuals who I am constantly inspired by.

Finally, I would like to thank my mother. I appreciate you always pushing me while still being so caring. I am truly indebted to you. I love you.

Table of Contents

1. Introduction	1-8
2. Results and Discussion	8-35
2.1 Ligand Development	8-15
2.2 Naphthindenyl Rhodium Complex Development	15-20
2.3 Predicting Planar Chiral Naphthindenyl Rhodium(III) Catalyst Reactivity	20-35
3. Conclusions and Future Directions	35-37
4. Supplemental Information	37-96
5. References	97-105

Figures

1. The Cp and Ind ligands.	2
2. The Ind catalyst developed by Baker.	3
3. The Ind catalyst developed by the Blakey group and its application towards asymmetric functionalization.	4
4. Modification of the Ind catalyst developed by the Blakey group.	5
5. Predicted nuances of the 4th-generation of the Blakey group's Ind catalyst.	6
6. Retrosynthetic analysis of desired rhodium(III) Ind and naphthindenyl complexes.	10
7. Current progress towards developing the linear naphthindenyl ligand scope.	11
8. Attempts at linear naphthindanone α -alkylation reaction.	12
9. Attempts at an alternative method for linear naphthindanone α -alkylation using an enolate trapped as a silyl enol ether.	13
10. Current progress towards developing the bent naphthindenyl ligand scope.	14

11. Current progress towards developing the rhodium(I)-COD naphthindenyl and indenyl complex scope.	16
12. Current progress towards developing the rhodium(I)-carbonyl naphthindenyl and indenyl complex scope.	17
13. Synthesis of planar chiral bent naphthindenyl rhodium(III) complex derived from bent naphthindene 5.	20
14. Simplified illustration of σ -donation, π -backbonding and alteration of metal center electron density by ligands.	21
15. Tolman electronic parameter analysis ranked by asymmetric stretch wavenumbers.	23
16. Heatmap displaying the J _{Rh-C} (Hz) of each Cp moiety carbon.	28
17. Crystal structures of bent naphthindenyl rhodium(I)-COD complex derived from bent naphthindene 4.	31
18. Crystal structures of linear naphthindenyl rhodium(I)-COD complex derived from linear naphthindene 7.	32
19. Crystal structures of Ind rhodium(I)-COD complex derived from indene 9.	32
20. Carbons used calculating for slip value Δ (Å).	33
21. Slip values (Å) for the benchmark indene and naphthindene ligands.	34
22. Characterizing the 4th generation naphthindenyl complexes relative to established scaffolds Cp and Ind.	36

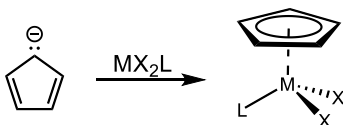
1 – Introduction

In modern organic chemistry, asymmetric functionalization of carbon-hydrogen bonds is a powerful method for revolutionizing synthetic strategy. Efforts in numerous fields— radical chemistry, electrochemistry, photocatalysis, biocatalysis, and more—have allowed for the synthesis of natural products, desired pharmaceutical targets, and diverse substrate scopes in methodological studies, but transition metal catalysis remains a dominant approach for achieving asymmetric C-H functionalization.¹⁻⁴ When conducting transition metal-catalyzed asymmetric C-H functionalization, a variety of factors are considered including but not limited to the transition metal species, directing groups, substrate structure, chiral additives, metal salts, Lewis or Brønsted acids and bases, oxidants and reductants, temperatures, and solvents; however, the design of ligands that complex with the transition metal can be particularly crucial for achieving preferred regio-, chemo-, and stereoselectivity.^{1,5-11}

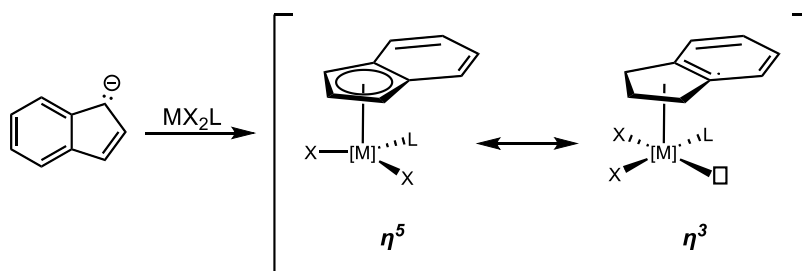
BOX, BINAP, BINOL, and NHC are some of the most prevalent chiral ligands utilized in asymmetric transition metal catalysis, but none exhibit the unique method of binding to a transition metal like that of the privileged cyclopentadienyl anion (Cp) ligand (**Figure 1A**).¹⁰ The 6 π -electron aromatic system can bind to a transition metal center in an η^5 mode, providing a stable Cp-metal complex (CpM); this contrasts to the use of heteroatoms or carbenes coordinating to the transition metal as observed in the other privileged ligand classes mentioned above.¹⁰ Realization of asymmetric transition metal catalyzed C-H functionalization reactions has been made possible by development of intricate, chiral versions of Cp by Cramer, Ward, Rovis, You, Wang, Antonchick, Waldmann, and many others, resulting in different stereoelectronics and steric effects at the metal center.¹⁰ Previous work in the Blakey group has involved the use of the Cp variant pentamethylcyclopentadienyl anion (Cp*) complexed with

Group IX transition metals (cobalt, rhodium, and iridium) to accomplish allylic C-H functionalization.¹²⁻¹⁶ While these reactions demonstrated regioselectivity, they were modestly stereoselective at best, so our focus shifted towards development of Group IX chiral Cp catalysts for improved enantioinduction.

A. Cyclopentadienyl (Cp)



B. Indenyl (Ind)



Note: Here, M represents a Group IX transition metal, but Cp is well established to coordinate with a variety of transition metals.

Figure 1 - The Cp and Ind ligands.

One particularly interesting variation of Cp is the indenyl (Ind) ligand, a Cp ring fused to a benzene ring (**Figure 1B**). During their studies of migratory insertion reactions by Ind-Mo complexes, Hart-Davis and Mawby observed a 10-fold increase in reaction rate by Ind-Mo compared to Cp-Mo.^{17,18} Even more significantly, Basolo and Rerek investigated a ligand exchange reaction between carbon monoxide and phosphine using Ind-Rh complexes and observed up to a 10⁸-fold increase in reaction rate by Ind-Rh compared to Cp-Rh.^{19,20} While mechanistic theories originally involved formation of unfavorable 20-electron metal complexes, Cramer and Seiwel suggested that “ring slippage” of the Ind ligand from an η⁵ species to an η³ species, motivated by the stabilization of the benzene backbone, led to the increase in reaction rates observed.^{17,20} This could occur due to the formation of a 16-electron complex as a result of

a ring slip from an η^5 species to an η^3 species, opening a coordination site for another ligand to associate. The plethora of data collected supporting this theory led Basolo and Rerek to establish the indenyl ligand effect: increased reaction rate due to the nature of the indenyl ligand's ability to ring slip.^{17,21}

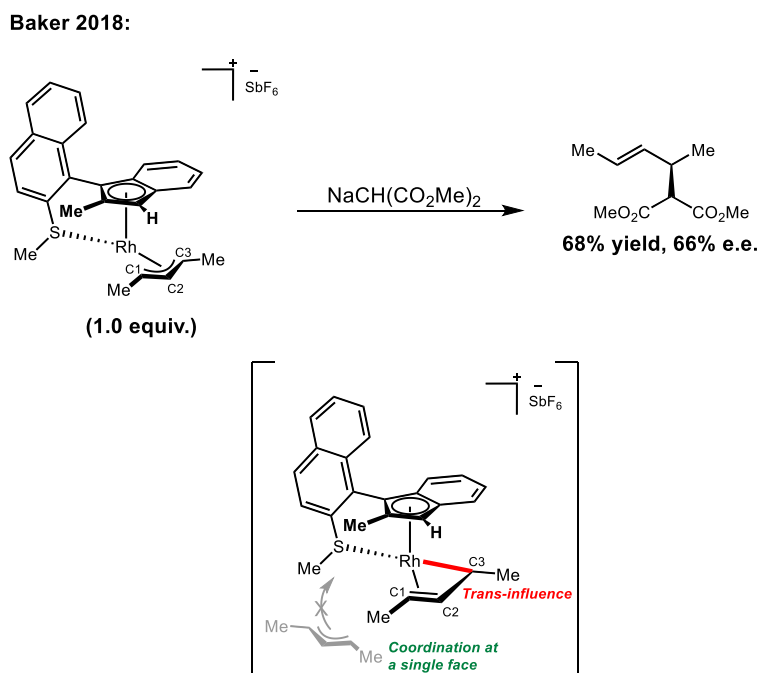
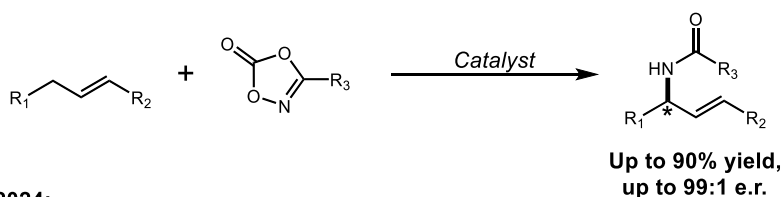


Figure 2 - The Ind catalyst developed by Baker.

The Ind scaffold has been subjected to many structural modifications and paired with early and late transition metals alike to perform transformations on small molecules as well as polymerization reactions in regio-, chemo-, and stereoselective manners.^{17,21} Of interest to the Blakey group was work by Baker in 2018: an indenyl-sulfanyl rhodium(III) complex capable of asymmetric allylic C-H functionalization (**Figure 2**).²² This ligand directly influenced enantioinduction by permitting the allylic substrate to selectively coordinate a single face of the complex and more critically, by inducing electronic asymmetry of the rhodium center.²² The thioether moiety aided the selective coordination of the allylic substrate by blocking one coordination site of the complex such that only a single face of the catalyst was available.^{19,22,23}

Electronic asymmetry of the rhodium center is a result of the η^5 - η^3 ring slippage causing an increase in trans-influence by the η^3 -coordinated carbons, effectively weakening the bond between the rhodium center and carbon C3 of the π -allyl substrate.^{19,22,23} Dimethyl malonate anions then preferentially attack this weakened bond to afford an asymmetric product.^{19,22,23} Unfortunately, the modest yield and enantioselectivity, the use of stoichiometric amounts of rhodium, and the potential for oxidation of the thioether causing unwanted side reactivity limited the impact of Baker's catalyst.^{22,23} Despite this, the Blakey group believed this Ind scaffold was a promising way for achieving allylic C-H functionalization asymmetrically and sought to further modify it.

Blakey 2020:



Blakey 2024:

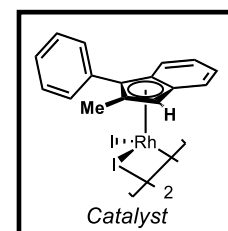
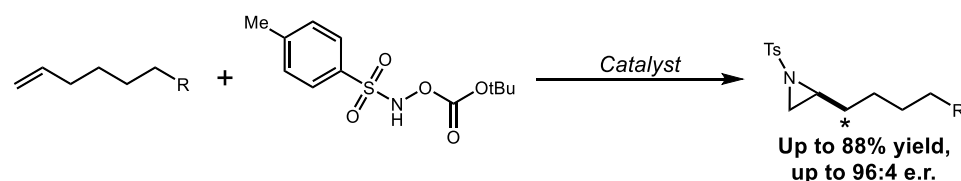


Figure 3 - The Ind catalyst developed by the Blakey group and its application towards asymmetric functionalization.

In 2020, the Blakey group detailed the development of a planar chiral rhodium(III) Ind catalyst for regio- and enantioselective allylic C-H amidation (**Figure 3**). This variation improved yields and enantioinduction using only catalytic amounts of rhodium.²³ The prochiral Ind ligand, easily synthesized in two steps, induced asymmetric electronics seen in the Baker catalyst and promoted desired substrate interactions through the substitution of the thioether moiety with a phenyl group providing steric blocking instead.²³ The racemic mixture of planar chiral COD complex could be easily resolved using chiral HPLC, providing an alternative

method for accessing chiral catalysts to the development of C₂-symmetric ligands.^{23,24} While early transition metal planar chiral catalysts have been explored, late transition metal planar chiral catalysts have yet to be largely explored due to synthetic constraints and difficulties with stereochemical assignment, demonstrating other contributions of this catalyst outside of reactivity.²⁴ In 2024, the Blakey group utilized this catalyst again to perform enantioselective aziridination of unactivated terminal alkenes (**Figure 3**).²⁵ A second generation of this Ind ligand, focused on modifying the electronics of the phenyl substituent, helped increase yield through the substitution of a tert-butyl group *para* to the Ind moiety (**Figure 4**). To increase the electron density of the Ind scaffold itself, a third generation of this Ind ligand was synthesized that included methylation throughout the benzene backbone, increasing yield even more significantly (**Figure 4**). Despite this promising result, the third-generation catalyst was not able to be resolved by chiral HPLC nor other tactics such as adduct separation, so the catalyst could only be used as a racemic mixture. Consequently, the first generation of the Ind catalyst was applied to this aziridination chemistry.

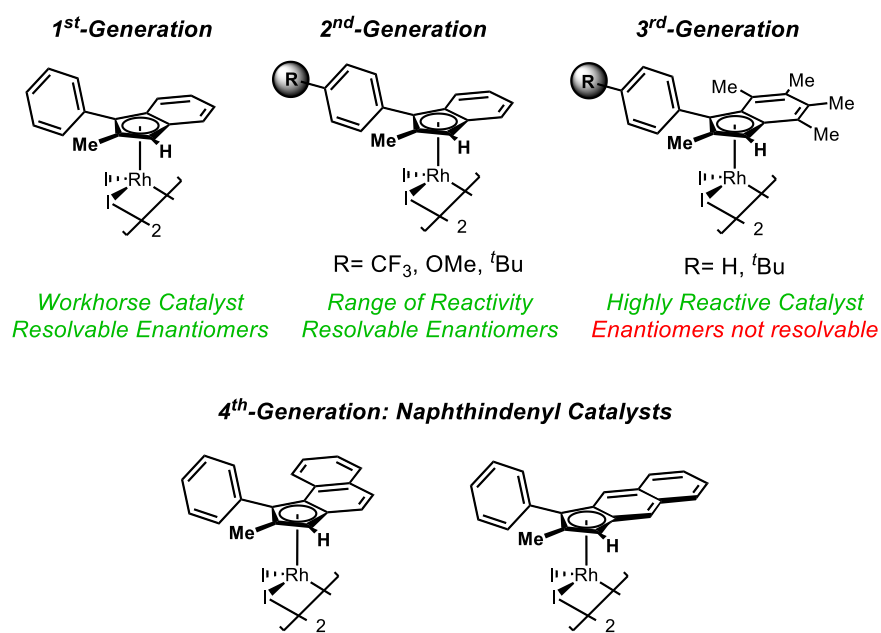


Figure 4 - Modification of the Ind catalyst developed by the Blakey group.

Three works done by Heller and colleagues are the only other example of Group IX (cobalt) asymmetric transition metal Ind catalysts, with one catalyst being planar chiral.^{26–28} Continued development of these planar chiral Ind ligands is important for further expanding this field and unlocking new reactivity as evidenced by the third generation of the Blakey group's catalysts, with primary challenges being chiral resolution. We aimed to further tune the electronic and steric profile in a fourth generation through two main modifications: extension of the aromatic backbone and substitution around the Cp moiety (**Figure 4**).

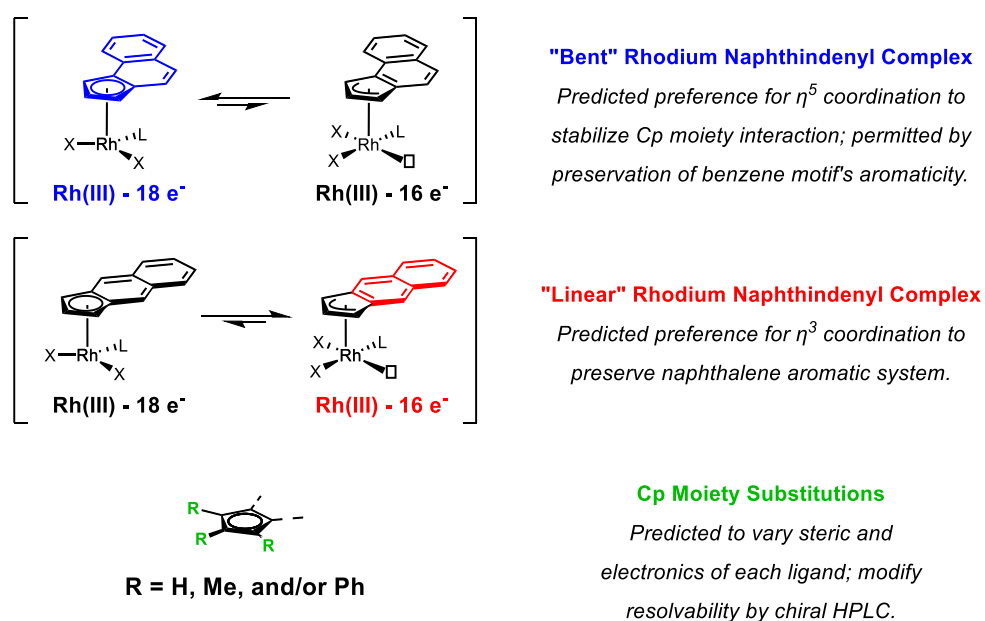


Figure 5 - Predicted nuances of the 4th-generation of the Blakey group's Ind catalyst.

Firstly, we envisioned extending the aromatic backbone of Ind by fusing naphthalene to the Cp ring instead of benzene. We chose to orient the naphthalene backbone in a “linear” (benz[f]indenyl) and “bent” (benz[e]indenyl) fashion and predicted that this would lead to subtle differences in the preferred hapticity of the Cp moiety (**Figure 5**). For the linear naphthindenyl ligand, we hypothesized that ring slippage would tend towards an η^3 coordination to preserve the naphthalene backbone's aromatic system; an η^5 coordination would require the incorporation of 2 π -electrons from the naphthalene backbone, leading to the complete loss of aromatic

stabilization. For the bent naphthindenyl ligands, we hypothesized that ring slippage would tend towards an η^5 coordination to further stabilize the interaction between the Cp moiety and the metal. While the incorporation of 2 π -electrons from the naphthalene backbone to give η^5 coordination would result in de-aromatization of the naphthalene system, a benzene motif would still remain in the backbone. The preservation of the strongly aromatic benzene would provide stability necessary to permit η^5 coordination to occur. We anticipated that the linear naphthindenyl and bent naphthindenyl ligands would lead to ring slippage behavior less and more like the privileged Cp, respectively. The electronics (outside of the influences of the aromatic system on the Cp moiety coordination) and steric profile of the backbones of these ligands may also have interesting implications on reactivity. To the best of our knowledge, previous transition metal catalysis research with either linear or bent naphthindenyl ligands have only been in the context of polymerization, and no modifications of the Cp moiety that would influence planar chirality have been made.^{29–35} Additionally, only one example of late transition metal catalysis using such ligands is available; use of Group IV transition metals (titanium, zirconium, hafnium) has been predominant.^{29–35}

Secondly, the substitution of the Cp moiety is also predicted to vary the sterics and electronics of each ligand (**Figure 5**). Again, the lone phenyl ring in these Ind catalysts have contributed to enantioinduction by acting as a steric block to promote favored interactions between coordinated substrates. We hoped to investigate the ability for other groups to perform this function, as well as better understand how they might change the electronics of the ligand. The influence of these groups on the planar chirality of these ligands is also of importance for chiral resolution of the catalyst racemates. While the bent naphthindenyl ligand skeleton already

has innate planar chirality without Cp moiety substituents, the linear naphthindenyl ligand requires further modification to give planar chirality.

In this work, we describe the synthesis of variants of the linear naphthindenyl ligands, bent naphthindenyl ligands, and various rhodium(I) complexes using these ligands. We detail the efforts towards accessing the rhodium(III) complexes for the use in reaction rate studies and stereoselective catalytic transformations. We also discuss progress made towards analyzing levels of hapticity between these ligands relative to the Ind catalysts we have developed, which we correlate with preferred level of ring slippage. The Rovis group has done extensive work clarifying how modifications to Cp impact its catalytic activity, and we hoped to place our Ind and naphthindenyl catalysts in the context of this work through a common method of measurement that simultaneously provide insight into hapticity: the Tolman electronic parameter.^{36,37} We then gauge hapticity tendencies of each ligand by taking advantage of rhodium's NMR activity, which allows us to examine the level of interaction between each carbon of the Cp moiety and the rhodium metal center via ^{103}Rh - ^{13}C coupling constants. Also, solid-state structure analysis is performed, and previously defined parameters for characterizing slippage using this solid-state structure data are implemented. Finally, we highlight the future directions of this project.

2 – Results and Discussion

2.1 – Naphthindene Synthesis

The retrosynthetic analysis is shown below (**Figure 6**). We believed the rhodium(III) naphthindenyl species could be produced by complexation of rhodium(I) with naphthindenes followed by subsequent oxidation of the rhodium center. This would involve employing robust

methods that we used to create our previous Ind catalysts. To synthesize the naphthindenes, we looked again to our previous work: the indene used for our first-generation Ind ligand was particularly attractive due to its two-step, high-yielding, modular synthesis from indanone. This later enabled easy access to our second generation via modification of the phenyl ring added through Grignard addition. We proposed a similar approach to the naphthindenyl ligands through the linear and bent naphthindanones, for which several synthetic protocols have been developed. Various decorations of the naphthindene Cp moiety were thought to be accessible via modifications to previous work performed accessing naphthindanones or by simple reactions with the naphthindanone skeletons. However, this turned out to be a non-trivial task that required extensive study.

We imagined several different naphthindenes to best explore the phenomena of interest (**Figure 6**). Firstly, we hoped to utilize the same, key motifs that have been incorporated in every generation of the planar chiral rhodium(III) Ind catalyst developed by our lab—the methyl and phenyl that decorate the Cp moiety of the Ind ligand. As such, we aimed to synthesize the linear naphthindene **6** and bent naphthindene **2** which use these same groups to understand how they would differ in reactivity compared to the first generation Ind ligand (indene **8**) as a result of the difference in the aromatic backbone and resulting ring slippage. The preservation of the phenyl but removal of the methyl in **4** and **7** would serve to maintain the planar chiral character of the ligand once complexed while concurrently allowing us to examine the significance of the methyl on reactivity and further probe the effects of aromaticity on ring slippage; Ind derivative **9** was included in this scope to serve as a control to compare these derivatives against. We predicted that variations **1**, **3**, and **5** would increase the stereoelectronic contribution of these naphthindenyl ligands to the rhodium metal center in incremental fashions, and by characterizing each one, we

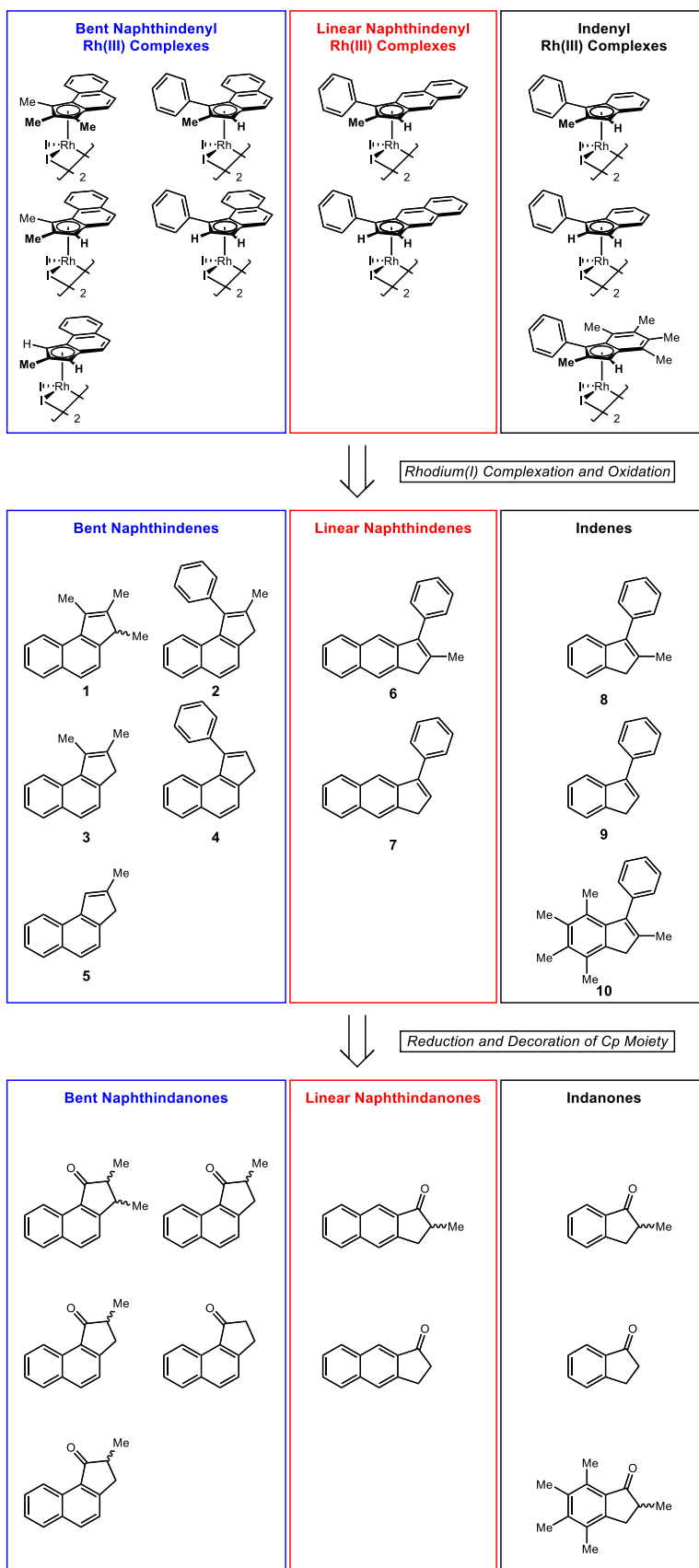


Figure 6 - Retrosynthetic analysis of desired rhodium(III) Ind and naphthindenyl complexes.

would be able to understand the sum effect of additional substituents to the Cp moiety. Finally, we included indene **10** based on our observations of its improved reactivity in the third generation of catalysts screened in our aziridination chemistry and its current applications towards unpublished work on asymmetric 1,2-oxyamidation of dienes.

Indenes were synthesized by former lab member Patrick Gross (PhD) (**8** and **9**) and current lab member Ethan Heyboer (**10**). Access to naphthindenes was a result of efforts by current lab member Harry Ung (**2**, **3**, and **5**) and myself (**1**, **4**, **6**, and **7**).

The synthesis of linear naphthindenes **6** and **7** is detailed below (**Figure 7**). McLaughlin and colleagues established a tandem Diels-Alder aromatization reaction that generates the desired linear naphthindanone framework in a 57% yield, which was able to be closely replicated here in a 50% yield.³⁸ Then, generally following the procedure used by the Blakey group in the development of the first-generation Ind, a Grignard addition using phenyl magnesium bromide followed by an elimination using concentrated hydrochloric acid was performed to give **7** in a 64% yield. It is worth noting that extended stirring of phenyl magnesium bromide in a 0.5 M solution of LiCl in THF prior to addition of the linear naphthindanone greatly improved yields of this reaction. This is likely due to the ability for LiCl to break up aggregates of the phenyl magnesium bromide to produce a more reactive complex of the reagent.³⁹

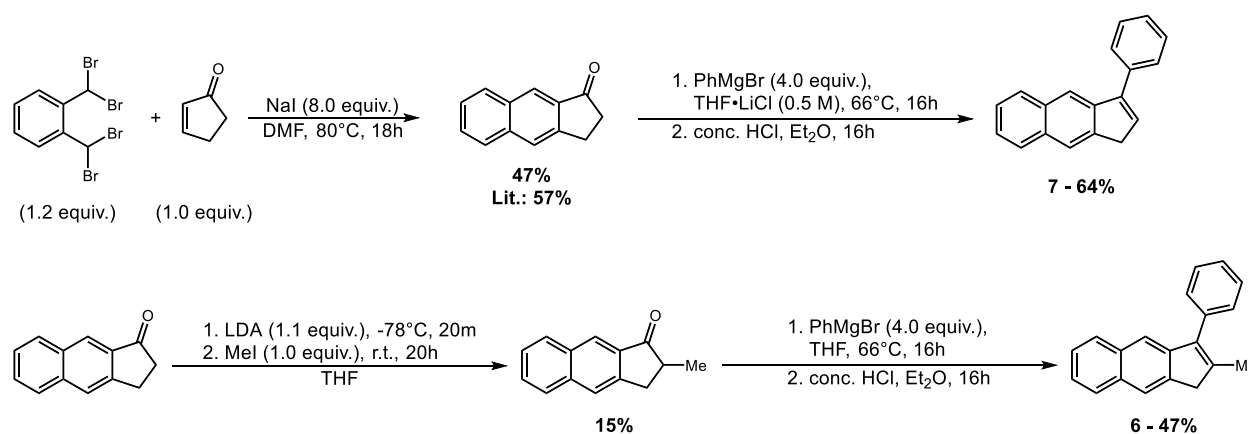
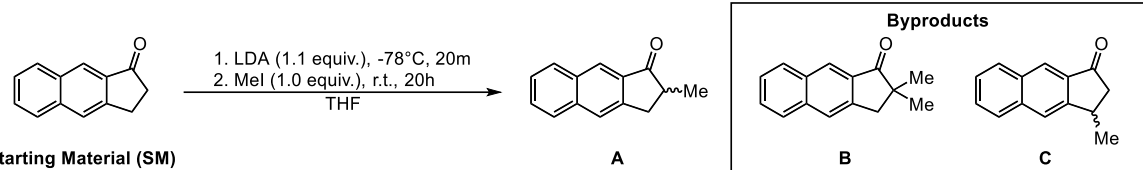


Figure 7 - Current progress towards developing the linear naphthindenyl ligand scope.

We believed that **6** could be synthesized by alkylation of the linear naphthindanone's enolate followed by a Grignard addition and elimination like what was detailed above. Two works detail formation of the α -alkylated naphthindanone but require specific substrates and transition metal catalysis, leading to our use of this approach instead.^{40,41} The initial reaction conditions of the enolate alkylation were low yielding, but efforts to drive the alkylation reaction forward by increasing equivalences of the electrophile and non-nucleophilic base, inclusion of polar, aprotic solvents, modification of addition techniques, and use of alternative bases only gave rise to unwanted byproducts (**Figure 8**). Excessive equivalents of base and electrophile were likely to explain formation of both byproduct B and C (verified using literature spectral data), and the unexpected β -alkylation of product C was hypothesized to occur due to a second deprotonation at the β -carbon following formation of the enolate.^{42,43}



Entry	Base	Electrophile	Additive	Starting Material	Yield - A	Note
1	LDA (1.1 equiv.)	MeI (1.0 equiv.)		44%	7%	
2	LDA (5.1 equiv.)	MeI (10.0 equiv.)		31%	15%	Formation of C observed.
3	LDA (8.1 equiv.) (3h)	MeI (10.0 equiv.) (72h)		--%	--%	Formation of B only.
4	LDA (5.1 equiv.) (3h)	MeI (10.0 equiv.)	DMPU (4:1 THF:DMPU)	--%	--%	Formation of several unidentified
5*	LDA (5.1 equiv.) (3h)	MeI (10.0 equiv.)		--%	--%	Formation of several unidentified byproducts.
6	HMDS (5.1 equiv.) (3h)	MeI (10.0 equiv.)		--%	--%	Formation of B only.

Run on -2,000 mmol scale for entries 1-3, and -1,000 mmol scale for 4-6. Byproduct identity verified using literature spectral data.
* = Starting material was chilled to -78 °C and added dropwise into LDA solution as opposed to dropwise addition of a room temperature solution.

Figure 8 - Attempts at linear naphthindanone α -alkylation reaction.

Though further studies could have been undertaken to optimize this reaction, an alternative method for α -alkylation of the linear naphthindanone was investigated: trapping of the enolate as a silyl enol ether followed by exposure to the electrophile. This approach would allow us to verify the formation of the enolate, and due to the absence of base when exposed to

the electrophile, would hypothetically prevent formation of byproduct B. Previous α -alkylation studies have only examined Lewis acid-mediated alkylation of cyclopentanone silyl enol ethers, so a model study was conducted on indanone to examine the feasibility of this reaction.⁴⁴

Preparation of the indanone silyl enol ether was preceded, and the formation of the silyl enol ether was confirmed by ^1H NMR.⁴⁵ Subjecting the obtained indanone silyl enol ether to the conditions prescribed by the sole study provided the alkylated indanone in a modest 22%, which provided enough grounds to apply this system to the linear naphthindanone (**Figure 9A**). While the 84% return of starting material was an improvement relative to the *in situ* enolate formation leading to full consumption of starting material, the 6% yield was not enough to provide traction for further optimization (**Figure 9B**). While disappointing, this does suggest that the formation of the enolate occurs readily, and that challenges lie in the interaction between the electrophile and enolate. Further studies using stronger electrophiles might be of interest. Following this effort, focus shifted towards moving forward with the α -alkylated linear naphthindanone that had been accrued, which underwent Grignard addition and elimination for a 47% yield of **6** (**Figure 8**). This reaction was performed prior to the knowledge of the improved reactivity associated with $\text{LiCl}\cdot\text{THF}$ solution, which may explain the slightly lower yield of **6** versus **7**.

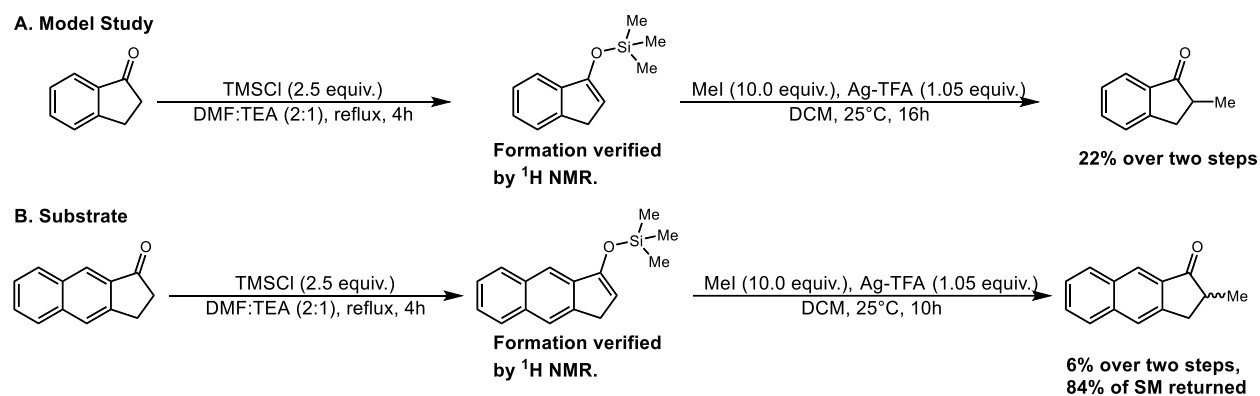


Figure 9 - Attempts at an alternative method for linear naphthindanone α -alkylation using an enolate trapped as a silyl enol ether.

The synthesis of bent naphthindenes **1** and **4** is detailed below (**Figure 10**). Precedent for the desired naphthindanone precursor of **1** does exist, but is relatively lengthy; instead, we envisioned adapting a synthetic method that utilized a Friedel-Crafts acylation followed by a Nazarov cyclization to obtain a bent naphthindanone bearing the α,β -dimethyl substitution as an alternative procedure for access to **1**.^{46,47} While the α,β -dimethyl indanone precedent observed a 92% yield, the naphthindanone precursor of **1** was only isolated in a 9% yield. However, our focus remained on simply obtaining the naphthindene to explore reactivity, so a Grignard addition and elimination was performed to obtain **1** in an 84% yield. A synthetic scheme for the bent naphthindanone precursor of **4** exists, proceeding through both a Friedel-Crafts acylation and Friedel-Crafts alkylation to obtain the desired bent naphthindanone framework in a 70% yield.^{48,49} Though the reaction went poorly in this instance, giving a 14% yield, it provided enough of the bent naphthindanone to proceed to the Grignard addition and elimination step to afford a 66% yield of **4**.

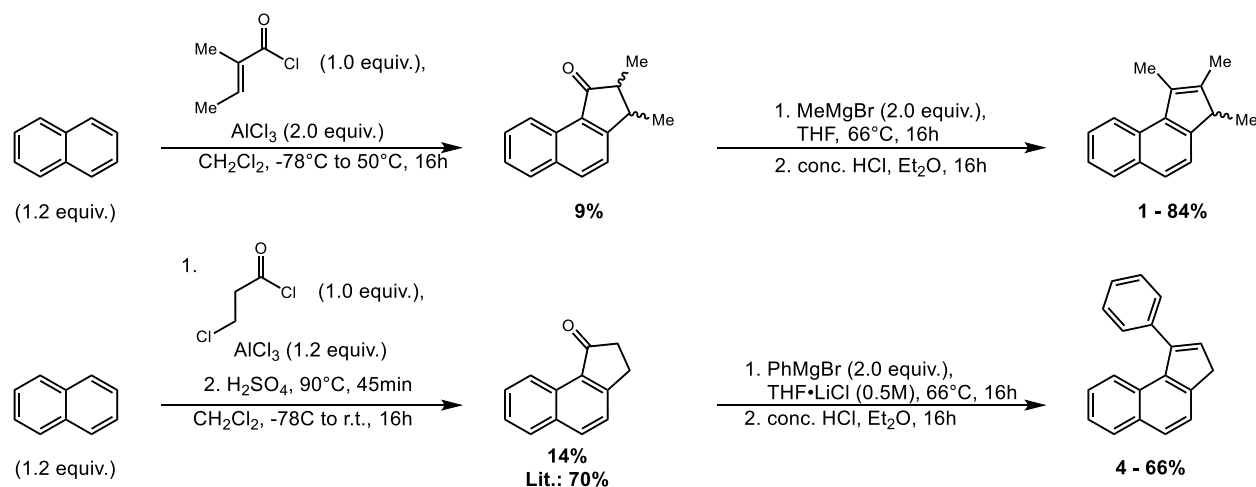


Figure 10 - Current progress towards developing the bent naphthindenyl ligand scope.

There remains a substantial opportunity for improvement in many of the unsuccessful reactions presented here, but the intended value of this work is the exploration of ligands that may unlock asymmetric catalytic activity rather than the optimization of the synthesis of a

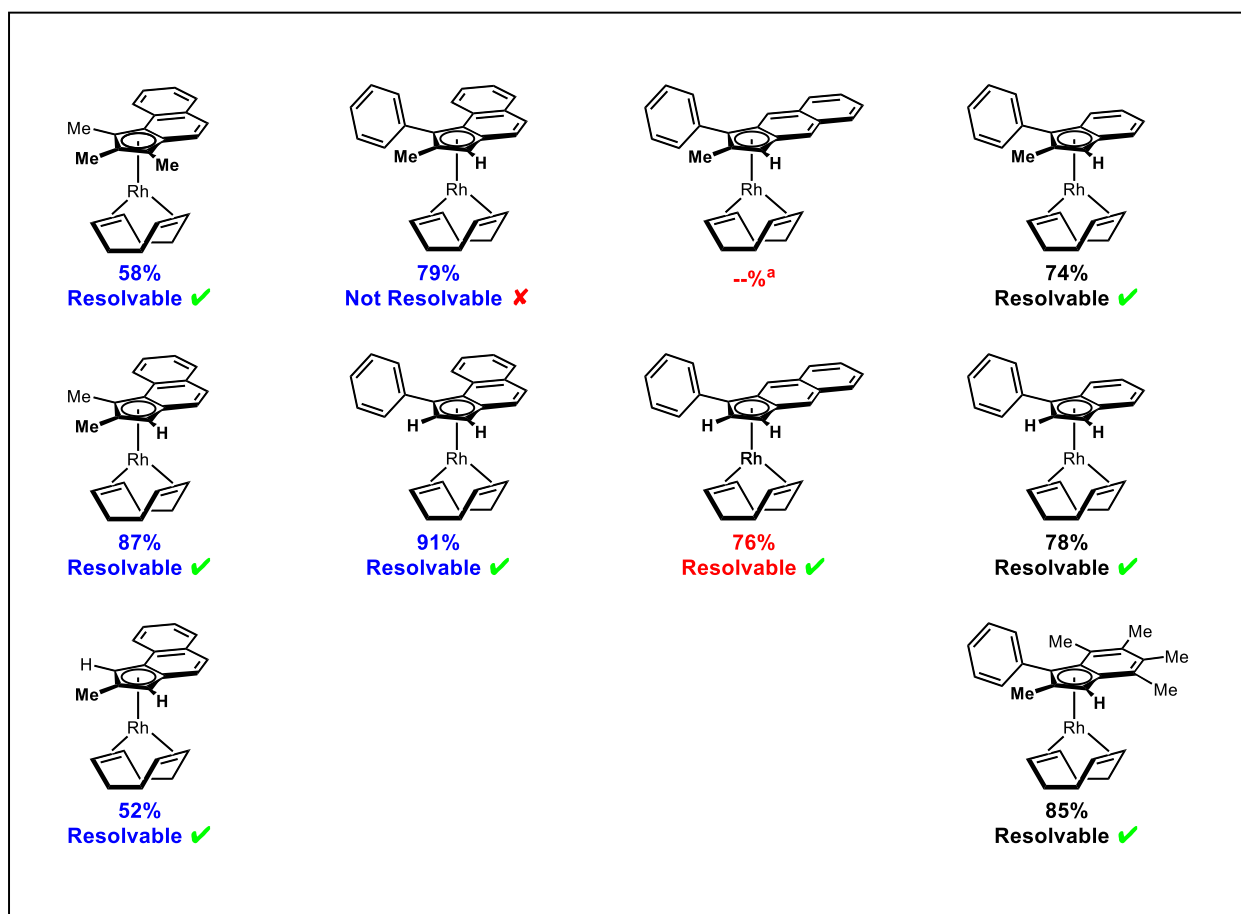
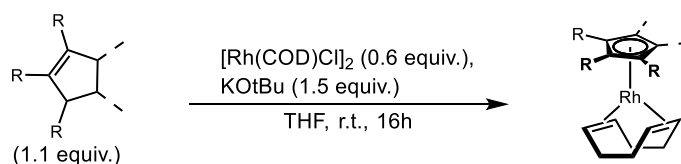
molecule. As such, the production of enough of each of these ligands such that their reactivity can be evaluated is significantly more important. Some ligands may not end up having the desired reactivity, so expenditure of additional time and energy on their synthesis will be fruitless. In the case that they do, further work can be performed to refine the synthetic pathways such that higher yields are obtained.

2.2 – Naphthindenyl Rhodium Complex Development

As suggested during the retrosynthetic analysis, complexation of naphthindene and indene molecules of interest with rhodium(I) species followed by oxidation of the rhodium center would give the desired rhodium(III) complexes. We hoped to again apply the same method used for the development of the first-generation catalyst, which involves exposure of cyclooctadiene (COD) rhodium(I) chloride dimer to the indenyl anion generated in the presence of strong base potassium *tert*-butoxide.²³ Thankfully, each naphthindene/indene rhodium(I)-COD complex was generated in good yield (**Figure 11**).²³ At this stage of the synthesis, the prochiral naphthindene and indene compounds become planar chiral, warranting separation of the two enantiomers formed from one another by chiral HPLC.²³ Remarkably, every complex could be resolved by the analytical chiral HPLC except for the bent naphthindenyl version of our first-generation catalyst, derived from bent naphthindene **2**.

Unfortunately, naphthindene **6** was unstable and decomposed under ambient conditions, and the corresponding Rh(I) complex could not be synthesized. After this observation, each naphthindene was moved from benchtop storage to the freezer to mitigate any other decomposition. Additionally, the re-synthesis of linear naphthindene **6** was put on hold due to the difficulties involved in accessing it, and our benchmark ligands for analyzing ring slippage

and consequent reactivity became the phenyl-substituted naphthindenyl and Ind ligand series instead (4,7, and 9).

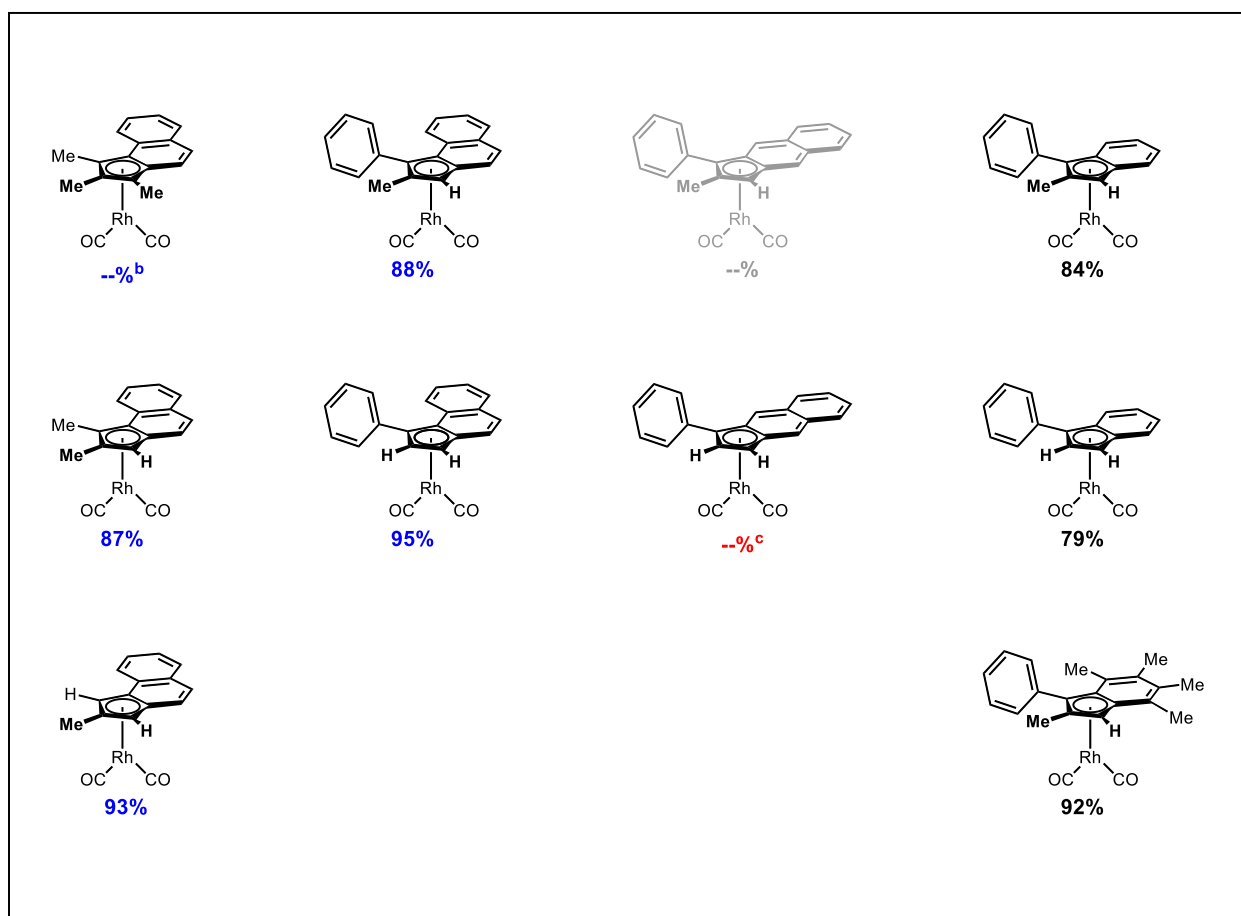
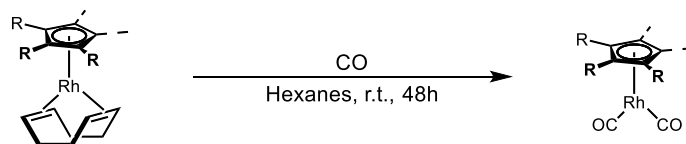


a = Decomposition of ligand prevented this complex from being synthesized.

Figure 11 - Current progress towards developing the rhodium(I)-COD naphthindenyl and indenyl complex scope.

Prior to synthesizing the rhodium(III) species of these complexes, we elected to convert each rhodium(I)-COD complex to the rhodium(I)-carbonyl complex to collect the infrared stretching frequencies needed for the Tolman electronic parameter, which will be described in section 2.3. Rhodium(I)-COD complexes were simply subjected to a CO atmosphere, where a ligand exchange reaction like that observed in the formation of rhodium(I)-COD complexes is

expected to occur. The anticipated products were isolated for most of the rhodium(I)-CO complexes (**Figure 12**). However, we noticed rapid increases in impurities following purification on the timescale of hours to days, depending on the complex. The presence of impurities was detected by ^1H NMR, where the most visible non-product peaks would often appear to correspond with the



^b = Unreacted starting material was returned with small amounts of product observed. A CO infrared stretch was able to be collected.

^c = Rapid decomplexation of this ligand was believed to have been observed, but a CO infrared stretch was able to be collected.

Figure 12 - Current progress towards developing the rhodium(I)-carbonyl naphthindenyl and indenyl complex scope.

naphthindene or indene's aliphatic protons that are typically deprotonated during the rhodium(I)-COD complexation reaction. Qualitatively, there appeared to be a general trend that the level of

impurities would grow slowly in bent naphthindenyl rhodium(I)-CO complexes but quite quickly in indenyl rhodium(I)-CO complexes. Additionally, a rapid color change of these complexes from yellow to brown/black was observed following evaporation of solvent from purification fractions, suggesting a possible stabilization of these complexes by solvents.

Along with this, we were unable to isolate the linear naphthindenyl rhodium(I)-CO complex derived from linear naphthindene **7** due to significant amounts of persistent impurities, with the non-coordinated linear naphthindene seeming to be the most prevalent product present besides the rhodium(I)-CO complex by ^1H NMR. Attempts to conduct and purify this reaction in deuterated benzene to minimize destabilization related to evaporation of solvent were unsuccessful. Future studies may include purification under inert conditions to minimize the effects of various reactive species in the normal atmosphere.

The bent naphthindenyl rhodium(I)-CO complex derived from naphthindene **1** also posed a challenge to develop. Under the given conditions, TLC studies suggested that the conversion of bent naphthindenyl rhodium(I)-COD was extremely slow, hardly converting over the span of the 48-hour reaction. This was confirmed by ^1H NMR, which showed that much of the starting material remained. Future work may include either running this reaction on a much longer timescale or attempting a procedure by Rovis and colleagues involving a reduction and carbonylation of the rhodium(III) species.³⁶

Our qualitative observations and challenges synthesizing the linear and bent naphthindenyl rhodium(I)-CO complexes may suggest the lability of these compounds because of their willingness to ring slip, which we correlated with hapticity inferred from electronic density at the rhodium center. The bent naphthindenyl rhodium(I)-CO complex derived from naphthindene **1** is hypothesized to prefer η^5 coordination, with significant stereoelectronic

contributions from the three methyl decorations of the Cp moiety; we believe that this cumulative electronic contribution of the ligand serves to stabilize the rhodium center, decreasing the complex's lability. This could explain the extremely slow conversion that was observed: η^5 coordination with additional stereoelectronic stability from methyl groups could have prevented the association of CO due to the lack of a coordination site opening if proceeding through an associative pathway (which is commonly associated with the Ind ligand).¹⁹ Oppositely, naphthindene **7** of the linear naphthindenyl rhodium(I)-CO complex is hypothesized to prefer η^3 coordination and lacks the electronic density afforded by the methyl decoration of naphthindene **1**. We believe that this could increase the complex's lability through reduced stabilization of the rhodium center due to the lack of overall electronic contribution from the ligand, which in an ideal η^3 coordination would allow for the opening of a coordination site. This could explain the decreased stability of this complex, as CO, H₂O, and other common molecules in the environment could also coordinate and lead to undesired reactions like the dissociation and re-protonation to form naphthindene **7**.

Finally, progress towards the synthesis of rhodium(III) complexes from rhodium(I)-COD complexes has been hindered by challenges with purification. Rhodium(I)-COD complexes are subjected to I₂, leading to the formation of a rhodium(III) dimer. During the development of the first-generation catalyst, the purification method that was found to be successful was to wash the isolated solid with excess diethyl ether.²³ However, current lab member Ethan Heyboer found that this method was not successful for purification of the indenyl rhodium(III) dimer derived from naphthindene **10** even when paired with use of more polar solvents to wash,

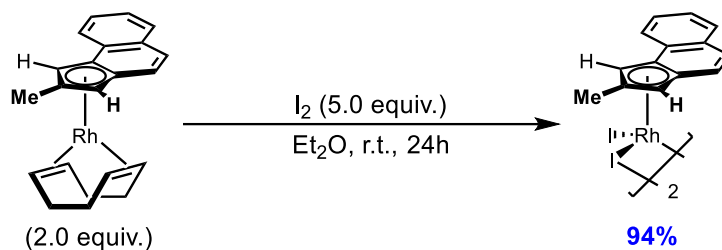


Figure 13 - Synthesis of planar chiral bent naphthindenyl rhodium(III) complex derived from bent naphthindene 5.

excessive agitation by sonication and scraping, and more. While these complexes often have extremely low solubility, it was found that a DCM:MeOH solvent system solubilized the product just enough that it could be purified by column chromatography. For the synthesis of the indenyl rhodium(III) dimer derived from naphthindene **5**, the vigorous washing methods still left small amounts of unidentifiable impurities. As a result, column chromatography was applied, and despite extremely low solubility of the complex, successful isolation of the desired rhodium(III) species was accomplished in a 94% yield (**Figure 13**). Unfortunately, attempts to purify other rhodium(III) species from the scope of this study have not yet been successful; primary challenges include tracking impurities that are not visible under UV light or with various stains and ensuring that the product remains solubilized for the duration of the purification.

2.3 – Predicting Planar Chiral Naphthindenyl Rhodium(III) Catalyst Reactivity

The Tolman electronic parameter, a measure of the electron-donating or electron-withdrawing capabilities of a ligand, has been utilized by the Rovis group to characterize the electron density at the rhodium metal center of a wide variety of Rh(I)-Cp complexes, including Ind*.³⁶ The classical application of this parameter is for evaluating the electron-donating and electron-withdrawing character of phosphine ligands, but work by Basolo and Marder have allowed for the parameter to be extended to metal-Cp and metal-Ind complexes.^{50–52} The premise behind this parameter is the ability of carbon monoxide (CO) to behave as both a σ -donor and π -

acceptor: while the CO molecule's HOMO (a lone pair located on the carbon atom) donates into the d-orbitals of the metal center, the metal-centered d-orbitals simultaneously participate in π -backbonding by donating into the CO molecule's LUMO (the π^* -orbital) (**Figure 14**).⁵⁰ A metal center with higher electron density will be able to perform more π -backbonding, inducing a weaker, longer CO bond. Oppositely, a metal center with lower electron density will be able to perform less π -backbonding, allowing for a stronger, shorter CO bond. The stretching of the CO bond can be measured using infrared spectroscopy; two unique signals associated with two different stretching modes—antisymmetric and symmetric— will be visible, reflecting the infrared energy that was needed to excite the CO bond. Weakened CO bonds (associated with higher π -backbonding and metal center electron density) will require less energy to excite, appearing as a lower wavenumber ν (cm^{-1}) in the IR spectrum. Strengthened CO bonds (associated with lower π -backbonding and metal center electron density) will require more energy to excite, appearing as a higher wavenumber ν (cm^{-1}). Since metal center electron density can be a result of the electronic influences of coordinated ligands like phosphines, Cp, and Ind,

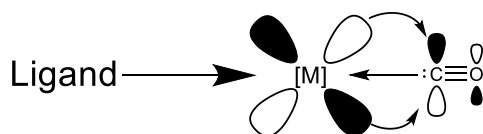
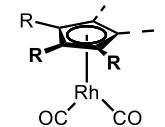
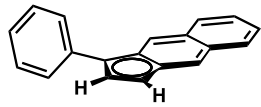
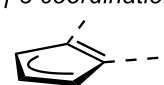
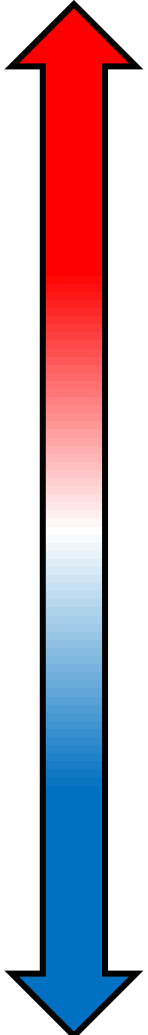
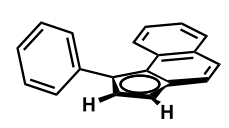
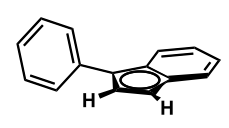
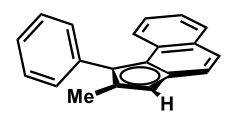
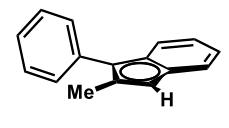
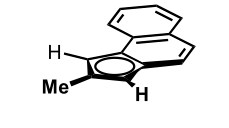
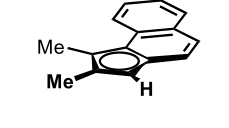
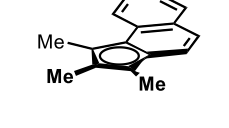
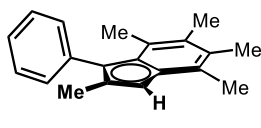


Figure 14 - Simplified illustration of σ -donation, π -backbonding, and alteration of metal center electron density by ligands.

we hoped to apply the Tolman electronic parameter to compare the electron density of each naphthindene and indene ligand of interest (**Figure 14**). We would then use this to gauge the hapticity that the ligand might favor since differences in hapticity of these ligands is associated with a different number of electrons—four electrons for true η^3 coordination and six electrons for true η^5 coordination. As such, we predicted that ligands demonstrating more η^3 character—the linear naphthindenyl rhodium(I)-CO complex derived from linear naphthindene **7**—would

contribute less electron density to the rhodium center, resulting in a higher-frequency CO stretch. We predicted that ligands demonstrating more η^5 character—the bent naphthindenyl rhodium(I)-CO complex derived from bent naphthindene **4**—would contribute more electron density to the rhodium center, resulting in a lower-frequency CO stretch. Marder and colleagues suggested that there was a hyperconjugative influence from different substitutions to both the Cp moiety and the aromatic backbone of Ind variants after observing altered electron density of the rhodium metal center in rhodium(I)-Ind complexes via the Tolman electronic parameter.⁵² This could add additional nuance to the trends observed with the naphthindenyl complexes examined here. We predicted that ligands with extensive substitution—the bent naphthindenyl rhodium(I)-CO complex derived from bent naphthindene **1**—would contribute more electron density to the rhodium center, resulting in lower-frequency CO stretches.

The CO infrared stretches are shown below, ordered by largest to smallest anti-symmetric stretches (**Figure 15**). We chose this method for displaying the data as it is what Rovis and colleagues did during their analysis of Cp variants.³⁶ However, while studying Ind variants, Marder and colleagues chose to average both values as well as find the difference relative to the classical, non-decorated Ind ligand, which could be another method for displaying this data.⁵² It must be noted that the infrared spectra for the linear naphthindenyl rhodium(I)-CO complex derived from linear naphthindene **7** and bent naphthindenyl rhodium(I)-CO complex derived from bent naphthindene **1** could still be taken despite the difficulties with their synthesis. Additionally, to make comparisons between the Cp study done by Rovis and colleagues, all samples' IR spectra were obtained in deuterated benzene except for the Blakey group's first-

	$\nu(\text{CO}) \text{ (cm}^{-1}\text{)}$		
	anti-sym ν	sym ν	
	2041.26*	1980.03*	<div style="border: 2px solid black; padding: 10px; text-align: center;"> <p style="color: red; font-weight: bold;">Less electron-donating</p> <p>η-3 coordination</p>   <p style="color: blue; font-weight: bold;">More electron-donating</p> <p>η-5 coordination</p>  </div>
	2036.87	1976.32	
	2036.77	1974.93	
	2033.62	1971.74	
	2032.58 ^d	1972.56 ^d	
	2032.34	1969.02	
	2029.25	1970.41	
	2026.99 ^{*d}	1968.27 ^{*d}	
	2026.65	1966.14	

All infrared stretches taken in deuterated benzene unless indicated.

d = Infrared stretch taken in hexanes.

* = Infrared stretch taken in spite of impure product.

Figure 15 - Tolman electronic parameter results ranked by asymmetric stretch wavenumbers.

generation catalyst. Future efforts to collect the first-generation catalyst CO stretches in deuterated benzene are anticipated.

As expected, the linear naphthindenyl rhodium(I)-CO complex derived from linear naphthindene **7** appears to have the lowest level of electron density at the rhodium center, which we predicted would occur because of its tendency towards an η^3 -coordination (4 electron coordination) to preserve the aromaticity of the naphthalene backbone. It is also very interesting to see that the indenyl and bent naphthindenyl rhodium(I)-CO complex derived from indene **9** and bent naphthindene **4** appear to have nearly identical amounts of electron density at the rhodium center. This could suggest that they have similar hapticity. Alternatively, there could be a complex combination of hyperconjugative effects from the phenyl ring and different aromatic backbones that result in each rhodium center having similar electron density but with different levels of preferred coordination by each ligand. The bent naphthindenyl and indenyl complex derived from **4** and **9**, respectively, are also approximately five wavenumbers lower than the linear naphthindenyl complex derived from **7**, which offers promising support that the bent aromatic backbone results in different hapticity to significantly modify electronic density of the rhodium metal center as there are no differences in the Cp moiety substituents. It is also fascinating to see that there is an almost linear decrease in wavenumber as the number of methyl decorations to the Cp moiety increase, which culminates in the most electron dense rhodium centers being coordinated with the bent naphthindenyl ligand derived from **1** and the Ind ligand derived from **10**, which are the ligands with the most methyl decorations. This is likely explained by the increase in hyperconjugative effects from each methyl group, which was also anticipated. It appears that the naphthindene variations have much less electron density on the rhodium center relative to the Cp derivatives developed by Rovis and colleagues; many of their complexes are a

minimum of 10 wavenumbers lower than the most-electron-rich rhodium center complexes derived from **1** and **10**.³⁶

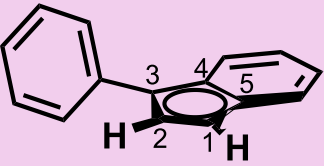
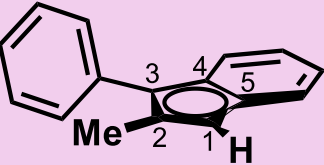
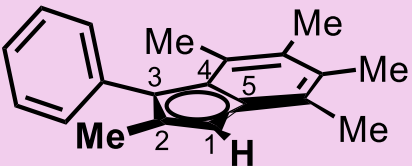
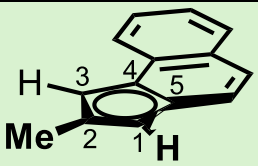
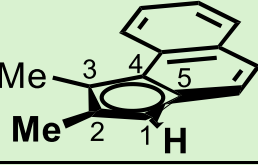
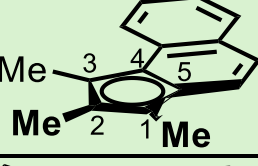
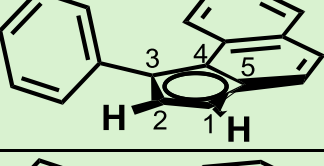
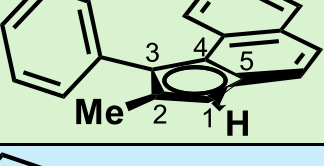
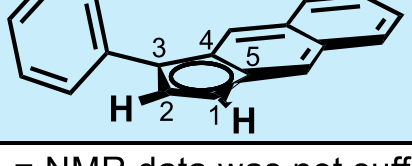
While the Tolman electronic parameter offered insight into the contribution of the ligand to the electronic density localized on the rhodium metal center, we hoped to more closely examine the relationship between each carbon involved in the Cp moiety and the rhodium metal center itself through NMR studies. The naturally occurring NMR-active isotope ^{103}Rh can directly interact with carbon nuclei; as such, in a ^{13}C NMR, certain carbons whose chemical environments directly involve rhodium experience ^{103}Rh - ^{13}C coupling. This is visible due to splitting of the ^{13}C signal by ^{103}Rh and a corresponding J -value (coupling constant) that quantifies the strength of the interaction, with large J -values representing more significant interactions between the carbon and rhodium nuclei. Other common NMR studies that take advantage of rhodium's NMR-activity include ^{31}P NMR of rhodium-phosphine complexes and ^{13}C NMR of rhodium-carbonyl complexes to directly examine the electronic influence of the metal center on phosphine (characterized using $J_{\text{Rh-P}}$) and carbonyl ligands (characterized using $J_{\text{Rh-C}}$), respectively.^{36,53} However, this only provides insight into the general electronic density located at the rhodium center similar to the Tolman electronic parameter, while we are more interested in examining the interactions of each carbon of the Cp moiety and the rhodium center to characterize hapticity. One study does specifically examine the chemical shifts of each Ind carbon in Ind-Cr, Ind-Fe, Ind-Co, and Ind-Ni complexes to characterize hapticity, but these shifts are not solely due to the interaction of the carbon with the metal center—they rely on the surrounding chemical environment like nearby carbons and hydrogens as well.⁵⁴ As such, specifically characterizing the interaction of the rhodium and the carbon nuclei through the ^{103}Rh - ^{13}C coupling constants provides another view into the naphthindenyl and Ind ligand

hapticity, which we then correlate with ring slippage. For η^3 -favoring ligands, we predicted that we would see small $J_{\text{Rh-C}}$ -values for the two carbons shared by the aromatic backbone and Cp moiety, and then larger $J_{\text{Rh-C}}$ -values for the other three carbons within the Cp moiety. For η^5 -favoring ligands, we would anticipate similar coupling constants between the Rh and all five of the Cp carbons. We predicted that the three carbons within the Cp moiety not shared by with the aromatic backbone might still have a slightly larger $J_{\text{Rh-C}}$ -values than for the two carbons shared by the aromatic backbone and Cp moiety due to possible ring slippage. We would also anticipate that the increased cumulative stereoelectronic effect of Cp substituents effectively donating more electron density into the rhodium metal center could lead to increased interaction between the carbons and rhodium.

To accomplish this, we planned to identify each carbon in the Cp moiety of the rhodium(I)-COD complexes through a variety of different NMR studies including ^1H , ^{13}C , DEPT90, DEPT135, HSQC, HMBC, COSY, and NOESY. Then, the ^{103}Rh - ^{13}C coupling constant would be collected and assigned to the correct carbon. The data is compiled and displayed below, with the ligands organized as indene-derived (pink), bent naphthindene-derived (green), or linear naphthindene-derived (blue) (**Figure 16**). All ^{103}Rh - ^{13}C coupling constants were calculated manually using MestReNova's peak selection system. To better visualize the differences in coupling constants across the various Rh complexes, a heatmap was employed where coupling constants below 2.00 and above 5.00 were colored dark blue and red, respectively. For values between 2.00 and 5.00, a color gradient transitioning from dark blue to red was developed based on 0.25 Hz increments of coupling constants. It is worth noting that in the series of bent naphthindenyl rhodium(I)-COD complexes derived from naphthindenes **1**, **3**, and **5**, the provided data is not sufficient to make a conclusive assignment as several of the carbon signals were

extremely close together, leading to overlapping signals. As a result, these signals were placed in the heatmap based on their anticipated location. While this might be seen as a misleading way of displaying the data, the data points were marked to clarify their ambiguity. Additionally, for the carbon assignments that were confirmed, similar values were observed in the same carbons of related ligands, leading to the prediction that minimal modification such as the addition of a methyl would not drastically alter the coupling constant. These considerations led to the placement of coupling constants at the locations they are displayed in.

Overall, it appears that the carbons shared by the fused aromatic backbone and Cp moiety—C4 and C5—experience weaker interactions with the rhodium metal center compared to the non-fused carbons—C1, C2, and C3—as seen by the smaller $J_{\text{Rh-C}}$ -values of C4 and C5 (more blue) compared to C1, C2, and C3 (more red). However, that does not mean that each complex is demonstrating perfect η^3 coordination as closer examination of the differences in the $J_{\text{Rh-C}}$ -values seem to show that there are stronger levels of interaction between C4 and C5 and the rhodium metal center in the bent ligands than either the indenyl or linear. The linear naphthindenyl complex derived from naphthindene **10** does seem to tend towards η^3 coordination as evidenced by the lack of interaction between Rh-C5, relatively small interaction between the Rh-C4, and extremely large $J_{\text{Rh-C}}$ -values for C2 and C3 of this complex. The asymmetric level of interaction between Rh-C5 and Rh-C4 may suggest an asymmetric electronic density as well, which could be interesting for enantioinduction. The Ind family also demonstrates strong interactions of the rhodium center with C1, C2, and C3 along with smaller, asymmetric interactions with C4 and C5 in a way that is very reminiscent of the linear naphthindenyl example. It appears that there are stronger interactions between Rh-C4 and Rh-C5 for this group of ligands than for the linear example, which could suggest a weaker preference for η^3 compared

	C1	C2	C3	C4	C5
	4.72	5.05	3.77	2.39 ^e	1.50 ^e
	4.56	5.11	3.71	2.26	2.52
	4.53	5.00	4.35	3.30	2.22
	3.75	4.65 ^e	3.77	2.92	2.73 ^e
	4.29	5.06 ^e	3.74 ^e	3.14	3.04
	4.44	4.97 ^e	4.54 ^e	3.36	3.05
	4.32	3.74	3.72	2.72	2.92
	4.37	3.73	4.22	2.98	2.96
	4.95	5.74	4.06	2.21	0.00 ⁺

e = NMR data was not sufficient to provide definitive assignment of carbon.

Figure 16 - Heatmap displaying the J_{Rh-C} (Hz) of each Cp moiety carbon.

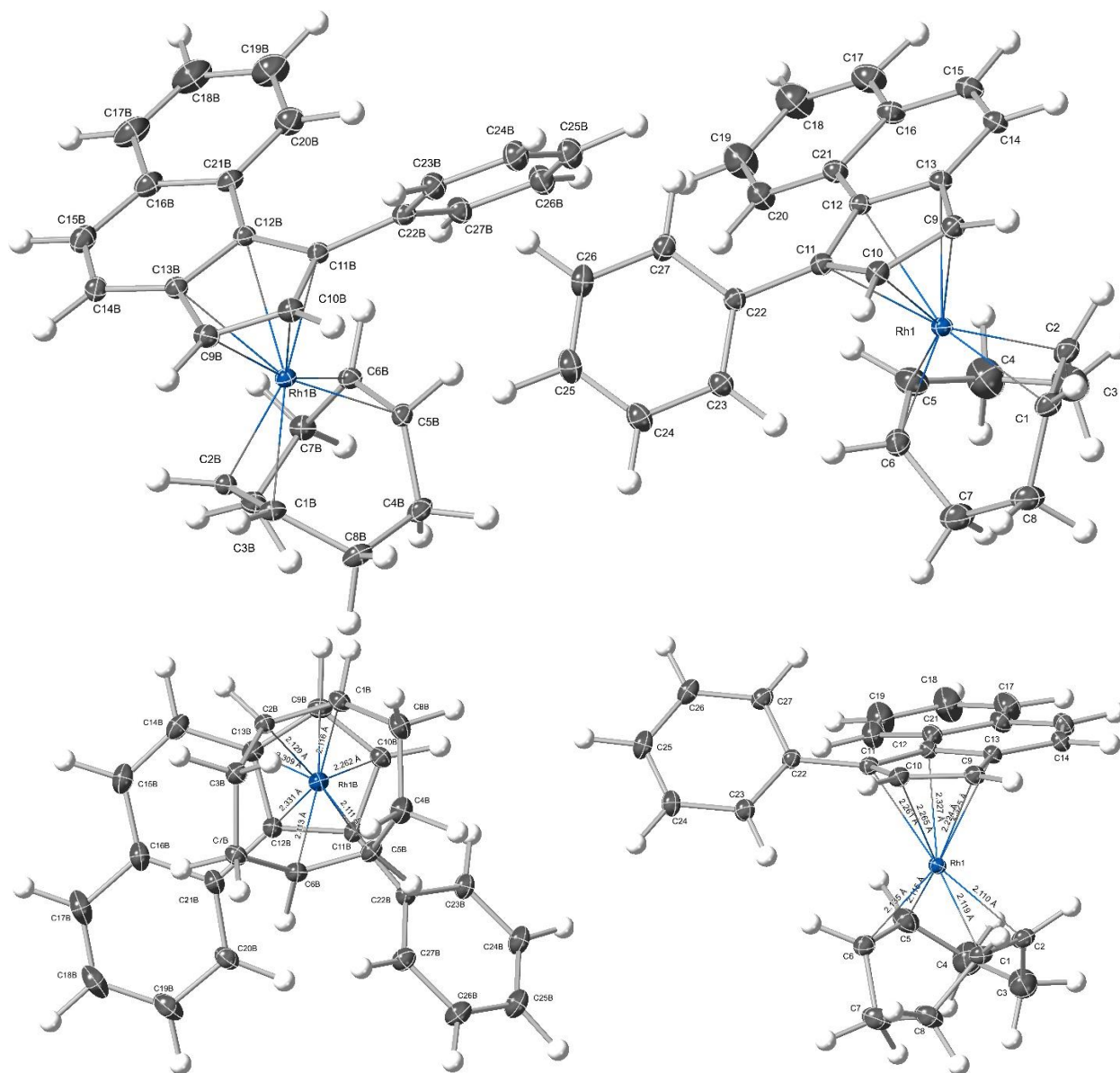
to the linear naphthindenyl example such that ring slippage might be more permissible. The bent naphthindene family shows the slightly weaker interactions of the rhodium center with C1, C2, and C3 along with much larger and more symmetric interactions with C4 and C5. While the difference in the level of interaction between Rh-C1-3 and Rh-C4/5 is still quite major, it is smaller than what was seen for the Ind and linear naphthindenyl examples, suggesting an even weaker preference for η^3 or a stronger preference for η^5 . It becomes unclear whether the bent naphthindenyl family might favor η^5 strongly enough that it does not participate in significant amounts of ring slippage like the classic Cp, or if it will still be capable of ring slippage like that observed with Ind complexes.

Addition of methyl substituents around the Cp moiety did appear to increase the strength of interaction of all five carbons of the Cp moiety, which demonstrates that stereoelectronic contributions via hyperconjugation may be non-trivial to a ligand's behavior. One seemingly bizarre observation was the weak interaction between Rh-C2 in the bent naphthindenyl complexes derived from bent naphthindene **2** and **4**. The added methyl in the bent naphthindenyl complex derived from bent naphthindene **2** did not seem to recover the level of Rh-C2 interaction seen with the methylated bent naphthindenyl complexes, which was puzzling. One potential explanation could be the electron-withdrawing behavior of the phenyl ring due to the sp^2 -hybridization of its carbons. This could result in inductive withdrawing of electron density from the C2 carbons that is then centralized on the C3 carbon. This would provide excess electron density at C3 to facilitate a stronger Rh-C3 interaction while weakening the Rh-C2 interaction due to the lost electron density. The added methyl in the bent naphthindenyl complex derived from bent naphthindene **2** could be the source of electron density that is withdrawn away from C2 towards C3, which could explain the increase in Rh-C3 interaction while preserving the

lower Rh-C2 interaction for this complex compared to the bent naphthindenyl complex derived from bent naphthindene **4**. Upon closer examination of the Rh-C4 interaction in these two derivatives, we also observe a slight decrease in interaction, which is opposite of what was seen with the methylated bent naphthindenyl complexes—the interaction of Rh-C4 was stronger than Rh-C5. This provides further support for the inductive withdrawing performed by the phenyl group, accumulating electronic density on C3. Many interesting nuances are shown here that were not observed from the Tolman electronic parameter, so future study into the $J_{\text{Rh-C}}$ -values of previous generations of the Ind catalyst developed in the Blakey lab along with other popular Ind variants could be highly interesting.

Finally, the data provided by solid-state structures is invaluable. Bond lengths, bond angles, and torsion angles can provide extensive insight into a variety of different characteristics of a molecule. With the help of John Bacsá (PhD), we were able to grow crystals of complexes containing our benchmark ligands: bent naphthindenyl rhodium(I)-COD complex derived from bent naphthindene **4** (**Figure 17**), linear naphthindenyl rhodium(I)-COD complex derived from linear naphthindene **7** (**Figure 18**), and Ind rhodium(I)-COD derived from indene **9** (**Figure 19**). For the bent benchmark, two structures of the complex were identified as the crystal included both structures. Additionally, the thermal ellipsoid of the rhodium was elongated in the same direction as the plane of the aromatic backbone, pointing to a displaced rhodium. The displacement of the rhodium center in the direction of the aromatic backbone could be indicative of the rhodium center slipping between η^5 and η^3 coordination modes. For the linear benchmark, we were able to capture what we believe are two coordination modes, where the rhodium metal center of the two modes is approximately 0.2 Å apart. This was promising as each mode could represent both the η^3 -like coordination predicted to result from the maintenance of aromaticity in

the naphthalene backbone along with the less-favored η^5 coordination. However, the complex was observed to be highly reactive and unstable during crystallization, so further studies to ensure that this data is valid will be pursued.



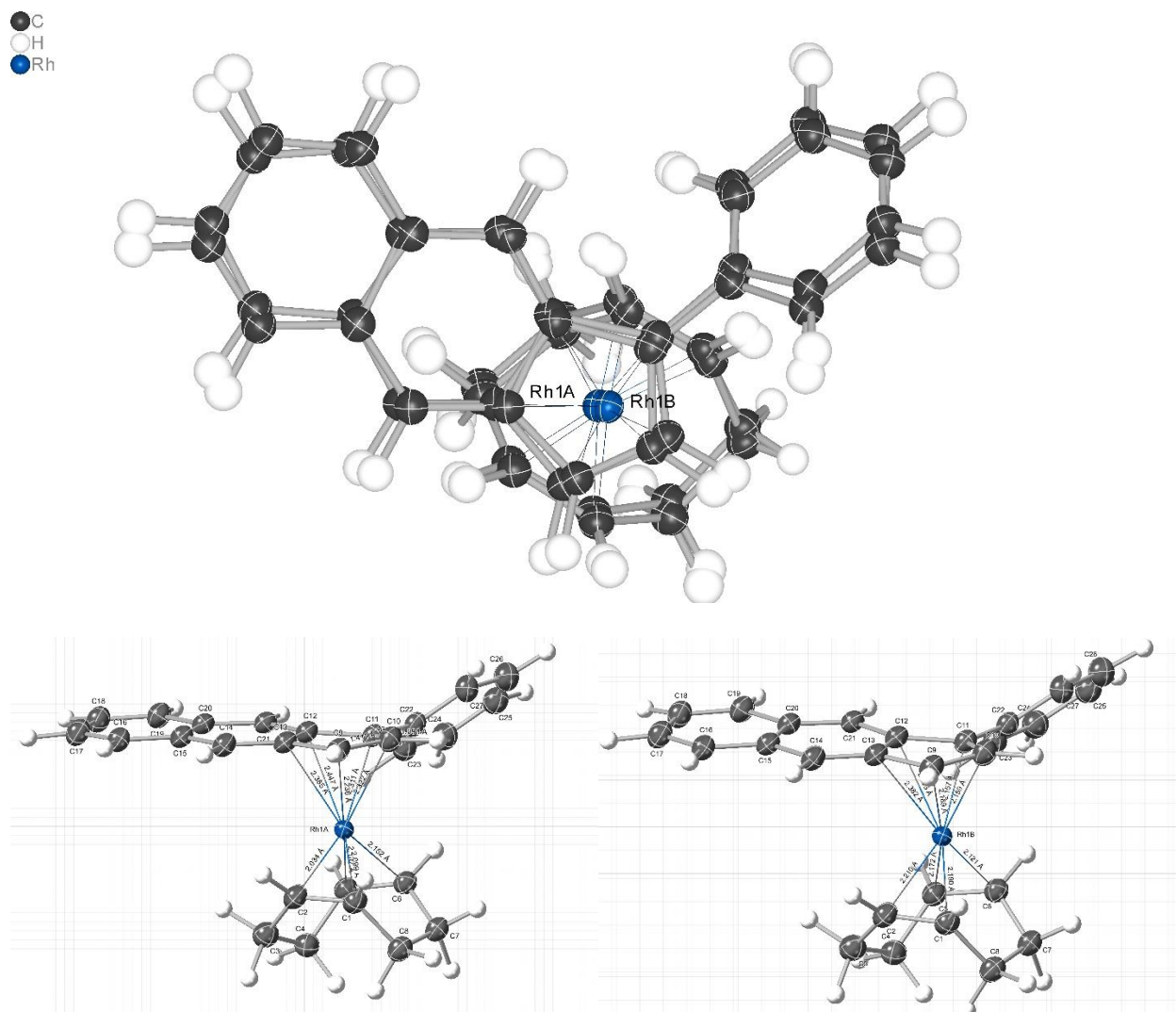


Figure 18 - Crystal structures of linear naphthindenyl rhodium(I)-COD complex derived from linear naphthindene 7.

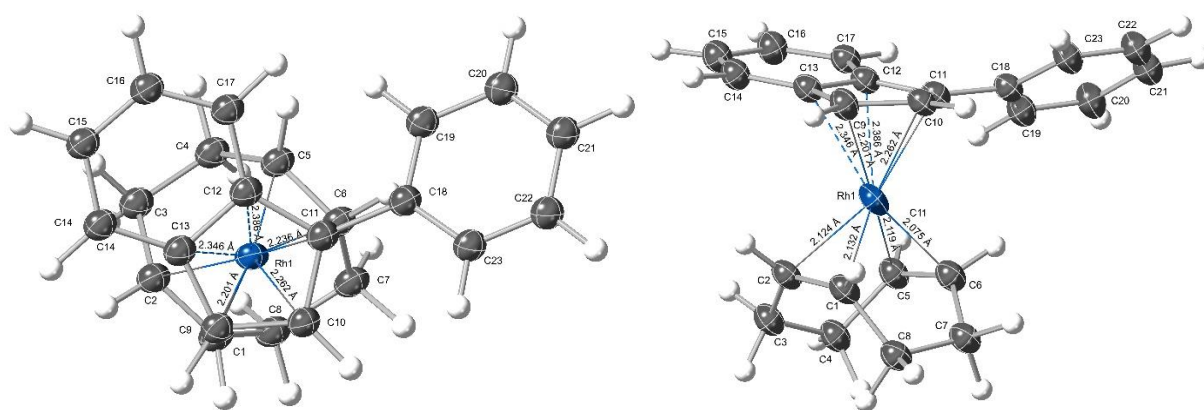


Figure 19 - Crystal structures of Ind rhodium(I)-COD complex derived from indene 9.

In addition to the general observations of this process, we hoped to utilize an established method of interpretation of this data that might shed final insights on the hapticity and ring slippage character resulting from the different aromatic backbones. Previously, Marder and colleagues collected solid-state structural data of Ind complexed iron, cobalt, rhodium, and nickel, during which they utilized a parameter titled “slip value”.^{55,56} This value represents the relative slippage of the metal center away from the Cp moiety’s centroid, which is where it would be positioned in a true η^5 ligand.^{55,56} The definition of slip values is the following:^{55,56}

$$\Delta = \text{avg } d(M - C(4), C(5)) - \text{avg } d(M - C(1), C(3))$$

where d is the distance of the bond $M - C(x)$ and the carbon assignments are

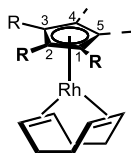


Figure 20 - Carbons used calculating for slip value Δ (Å).

For a true η^5 Ind ligand, the slip value should be 0 Å since the bond lengths from the rhodium to each carbon would be the same. It is difficult to establish a metric for a true η^3 Ind ligand, but previously reported values ranged from 0.69-0.79 Å.⁵⁶ This parameter was utilized for the complexes using the classical, unvaried Ind, which may make comparison of slip values for our planar chiral indene and naphthindenes not comparable to the values reported. However, this will still provide us insight into the general difference in slip values of the complexes compared to one another. The table of bond lengths and the slip value for each is shown below (**Figure 21**).

The slip values for the bent benchmark complex were expected to be closer to an η^5 slip value, which seemed to be true across both proposed crystal structures. It is quite interesting that we can observe a difference in the proposed coordination modes of the linear benchmark complex and to a certain extent, quantify this using the slip value. We also expected the linear

benchmark complex slip value to be greater than the bent benchmark complex due to the hypothesized η^3 preference of linear naphthindenyl ligands, which is what we observe. Mode 2 appears to be more η^3 -like than Mode 1. It is also remarkable to see that the Ind benchmark complex slip value lies somewhere between both the bent and the linear benchmarks. This aligns with the NMR study, which showed the Ind complexes having stronger rhodium-carbon interactions than the bent ligand scope but weaker rhodium-carbon interactions than the linear

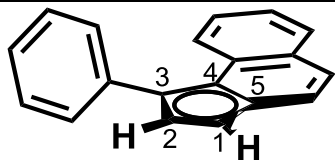
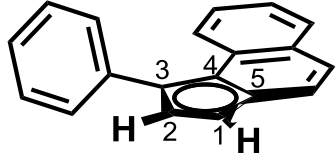
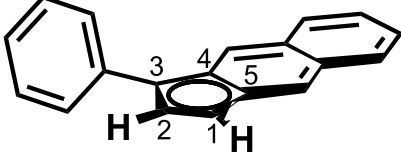
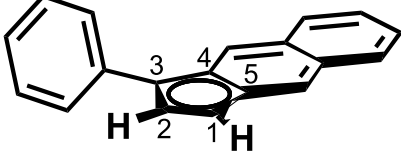
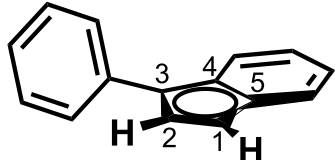
	Rh-C4	Rh-C5	Rh-C3	Rh-C1	Slip Value (Å)
 Crystal Structure 1	2.327	2.325	2.261	2.228	0.084
 Crystal Structure 2	2.331	2.308	2.251	2.219	0.085
 Mode 1	2.450	2.384	2.340	2.260	0.117
 Mode 2	2.390	2.393	2.130	2.160	0.247
	2.386	2.346	2.236	2.201	0.148

Figure 21 - Slip values (Å) for the benchmark indene and naphthindene ligands.

scope. Considering the Tolman electronic parameter, NMR studies, and solid-state structure analysis together, we believe that the influence of different orientations of the aromatic naphthalene backbone paired with Cp substituent modification allows for access to a range of different hapticities, and likely, levels of ring slippage, with Cp having little to none, bent naphthindenyls having less than Ind, and linear naphthindenyls having the most.

3 – Conclusions and Future Directions

In this work, we hoped to begin understanding what effect the extension of the indenyl ligand's aromatic backbone had alongside modification to substituents around the Cp moiety. This was in hopes of unlocking new reactivity using planar chiral rhodium(III) catalysts for the purpose of asymmetric C-H functionalization, but also asymmetric catalysis as a whole. We envisioned a naphthalene backbone oriented in a "linear" and "bent" fashion and predicted that this would lead to subtle differences in the preferred hapticity of the Cp moiety and preference to ring slip based on the resonance structures of this backbone. Initial efforts towards synthesis of two linear naphthindenes and two bent naphthindenes is described. Though the key conversion of naphthindanone precursors to naphthindenes has been established as a robust method, the development of the naphthindanone variants themselves proved challenging. Significant efforts were made to improve the yields of these reactions, but to little or no avail. In spite of this, we successfully generated the rhodium(I)-COD species and rhodium(I)-carbonyl species. One rhodium(III) iodine dimer was synthesized and purified, but challenges remain for successful purification of these rhodium(III) species. We also discussed the three methods that we used to gain insight into the hapticity of these complexes, which we hoped to correlate with a complex's desire to ring slip. The Tolman electronic parameter suggested the electron-donating capabilities

of each ligand within our scope, which could be correlated with hapticity based on the number of coordinated electrons. To better understand the individual interaction between the rhodium metal center and each carbon of the naphthindenyl and Ind Cp moiety, we identified each carbon in the Cp moiety using various NMR studies and identified their ^{103}Rh - ^{13}C coupling constants. Also, solid-state structure analysis was performed, and slip-value, a parameter used for characterizing ring slippage, was used to process this data.

Our data suggests that the new linear and bent naphthindenyl ligands may have different levels of ring slippage relative to both Cp and Ind. While the bent naphthindenyl ligands have more η^5 character than the Ind or linear naphthindenyl ligands, the Tolman electronic parameter suggests it is still more η^3 -like than the Cp ligands. Relative to the Ind ligands, the linear naphthindenyl ligand demonstrates a much stronger preference for η^3 coordination. As a result, the naphthalene aromatic backbone and its specific orientation allows for a spectrum of hapticities, and subsequently, potential levels of ring slippage, to be accessed, with modification of the Cp moiety substituents offering additional fine tuning (**Figure 22**). Ultimately, we hope that this will allow us to access a wide variety of different complexes with different asymmetric, catalytic, C-H functionalization capabilities.

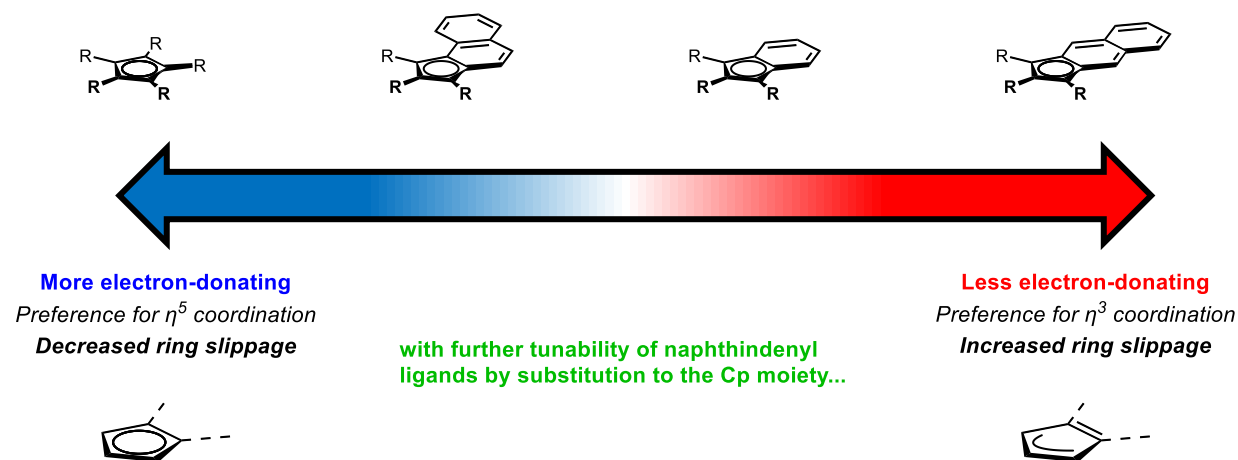


Figure 22 - Characterizing the 4th generation naphthindenyl complexes relative to established scaffolds Cp and Ind.

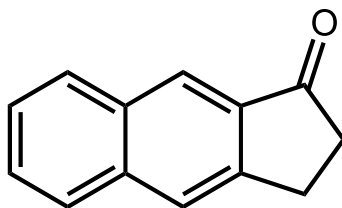
Future work includes completion of the rhodium(III) species scope, followed by use of these complexes in reactions to compare their reaction rates. This will allow us to gauge the level of ring slippage permitted by the bent and linear naphthalene backbones since the indenyl ligand effect relates the rate of a reaction to the ring slippage of Ind scaffolds. We also hope to observe how these catalysts behave in the different reactions that the Blakey group has developed using the first generation planar chiral Ind rhodium(III) catalyst. This would allow us to better understand how the steric profile and the electronic asymmetry was modified, and it could also potentially result in new reactivity. Finally, we plan to plot each of these different data sets against one another as well as other factors such as molecular orbital calculations in order to best characterize the level of hapticity and ring slippage that we predict is occurring.

4 – Supplemental Information

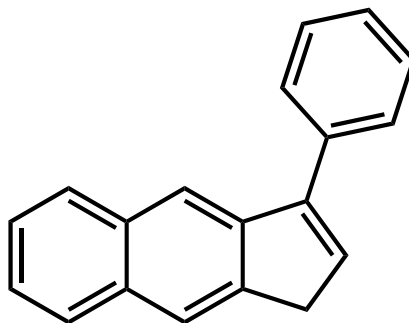
General Information

All reactions were conducted under nitrogen atmosphere with anhydrous solvents in oven- or flame-dried glassware using standard Schlenk technique, unless otherwise stated. Anhydrous dichloromethane (DCM), diethyl ether (Et₂O), tetrahydrofuran (THF), and hexanes were obtained by passage through activated alumina using a *Glass Contours* solvent purification system. Solvents for workup, extraction, and column chromatography were used as received from commercial suppliers without further purification. All other chemicals were purchased from Millipore Sigma, Strem Chemicals, Oakwood Chemicals, Alfa Aesar, TCI, Combi Blocks, or Ambeed and used as received without further purification, unless otherwise stated. ¹H and ¹³C nuclear magnetic resonance (NMR) spectra were recorded on a Bruker 800 spectrometer (800 MHz ¹H, 201 MHz ¹³C), a Bruker 600 spectrometer (600 MHz ¹H, 151 MHz ¹³C), Varian Inova

600 spectrometer (600 MHz ^1H , 151 MHz ^{13}C), a Varian Inova 500 spectrometer (500 MHz ^1H , 126 MHz ^{13}C), a Bruker 400 spectrometer (400 MHz ^1H , 126 MHz ^{13}C), and a Varian Inova 400 spectrometer (400 MHz ^1H , 126 MHz ^{13}C). Chemical shifts δ values were reported in parts per million (ppm) relative to CHCl_3 (7.26 ppm for ^1H , 77.16 ppm for ^{13}C) for CDCl_3 , relative to C_6H_6 (7.16 ppm for ^1H , 128.06 ppm for ^{13}C) for C_6D_6 , relative to DMSO (2.50 ppm for ^1H , 39.52 ppm for ^{13}C) for DMSO- d_6 . Coupling constants (J -values) were reported in Hz and multiplicities were indicated using the following abbreviations: s = singlet, d = doublet, t = triplet, q = quartet, qn = quintet, m = multiplet, br = broad. High resolution mass spectra (HRMS) were obtained using a Thermo Electron Corporation Finigan LTQFTMS (at the Mass Spectrometry Facility, Emory University). High Pressure Liquid Chromatography (HPLC) was performed on an Agilent 1100 series HPLC utilizing CHIRALPAK® AD-H, AS-H, CHIRALCEL® OD-H and OJ-H 4.6 x 150 mm analytical columns or on an Agilent 1260 Infinity II series HPLC utilizing CHIRALPAK® IA, IB, IH, IJ, and IK 4.6 x 150 mm analytical columns. Analytical thin layer chromatography (TLC) was performed on precoated glass-backed Silicycle SiliaPureR 0.25 mm silica gel 60 plates and visualized with UV light. Silica gel column chromatography was performed using Silicycle SiliaFlashR F60 silica gel (40- 63 μm). Flash column chromatography was performed using Silicycle SiliaFlashR F60 silica gel (40- 63 μm) on a Biotage Isolera One system.

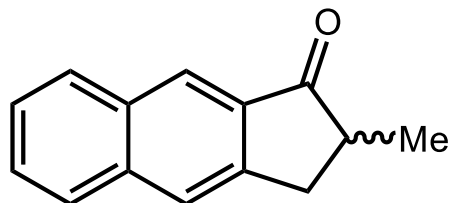
Experimental Section**S1** - 2,3-dihydro-1H-cyclopenta[b]naphthalen-1-one

A three neck round bottom flask equipped with a stir bar, a condenser, $\alpha,\alpha,\alpha',\alpha'$ -Tetrabromo-o-xylene (7.0100 g, 16.62 mmol, 1.2 equiv.), and sodium iodide (16.6153 g, 110.81 mmol, 8.0 equiv.) was placed under a nitrogen atmosphere. After adding 55 mL of DMF and stirring for 5 minutes, 2-cyclopentenone (1.20 mL, 13.85 mmol, 1.0 equiv.) was added. The reaction was then refluxed at 80°C for 18 hours, slowly becoming a dark red/purple color. The reaction was allowed to cool to room temperature and dumped onto 100 g of ice. 25 mL of sodium bisulfite solution immediately precipitated a yellow solid, which was collected using EtOAc. The solvent was then removed under reduced pressure and the resulting crude product was purified via silica gel column chromatography (20% EtOAc in hexanes) as a yellow solid. (1.1889 g, 47% yield) Spectroscopic data for **S1** matches those previously reported in literature.³⁸



S2 - 3-phenyl-1H-cyclopenta[b]naphthalene

A three neck round bottom flask equipped with a stir bar and a condenser was placed under a nitrogen atmosphere. The 2,3-dihydro-1H-cyclopenta[b]naphthalen-1-one (**S1**) (0.1007 g, 0.55 mmol, 1.0 equiv.) was dissolved in 5.0 mL of LiCl•THF solution (0.5M) and the reaction vessel was placed in an ice bath to cool to 0 °C. Once cooled, phenyl magnesium bromide (1.10 mL, 2.0M, 2.2 mmol, 4.0 equiv.) was slowly added to the reaction. Once the addition was complete the ice bath was removed and replaced with a heating block to reflux the reaction for 16 hours. The reaction was cooled to room temperature and placed in an ice bath before carefully quenching with DI H₂O. Concentrated HCl and Et₂O was added to the reaction vessel and stirred for an additional 24 hours at room temperature. The layers of the biphasic solution were separated, and the aqueous layer extracted with Et₂O three times. The combined organic layers were sequentially washed with NaHCO₃, DI H₂O and brine before being dried over MgSO₄. The solvent was removed under reduced pressure and the resulting crude product was purified via silica gel column chromatography (0% EtOAc in hexanes) as a yellow solid. (0.0859 g, 64% yield) **¹H NMR (400 MHz, CDCl₃)** δ 8.01 – 7.95 (m, 2H), 7.94 – 7.85 (m, 2H), 7.76 – 7.67 (m, 2H), 7.59 – 7.50 (m, 2H), 7.52 – 7.43 (m, 3H), 6.71 (t, *J* = 2.4 Hz, 1H), 3.69 (dd, *J* = 2.4, 1.2 Hz, 2H) ppm. **¹³C NMR (101 MHz, CDCl₃)** δ 145.08, 142.81, 142.48, 136.10, 132.78, 132.76, 131.90, 128.70, 128.22, 127.83, 127.81, 127.70, 125.22, 125.11, 122.51, 118.22, 77.37, 77.05, 76.73, 37.41 ppm. **HRMS (+APCI)** calculated for C₁₉H₁₅ [M+H]⁺ 243.11737, found 243.11683.



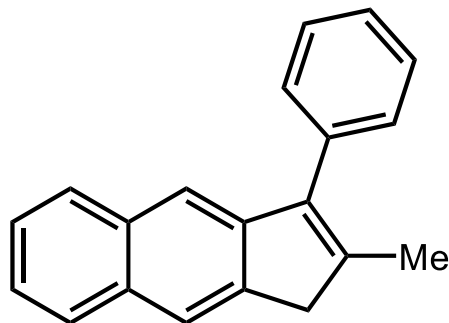
S3 - 2-methyl-2,3-dihydro-1H-cyclopenta[b]naphthalen-1-one

Lithium diisopropylamide approach: Several different conditions were attempted for the synthesis of **S3** (**Figure 8**). For entries 1-4 and 6, a two neck round bottom flask equipped with a stir bar and 2,3-dihydro-1H-cyclopenta[b]naphthalen-1-one (**S1**) (~2.00 mmol for entries 1-3, ~1.00 mmol for entries 4-6), and was placed under a nitrogen atmosphere. In a separate three neck round bottom flask equipped with a stir bar, n-butyllithium was added dropwise to a solution of diisopropylamine chilled to -78°C to generate lithium diisopropylamide (LDA) *in situ* (for entry 6, HMDS was used instead to generate LiHMDS). Between 4.0 and 8.0 mL of THF was added to each round bottom flask in each entry, with entry 4 requiring a 4:1 mixture of THF:DMPU. Then, the solution of 2,3-dihydro-1H-cyclopenta[b]naphthalen-1-one (**S1**) was added dropwise to the LDA and allowed to stir for 20 minutes in entries 1 and 2, and 3 hours in entries 3-6. In entry 5, the solution of 2,3-dihydro-1H-cyclopenta[b]naphthalen-1-one (**S1**) was also chilled to -78°C prior to dropwise addition. Finally, iodomethane was added dropwise (1.0 equiv. in entry 1, 10.0 equiv. in entry 2-6). The reaction was quenched using ammonium chloride, and the solvent was removed under reduced pressure. The resulting crude product was purified via silica gel column chromatography (0-20% EtOAc in hexanes), which revealed the formation of undesired byproducts. TLC was used to examine if the desired product was formed in entries 3-6; crude reaction mixtures were not purified if no product was observed. (Entry 1: 0.0313, 17% Entry 2: 0.0655, 15%)

Silyl enol ether approach: In the model indanone study, 1-indanone (0.3958 g, 2.99 mmol, 1.0 equiv.) was dissolved in a 2:1 DMF:TEA solution (13.2 mL DMF, 6.6 mL TEA) in a three neck round bottom flask equipped with a stir bar and condenser. Trimethylsilyl chloride (0.94 mL, 7.48 mmol, 2.5 equiv.) was added. This mixture was refluxed for 4 hours. 10 mL of pentanes was added, washed with saturated sodium bicarbonate solution, and dried over MgSO₄. Solvent was removed under reduced pressure, and conversion to the silyl enol ether was confirmed by ¹H NMR. To complete the alkylation, the silyl enol ether was placed under a nitrogen atmosphere and dissolved in 2.0 mL DCM. A suspension of silver trifluoroacetate (0.6978 g, 3.145 mmol, 1.05 equiv.) in 5.0 mL of DCM in a separate three neck round bottom flask equipped with a stir bar and under nitrogen was chilled to 0°C. The silyl enol ether was then added to the silver trifluoroacetate solution and iodomethane (0.20 mL, 3.145 mmol, 1.05 equiv.), and the reaction was stirred for 10 minutes. The mixture was filtered over celite, the solvent was removed under reduced pressure, and the resulting crude product was purified via silica gel column chromatography (10% EtOAc in hexanes) as a yellow solid. (0.0703 g, 22%)

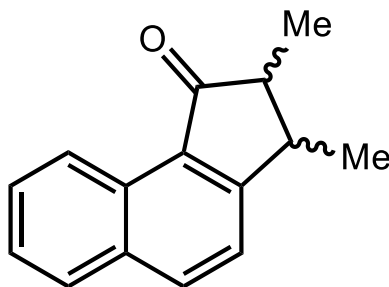
In linear naphthindanone study, 2,3-dihydro-1H-cyclopenta[b]naphthalen-1-one (**S1**) (0.1101 g, 0.60 mmol, 1.0 equiv.) was dissolved in a 2:1 DMF:TEA solution (1.60 mL DMF, 0.80 mL TEA) in a three neck round bottom flask equipped with a stir bar and condenser. Trimethylsilyl chloride (0.15 mL, 1.21 mmol, 2.5 equiv.) was added. This mixture was refluxed for 4 hours. 10 mL of pentanes was added, washed with saturated sodium bicarbonate solution, and dried over MgSO₄. Solvent was removed under reduced pressure, and conversion to the silyl enol ether was confirmed by ¹H NMR. To complete the alkylation, the silyl enol ether was placed under a nitrogen atmosphere and dissolved in 2.0 mL DCM. A suspension of silver trifluoroacetate (0.1408 g, 0.63 mmol, 1.05 equiv.) in 2.0 mL of DCM in a separate three neck round bottom

flask equipped with a stir bar and under nitrogen was chilled to 0°C. The silyl enol ether was then added to the silver trifluoroacetate solution and iodomethane (0.19 mL, 3.021 mmol, 1.05 equiv.), and the reaction was stirred for 72 hours. The mixture was filtered over celite, the solvent was removed under reduced pressure, and the resulting crude product was purified via silica gel column chromatography (10% EtOAc in hexanes) as a yellow solid. (0.0172 g, 6%) Spectroscopic data for **S3** matches those previously reported in literature.^{40,41}



S4 – 2-methyl-3-phenyl-2,3-dihydro-1H-cyclopenta[b]naphthalene

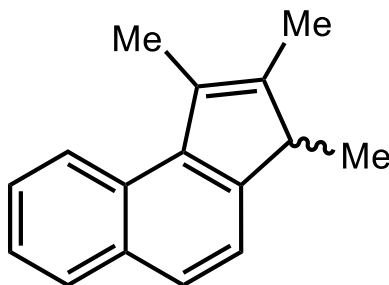
A three neck round bottom flask equipped with a stir bar and a condenser was placed under a nitrogen atmosphere. The 2-methyl-2,3-dihydro-1H-cyclopenta[b]naphthalen-1-one (**S3**) (0.1290 g, 0.65 mmol, 1.0 equiv.) was dissolved in 6.0 mL of THF and the reaction vessel was placed in an ice bath to cool to 0 °C. Once cooled, phenyl magnesium bromide (0.65 mL, 2.0M, 1.3 mmol, 2.0 equiv.) was slowly added to the reaction. Once the addition was complete the ice bath was removed and replaced with a heating block to reflux the reaction for 16 hours. The reaction was cooled to room temperature and placed in an ice bath before carefully quenching with DI H₂O. Concentrated HCl and Et₂O was added to the reaction vessel and stirred for an additional 24 hours at room temperature. The layers of the biphasic solution were separated, and the aqueous layer extracted with Et₂O three times. The combined organic layers were sequentially washed with NaHCO₃, DI H₂O and brine before being dried over MgSO₄. The solvent was removed under reduced pressure and the resulting crude product was purified via silica gel column chromatography (0% EtOAc in hexanes) as a yellow solid. (0.0799 g, 47% yield) **¹H NMR (400 MHz, CDCl₃)** δ 7.88 – 7.77 (m, 3H), 7.61 (s, 1H), 7.58 – 7.49 (m, 4H), 7.48 – 7.40 (m, 3H), 3.61 (t, *J* = 1.1 Hz, 2H), 2.21 (d, *J* = 1.1 Hz, 3H) ppm. **¹³C NMR (101 MHz, CDCl₃)** δ 145.53, 142.60, 140.81, 138.71, 135.54, 133.13, 131.75, 129.35, 128.65, 128.03, 127.78, 127.32, 125.16, 124.68, 121.85, 116.76, 42.46, 15.38 ppm. **HRMS (+APCI)** calculated for C₂₀H₁₇ [M+H]⁺ 257.13302, found 257.13248.



S5 – 2,3-dimethyl-2,3-dihydro-1H-cyclopenta[a]naphthalen-1-one

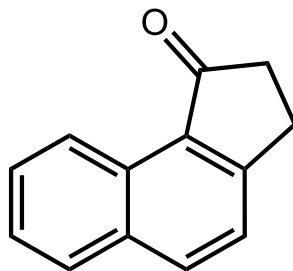
In a three neck round bottom flask equipped with a stir bar and reflux condenser, trans-2,3-dimethylacrylic acid (2.0381 g, 20.357 mmol, 1.0 equiv.) was placed under nitrogen and cooled to 0 °C. Thionyl chloride (2.22 mL, 30.535 mmol, 1.5 equiv.) was then added dropwise, and the mixture was refluxed for 2 hours. The mixture was allowed to cool to room temperature, and excess thionyl chloride was removed under reduced pressure. Formation of the acid chloride was confirmed by ¹H NMR. Then, in a new three neck round bottom flask equipped with a stir bar, naphthalene (2.6091 g, 20.356 mmol, 1.0 equiv.) was placed under nitrogen and dissolved in 40.0 mL of DCM. In an additional three neck round bottom flask equipped with a stir bar and reflux condenser, aluminum trichloride (5.4287 g, 40.713 mmol, 2.0 equiv.) was placed under nitrogen, chilled to 0 °C, and dissolved in 20.0 mL of DCM. The naphthalene solution was added dropwise to the aluminum trichloride. The acid chloride was also chilled to 0 °C, and then added to the aluminum trichloride-naphthalene mixture dropwise. This mixture was allowed to stir for 16 hours at 50°C. After allowing the mixture to cool to room temperature, it was poured over 250 g of ice mixed with 20 mL of concentrated HCl. The organic layer was washed with saturated sodium bicarbonate solution 3x. A crumbly black and brown solid made extraction extremely difficult and did not appear to be soluble in either water or organic solvents. The organic layer was dried over MgSO₄, and solvent was removed under reduced pressure. The resulting crude product was purified as a mixture of diastereomers via silica gel column chromatography (2%

EtOAc in hexanes) as a yellow solid. (0.4124 g, 9%) Spectroscopic data for **S5** resembles those previously reported in literature.⁴⁶



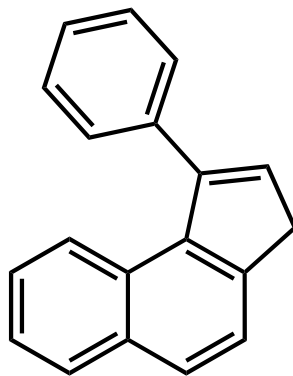
S6 - 1,2,3-trimethyl-3H-cyclopenta[a]naphthalene

A three neck round bottom flask equipped with a stir bar and a condenser was placed under a nitrogen atmosphere. The 2,3-dimethyl-2,3-dihydro-1H-cyclopenta[a]naphthalen-1-one (**S5**) (0.4124 g, 1.96 mmol, 1.0 equiv.) was dissolved in 12.0 mL of THF and the reaction vessel was placed in an ice bath to cool to 0°C. Once cooled, methyl magnesium bromide (1.56 mL, 2.5M, 3.92 mmol, 2.0 equiv.) was slowly added to the reaction. Once the addition was complete the ice bath was removed and replaced with a heating block to reflux the reaction for 16 hours. The reaction was cooled to room temperature and placed in an ice bath before carefully quenching with DI H₂O. Concentrated HCl and Et₂O was added to the reaction vessel and stirred for an additional 24 hours at room temperature. The layers of the biphasic solution were separated, and the aqueous layer extracted with Et₂O three times. The combined organic layers were sequentially washed with NaHCO₃, DI H₂O and brine before being dried over MgSO₄. The solvent was removed under reduced pressure and the resulting crude product was purified via silica gel column chromatography (0% EtOAc in hexanes) as a yellow oil. (0.3456 g, 84% yield) Spectroscopic data for **S6** matches those previously reported in literature.³⁴



S7 - 2,3-dihydro-1H-cyclopenta[a]naphthalen-1-one

A three neck round bottom flask equipped with a stir bar was placed under nitrogen. 5.0 mL of DCM was added to this flask, followed by 3-chloropropionyl chloride (1.48 mL, 18.6651 mmol, 1.2 equiv.). In a separate three neck round bottom flask equipped with a stir bar, aluminum trichloride (2.4888 g, 15.5542 mmol, 1.0 equiv.) was placed under nitrogen. 10.0 mL of DCM and naphthalene (1.9935 g, 15.55 mmol, 1.0 equiv.) were added to this flask and the solution was chilled to 0°C. The 3-chloropropionyl chloride solution was added dropwise, resulting in an orange solution. The reaction was stirred for 16 hours at room temperature. Then, the solution was chilled to 0°C and 40 mL of sulfuric acid was added. The mixture was refluxed for 90 minutes. Next, the mixture was cooled to room temperature and poured over 100 g of ice. The solution was extracted with EtOAc 3x and Et₂O 3x. The organic layers were combined and washed with DI H₂O, saturated sodium bicarbonate solution, and brine. The organic layers were dried over NaSO₄ and filtered, and the solvent was removed under reduced pressure. The resulting crude product was purified via silica gel column chromatography (5% EtOAc in hexanes) as an yellow oil. (0.4092 g, 14 % yield) Spectroscopic data for **S7** matches those previously reported in literature.^{48,49}

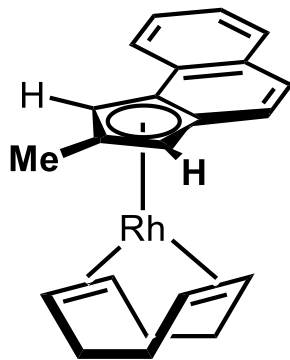


S8 - 1-phenyl-3H-cyclopenta[a]naphthalene

A three neck round bottom flask equipped with a stir bar and a condenser was placed under a nitrogen atmosphere. The 2,3-dihydro-1H-cyclopenta[a]naphthalen-1-one (**S7**) (0.0840 g, 0.39 mmol, 1.0 equiv.) was dissolved 4.0 mL of THF and the reaction vessel was placed in an ice bath to cool to 0 °C. Once cooled, phenyl magnesium bromide (0.53 mL, 1.5M, 0.79 mmol, 2.0 equiv.) was slowly added to the reaction. Once the addition was complete the ice bath was removed and replaced with a heating block to reflux the reaction for 16 hours. The reaction was cooled to room temperature and placed in an ice bath before carefully quenching with DI H₂O. Concentrated HCl and Et₂O was added to the reaction vessel and stirred for an additional 24 hours at room temperature. The layers of the biphasic solution were separated, and the aqueous layer extracted with Et₂O three times. The combined organic layers were sequentially washed with NaHCO₃, DI H₂O and brine before being dried over MgSO₄. The solvent was removed under reduced pressure and the resulting crude product was purified via silica gel column chromatography (0% EtOAc in hexanes). (0.0462 g, 55% yield) Spectroscopic data for **S8** matches those previously reported in literature.³⁸

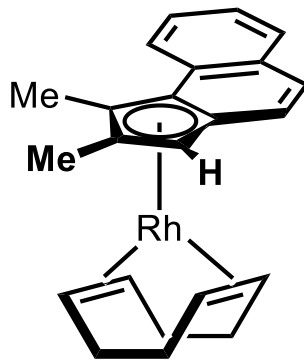
General Procedure A - (±)-1,5-cyclooctadiene(naphthindenyl/indenyl)rhodium(I) Complexes:

In a nitrogen-filled glovebox, naphthindene/indene **X** (1.1 equiv.), [Rh(COD)Cl₂] (0.6 equiv.), and potassium tert-butoxide (1.5 equiv.) were added to an oven-dried 4 mL vial equipped with a magnetic stir bar. A Teflon-septum screw cap was added, and the vial was brought out of the glovebox. THF (2.0 mL) was added to the vial and the reaction stirred at room temperature under a balloon of nitrogen for 16 hours. The reaction was filtered through a pipette containing celite with hexanes and the filtrate was concentrated under reduced pressure. Purification by flash chromatography on basified silica gel with 100% hexanes provided the desired complex, (±)-1,5-cyclooctadiene(naphthindenyl/indenyl)rhodium(I) as a yellow oil that would sometimes solidify.

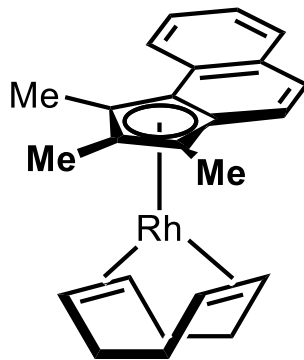


S9 - (±)-1,5-cyclooctadiene(η^5 -2-methyl-3H-cyclopenta[a]naphthalen-1H-yl)rhodium(I)

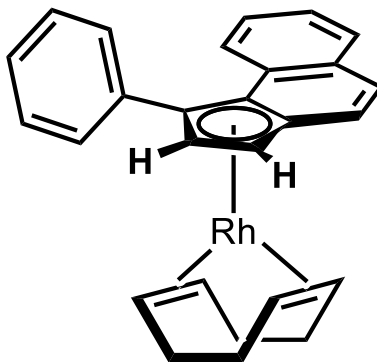
Prepared according to *General Procedure A* using 2-methyl-3H-cyclopenta[a]naphthindene (0.0537 g, 0.29 mmol, 1.1 equiv.), KO^tBu (0.0501 g, 0.45 mmol, 1.5 equiv.), and [Rh(COD)Cl]₂ (0.0881 g, 0.18 mmol, 0.6 equiv.). (0.0609 g, 52%) ¹H NMR (800 MHz, C₆D₆) δ 7.57 (d, J = 7.9 Hz, 1H), 7.55 (d, J = 8.0 Hz, 1H), 7.24 (ddd, J = 8.0, 7.0, 1.2 Hz, 1H), 7.18 (d, J = 8.7 Hz, 1H), 7.15 (ddd, J = 8.0, 7.0, 1.1 Hz, 1H), 7.01 (d, J = 8.7 Hz, 1H), 5.26 (d, J = 1.8 Hz, 1H), 4.79 (d, J = 1.8 Hz, 1H), 2.12 (s, 3H) ppm. ¹³C NMR (201 MHz, C₆D₆) δ 131.01, 129.24, 127.99, 127.68, 124.48, 123.24, 122.88, 119.85, 107.10 (d, J_{Rh-C} = 2.7 Hz), 107.01 (d, J_{Rh-C} = 4.7 Hz), 105.00 (d, J_{Rh-C} = 2.9 Hz), 80.72 (d, J_{Rh-C} = 3.7 Hz), 78.64 (d, J_{Rh-C} = 3.8 Hz), 70.30, 70.23, 67.19, 67.13, 32.26, 31.98, 14.81 ppm. HRMS (+APCI) calculated for C₂₂H₂₄Rh [M+H]⁺ 391.09330, found 391.09276.



S10 - (±)-1,5-cyclooctadiene(η^5 -1,2-dimethyl-3H-cyclopenta[*a*]naphthalen-1H-yl)rhodium(I)
 Prepared according to *General Procedure A* using 1,2-dimethyl-3H-cyclopenta[*a*]naphthindene (0.0330 g, 0.17 mmol, 1.1 equiv.), KO^tBu (0.0291 g, 0.26 mmol, 0.6 equiv.), and [Rh(COD)Cl]₂ (0.0512 g, 0.10 mmol, 0.6 equiv.). (0.0608 g, 87%) ¹H NMR (800 MHz, C₆D₆) δ 8.07 – 8.04 (m, 1H), 7.63 (dd, J = 8.0, 1.4 Hz, 1H), 7.29 (ddd, J = 8.2, 6.9, 1.4 Hz, 1H), 7.21 (d, J = 8.6 Hz, 1H), 7.19 (ddd, J = 8.0, 6.9, 1.2 Hz, 1H), 6.96 (d, J = 8.6 Hz, 1H), 4.77 (s, 1H), 3.37 (dtd, J = 27.8, 7.7, 4.3 Hz, 4H), 2.04 (d, J = 1.1 Hz, 3H), 1.88 (s, 3H), 1.72 – 1.61 (m, 4H), 1.61 – 1.55 (m, 2H), 1.55 – 1.48 (m, 2H) ppm. ¹³C NMR (201 MHz, C₆D₆) δ 131.72, 129.62, 129.31, 126.18, 123.97, 123.74, 123.13, 119.83, 106.76 (d, J_{Rh-C} = 5.0 Hz), 105.74 (d, J_{Rh-C} = 3.0 Hz), 103.34 (d, J_{Rh-C} = 3.1 Hz), 90.88 (d, J_{Rh-C} = 3.7 Hz), 79.38 (d, J_{Rh-C} = 4.3 Hz), 70.91, 70.84, 70.09, 70.02, 32.53, 31.73, 13.04, 12.24 ppm. HRMS (+APCI) calculated for C₂₃H₂₆Rh [M+H]⁺ 405.10895, found 405.10841.



S11 - (±)-1,5-cyclooctadiene(η^5 -1,2,3-trimethyl-3H-cyclopenta[a]naphthalen-1H-yl)rhodium(I)
 Prepared according to *General Procedure A* using 1,2,3-trimethyl-3H-cyclopenta[a]naphthindene (**S6**) (0.0179 g, 0.09 mmol, 1.1 equiv.), KO^tBu (0.0145 g, 0.13 mmol, 1.5 equiv.), and [Rh(COD)Cl]₂ (0.0254 g, 0.05 mmol, 0.6 equiv.). (0.0211 g, 58%) ¹H NMR (800 MHz, C₆D₆) δ 8.18 (dd, $J = 8.3, 1.2$ Hz, 1H), 7.79 (dd, $J = 8.0, 1.4$ Hz, 1H), 7.42 (ddd, $J = 8.2, 6.9, 1.4$ Hz, 1H), 7.39 (dt, $J = 8.7, 0.7$ Hz, 1H), 7.32 (ddd, $J = 8.0, 6.9, 1.2$ Hz, 1H), 7.16 – 7.13 (m, 1H), 3.37 (ddt, $J = 10.7, 7.4, 3.1$ Hz, 2H), 3.05 (td, $J = 7.6, 3.9$ Hz, 2H), 2.09 (d, $J = 1.3$ Hz, 3H), 2.04 (s, 3H), 1.85 (dtd, $J = 18.6, 7.8, 5.5$ Hz, 2H), 1.81 – 1.73 (m, 2H), 1.72 (s, 3H), 1.72 – 1.65 (m, 4H) ppm. ¹³C NMR (201 MHz, C₆D₆) δ 131.74, 129.62, 129.21, 126.14, 123.87, 123.36, 123.23, 118.15, 106.07 (d, $J_{Rh-C} = 5.0$ Hz), 105.79 (d, $J_{Rh-C} = 3.0$ Hz), 101.67 (d, $J_{Rh-C} = 3.4$ Hz), 89.06 (d, $J_{Rh-C} = 4.5$ Hz), 88.31 (d, $J_{Rh-C} = 4.4$ Hz), 73.48, 73.41, 71.22, 71.15, 32.35, 31.96, 12.39, 10.79, 8.53 ppm. HRMS (+APCI) calculated for C₂₄H₂₈Rh [M+H]⁺ 419.12460, found 419.12406.



S12 - (±)-1,5-cyclooctadiene(η^5 -1-phenyl-3H-cyclopenta[a]naphthalen-1H-yl)rhodium(I)

Prepared according to *General Procedure A* using 1-phenyl-3H-cyclopenta[a]naphthindene (**S8**)

(0.0202 g, 0.08 mmol, 1.1 equiv.), KO^tBu (0.014 g, 0.13 mmol, 1.5 equiv.), and $[\text{Rh}(\text{COD})\text{Cl}]_2$

(0.0246 g, 0.05 mmol, 0.6 equiv.). (0.0344, 91%) $^1\text{H NMR}$ (800 MHz, C_6D_6) δ 8.01 (d, $J = 8.2$

Hz, 1H), 7.71 (d, $J = 12.9$ Hz, 2H), 7.70 – 7.67 (m, 1H), 7.34 (d, $J = 8.7$ Hz, 1H), 7.24 (s, 1H),

7.23 (d, $J = 3.2$ Hz, 2H), 7.21 – 7.18 (m, 1H), 7.15 (d, $J = 7.8$ Hz, 1H), 7.09 (ddd, $J = 8.2, 6.9,$

1.4 Hz, 1H), 5.82 (dd, $J = 2.7, 1.2$ Hz, 1H), 4.86 (d, $J = 2.6$ Hz, 1H), 3.85 (tt, $J = 7.4, 3.1$ Hz,

2H), 3.44 (tt, $J = 7.4, 3.1$ Hz, 2H), 1.95 (dddd, $J = 13.8, 10.5, 7.4, 6.1$ Hz, 2H), 1.80 – 1.73 (m,

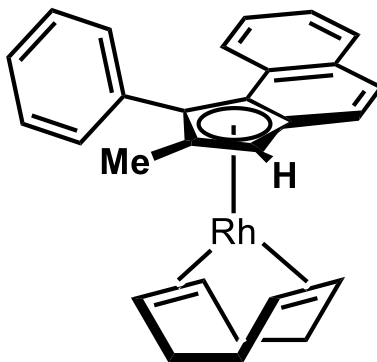
2H), 1.72 – 1.66 (m, 2H), 1.61 (dtd, $J = 13.5, 6.8, 4.0$ Hz, 2H) ppm. $^{13}\text{C NMR}$ (201 MHz, C_6D_6)

δ 137.38, 132.21, 130.55, 129.36, 128.55, 127.94, 127.40, 125.83, 124.78, 124.54, 124.04,

120.54, 108.36 (d, $J_{\text{Rh-C}} = 2.9$ Hz), 102.51 (d, $J_{\text{Rh-C}} = 3.7$ Hz), 101.02 (d, $J_{\text{Rh-C}} = 2.7$ Hz), 94.74

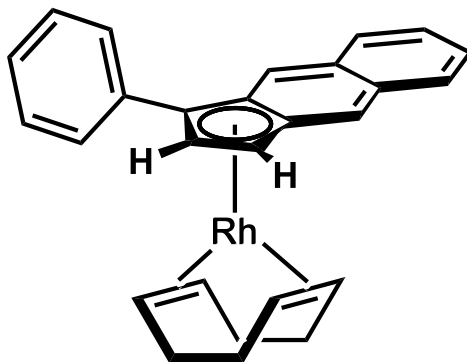
(d, $J_{\text{Rh-C}} = 3.7$ Hz), 77.24 (d, $J_{\text{Rh-C}} = 4.3$ Hz), 71.36, 71.29, 70.39, 70.32, 32.12, 32.02 ppm.

HRMS (+APCI) calculated for $\text{C}_{27}\text{H}_{26}\text{Rh}$ $[\text{M}+\text{H}]^+$ 453.10895, found 453.10841.



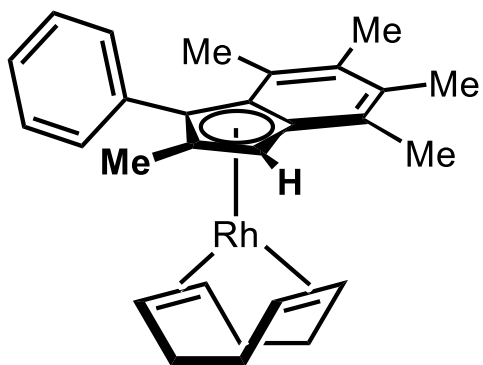
S13 - (±)-1,5-cyclooctadiene(η^5 -2-methyl-1-phenyl-3H-cyclopenta[a]naphthalen-1H-yl)rhodium(I)

Prepared according to *General Procedure A* using 2-methyl-1-phenyl-3H-cyclopenta[a]naphthindene (0.0260 g, 0.10 mmol, 1.1 equiv.), KO^tBu (0.0170 g, 0.15 mmol, 1.5 equiv.), and $[\text{Rh}(\text{COD})\text{Cl}]_2$ (0.0300 g, 0.06 mmol, 0.6 equiv.). (0.0417 g, 88%) **^1H NMR (800 MHz, C_6D_6)** δ 8.11 (dt, $J = 7.6, 1.7$ Hz, 1H), 7.68 (dd, $J = 8.2, 1.1$ Hz, 1H), 7.61 (dd, $J = 7.9, 1.3$ Hz, 1H), 7.43 (td, $J = 7.5, 1.5$ Hz, 1H), 7.31 (d, $J = 6.0$ Hz, 1H), 7.30 (d, $J = 7.2$ Hz, 1H), 7.22 (d, $J = 8.5$ Hz, 1H), 7.22 – 7.19 (m, 1H), 7.18 – 7.16 (m, 1H), 7.13 (ddd, $J = 8.0, 6.9, 1.2$ Hz, 1H), 7.00 (ddd, $J = 8.3, 6.9, 1.4$ Hz, 1H), 4.90 (s, 1H), 3.88 (tt, $J = 8.2, 3.2$ Hz, 2H), 3.04 (tt, $J = 7.9, 3.1$ Hz, 2H), 2.06 (dddd, $J = 13.0, 10.2, 7.5, 5.4$ Hz, 2H), 1.94 (s, 3H), 1.93 – 1.87 (m, 2H), 1.77 – 1.62 (m, 2H) ppm. **^{13}C NMR (201 MHz, C_6D_6)** δ 136.56, 132.54, 132.50, 131.99, 129.13, 128.69, 128.63, 128.61, 127.47, 125.73, 124.81, 124.38, 122.77, 120.94, 106.48 (d, $J_{\text{Rh-C}} = 3.7$ Hz), 105.05 (d, $J_{\text{Rh-C}} = 3.0$ Hz), 103.87 (d, $J_{\text{Rh-C}} = 4.2$ Hz), 99.70 (d, $J_{\text{Rh-C}} = 3.0$ Hz), 79.57 (d, $J_{\text{Rh-C}} = 4.4$ Hz), 73.30, 73.23, 68.75, 68.68, 32.34, 12.54 ppm. **HRMS (+APCI)** calculated for $\text{C}_{27}\text{H}_{26}\text{Rh}$ $[\text{M}+\text{H}]^+$ 467.12460, found 467.12406.



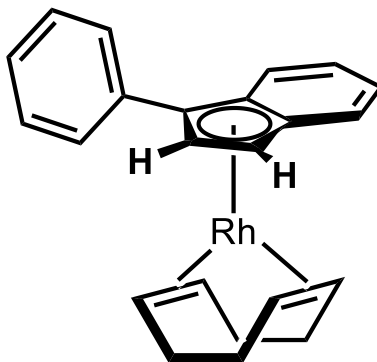
S14 - (±)-1,5-cyclooctadiene(η^5 -3-phenyl-1H-cyclopenta[b]naphthalen-1H-yl)rhodium(I)

Prepared according to *General Procedure A* using 3-phenyl-1H-cyclopenta[b]naphthindene (**S2**) (0.0201 g, 0.08 mmol, 1.1 equiv.), KO^tBu (0.0140 g, 0.12 mmol, 1.5 equiv.), and $[\text{Rh}(\text{COD})\text{Cl}]_2$ (0.0245 g, 0.05 mmol, 0.6 equiv.). (0.0256 g, 76%) $^1\text{H NMR}$ (800 MHz, C_6D_6) δ 8.14 (s, 1H), 7.85 – 7.81 (m, 1H), 7.80 – 7.77 (m, 1H), 7.69 – 7.63 (m, 2H), 7.58 (s, 1H), 7.32 – 7.27 (m, 2H), 7.22 (dddd, $J = 19.0, 7.9, 6.5, 1.4$ Hz, 2H), 7.14 (dt, $J = 7.4, 1.3$ Hz, 1H), 6.54 (t, $J = 2.4$ Hz, 1H), 5.02 (dd, $J = 2.8, 0.7$ Hz, 1H), 4.05 (s, 2H), 3.68 (t, $J = 7.5$ Hz, 2H), 1.69 – 1.49 (m, 8H) ppm. $^{13}\text{C NMR}$ (201 MHz, C_6D_6) δ 136.86, 131.83, 131.51, 129.19, 128.67, 128.26, 127.69, 126.66, 124.18, 124.15, 117.95 (d, $J_{\text{Rh-C}} = 2.2$ Hz), 116.44, 116.00, 114.59, 97.07 (d, $J_{\text{Rh-C}} = 5.7$ Hz), 92.01 (d, $J_{\text{Rh-C}} = 4.0$ Hz), 75.72, 72.75 (d, $J_{\text{Rh-C}} = 5.0$ Hz), 71.52, 31.62, 31.36 ppm. **HRMS** (+APCI) calculated for $\text{C}_{27}\text{H}_{26}\text{Rh}$ $[\text{M}+\text{H}]^+$ 453.10895, found 453.10841.



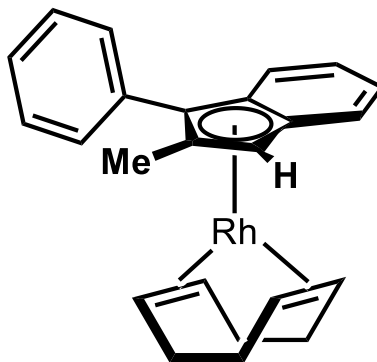
S15 - (±)-1,5-cyclooctadiene(η^5 -2,4,5,6,7-pentamethyl-3-phenylinden-1H-yl)rhodium(I)

Prepared according to *General Procedure A* using 2,4,5,6,7-pentamethyl-3-phenylindene (0.0412 g, 0.16 mmol, 1.1 equiv.), KO^tBu (0.0264 g, 0.24 mmol, 1.5 equiv.), and $[\text{Rh}(\text{COD})\text{Cl}]_2$ (0.0490 g, 0.09 mmol, 0.6 equiv.). (0.0632 g, 85%) Spectroscopic data for **S15** matches those previously reported in literature.²⁵



S16 - (±)-1,5-cyclooctadiene(η^5 -3-phenylinden-1H-yl)rhodium(I)

Prepared according to *General Procedure A* using 3-phenylindene (0.015 g, 0.08 mmol, 1.1 equiv.), KO^tBu (0.0131 g, 0.12 mmol, 1.5 equiv.), and [Rh(COD)Cl]₂ (0.0231 g, 0.05 mmol, 0.6 equiv.). (0.0245 g, 78%) **¹H NMR (800 MHz, C₆D₆)** δ 7.62 – 7.58 (m, 1H), 7.51 (dq, J = 8.0, 1.4 Hz, 2H), 7.24 – 7.17 (m, 3H), 7.13 – 7.07 (m, 3H), 6.26 (dd, J = 2.8, 1.8 Hz, 1H), 4.83 (dt, J = 2.6, 1.3 Hz, 1H), 3.91 (tt, J = 7.1, 3.1 Hz, 2H), 3.55 (dq, J = 6.9, 3.4 Hz, 2H), 1.89 – 1.80 (m, 4H), 1.70 – 1.59 (m, 4H) ppm. **¹³C NMR (201 MHz, C₆D₆)** δ 136.42, 129.03, 127.73, 126.61, 123.54, 123.01, 120.47, 118.70, 114.18 (d, J_{Rh-C} = 2.2 Hz), 111.76 (d, J_{Rh-C} = 1.5 Hz), 94.92 (d, J_{Rh-C} = 3.8 Hz), 92.63 (d, J_{Rh-C} = 5.1 Hz), 75.12 (d, J_{Rh-C} = 4.7 Hz), 72.84, 72.77, 68.79, 68.73, 31.80, 31.61. **HRMS** (+APCI) calculated for C₂₃H₂₄Rh [M+H]⁺ 403.09330, found 403.09276.

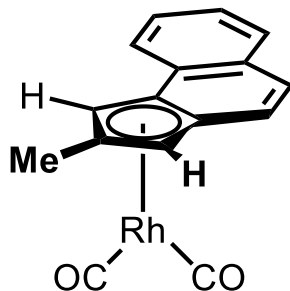


S17 - (\pm)-1,5-cyclooctadiene(η^5 -2-methyl-3-phenylinden-1H-yl)rhodium(I)

Prepared according to *General Procedure A* using 2-methyl-3-phenylindene (0.015 g, 0.07 mmol, 1.1 equiv.), KO^tBu (0.0122 g, 0.11 mmol, 1.5 equiv.), and $[\text{Rh}(\text{COD})\text{Cl}]_2$ (0.0215 g, 0.04 mmol, 0.6 equiv.). (0.0225 g, 74%) Spectroscopic data for **S17** matches those previously reported in literature.²³

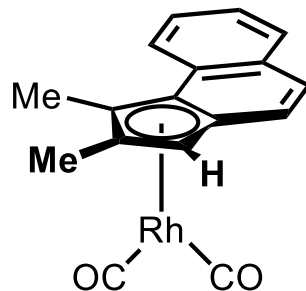
General Procedure B - (\pm)-dicarbonyl(naphthindenyl/indenyl)rhodium(I) Complexes:

A 20 mL scintillation vial containing (\pm)-1,5-cyclooctadiene(naphthindenyl/indenyl)rhodium(I) complex (1.0 equiv.) was placed under a nitrogen atmosphere. Then, 4.0 mL of hexanes was used to transfer the (\pm)-1,5-cyclooctadiene(naphthindenyl/indenyl)rhodium(I) complex to an oven-dried 7.0 mL vial equipped with a stir bar under a nitrogen atmosphere. Three sparges using carbon monoxide were performed before allowing the reaction to run for 48 hours under a balloon of carbon monoxide. Purification by flash chromatography on alumina with 100% hexanes provided the desired complex, (\pm)-dicarbonyl(naphthindenyl/indenyl)rhodium(I) as a yellow oil that became brown following drying.



S18 - (±)-dicarbonyl(η^5 -2-methyl-3H-cyclopenta[a]naphthalen-1H-yl)rhodium(I)

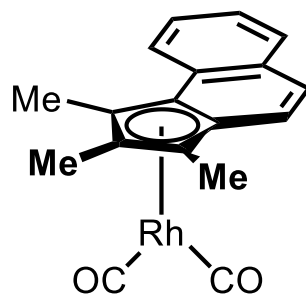
Prepared according to *General Procedure B* using **S9** (0.0270 g, 0.08 mmol, 1.0 equiv.). (0.0218 g, 93%) $^1\text{H NMR}$ (600 MHz, C_6D_6) δ 7.76 (ddt, $J = 8.1, 1.4, 0.7$ Hz, 1H), 7.54 (ddd, $J = 8.0, 1.3, 0.6$ Hz, 1H), 7.31 (ddd, $J = 8.2, 7.0, 1.3$ Hz, 1H), 7.26 – 7.20 (m, 2H), 6.93 (dd, $J = 8.7, 0.8$ Hz, 1H), 5.70 (d, $J = 1.9$ Hz, 1H), 5.19 – 5.16 (m, 1H), 1.94 (d, $J = 1.9$ Hz, 3H) ppm. $^{13}\text{C NMR}$ (151 MHz, C_6D_6) δ 191.42, 190.86, 131.50, 129.35, 127.00, 125.81, 125.60, 125.51, 122.94, 118.03, 114.15 (d, $J = 6.0$ Hz), 111.73 (d, $J = 2.8$ Hz), 110.25 (d, $J = 2.6$ Hz), 78.38 (d, $J = 3.4$ Hz), 76.07 (d, $J = 3.4$ Hz), 15.48. **HRMS** (+APCI) calculated for $\text{C}_{16}\text{H}_{12}\text{O}_2\text{Rh}$ $[\text{M}+\text{H}]^+$ 338.98923, found 338.98869.



S19 - (±)-dicarbonyl(η^5 -1,2-dimethyl-3H-cyclopenta[a]naphthalen-1H-yl)rhodium(I)

Prepared according to *General Procedure B* using **S10** (0.0303 g, 0.09 mmol, 1.0 equiv.).

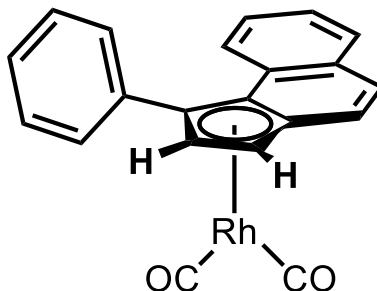
(0.0264 g, 87%) $^1\text{H NMR}$ (600 MHz, C_6D_6) δ 8.35 – 8.30 (m, 1H), 7.60 (ddt, $J = 8.1, 1.3, 0.6$ Hz, 1H), 7.34 (ddd, $J = 8.3, 6.9, 1.4$ Hz, 1H), 7.28 – 7.20 (m, 2H), 6.92 (d, $J = 8.6$ Hz, 1H), 5.08 (s, 1H), 2.31 (s, 3H), 1.90 (dd, $J = 1.9, 0.5$ Hz, 3H) ppm. $^{13}\text{C NMR}$ (151 MHz, C_6D_6) δ 192.15, 191.59, 132.23, 129.80, 127.60, 126.89, 125.96, 125.06, 123.17, 118.18, 113.51 (d, $J = 6.0$ Hz), 109.72 (d, $J = 2.8$ Hz), 109.24 (d, $J = 2.7$ Hz), 94.28 (d, $J = 3.1$ Hz), 75.86 (d, $J = 3.8$ Hz), 14.43, 13.66 ppm. **HRMS** (+APCI) calculated for $\text{C}_{17}\text{H}_{14}\text{O}_2\text{Rh}$ $[\text{M}+\text{H}]^+$ 353.00488, found 353.00434.



S20 - (±)-dicarbonyl(η^5 -1,2,3-trimethyl-3H-cyclopenta[a]naphthalen-1H-yl)rhodium(I)

Prepared according to *General Procedure B* using **S11** (0.0102 g, 0.03 mmol, 1.0 equiv.).

(significant amounts of unreacted starting material present, so yield not found; product is presumed to be present due to the presence of additional ^1H NMR peaks that do not align with the starting material)

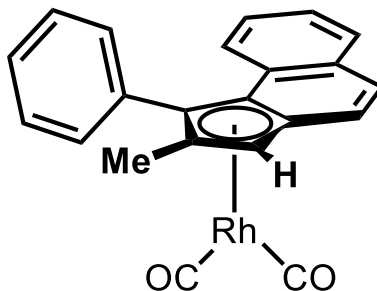


S21 - (±)-dicarbonyl(η^5 -1-phenyl-3H-cyclopenta[a]naphthalen-1H-yl)rhodium(I)

Prepared according to *General Procedure B* using **S12** (0.0148 g, 0.04 mmol, 1.0 equiv.).

(0.0125 g, 95%) $^1\text{H NMR}$ (600 MHz, C_6D_6) δ 7.98 (ddt, $J = 8.4, 1.4, 0.8$ Hz, 1H), 7.93 – 7.27 (m, 3H), 7.29 – 7.22 (m, 1H), 7.15 – 7.07 (m, 4H), 7.02 – 6.93 (m, 2H), 5.74 (dd, $J = 2.8, 2.0$ Hz, 1H), 5.15 (d, $J = 2.9$ Hz, 1H) ppm. $^{13}\text{C NMR}$ (151 MHz, C_6D_6) δ 191.20, 190.63, 135.61, 132.55, 131.85, 129.54, 128.65, 128.48, 126.77, 126.69, 125.75, 124.14, 118.50, 112.27 (d, $J = 2.6$ Hz), 108.35, 105.53 (d, $J = 3.7$ Hz), 98.68 (dd, $J = 5.3, 1.9$ Hz), 74.12 (d, $J = 3.7$ Hz).

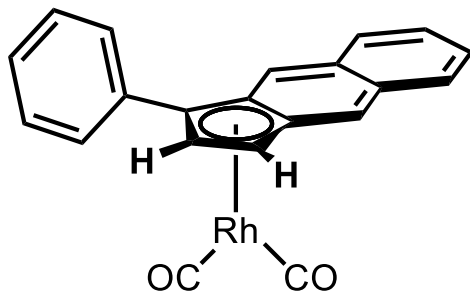
HRMS (+APCI) calculated for $\text{C}_{21}\text{H}_{14}\text{O}_2\text{Rh}$ $[\text{M}+\text{H}]^+$ 401.00488, found 401.00434.



S22 - (±)-dicarbonyl(η^5 -2-methyl-1-phenyl-3H-cyclopenta[a]naphthalen-1H-yl)rhodium(I)

Prepared according to *General Procedure B* using **S13** (0.0195 g, 0.05 mmol, 1.0 equiv.).

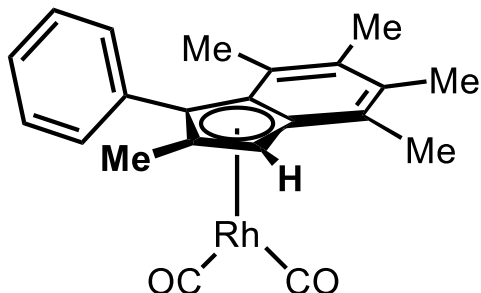
(0.0153 g, 88%) **$^1\text{H NMR}$ (600 MHz, C_6D_6)** δ 7.98 – 7.94 (m, 1H), 7.78 (dq, $J = 8.4, 0.9$ Hz, 1H), 7.60 – 7.53 (m, 1H), 7.33 – 7.24 (m, 2H), 7.18 – 7.10 (m, 4H), 7.06 (d, $J = 8.7$ Hz, 1H), 6.99 (ddd, $J = 8.4, 6.9, 1.4$ Hz, 1H), 5.20 – 5.16 (m, 1H), 1.86 (d, $J = 1.8$ Hz, 3H) ppm. **$^{13}\text{C NMR}$ (151 MHz, C_6D_6)** δ 191.68, 191.11, 134.77, 134.25, 132.45, 131.01, 129.52, 129.31, 128.70, 128.40, 126.65, 126.56, 125.88, 125.43, 123.82, 118.11, 114.59 (d, $J = 5.6$ Hz), 110.57 (d, $J = 2.8$ Hz), 108.52 (d, $J = 2.5$ Hz), 105.27 (d, $J = 3.5$ Hz), 75.21 (d, $J = 3.7$ Hz), 13.80 ppm. **HRMS** (+APCI) calculated for $\text{C}_{22}\text{H}_{16}\text{O}_2\text{Rh}$ $[\text{M}+\text{H}]^+$ 415.02053, found 415.01999.



S23 - (±)-dicarbonyl(η^5 -3-phenyl-1H-cyclopenta[b]naphthalen-1H-yl)rhodium(I)

Prepared according to *General Procedure B* using **S14** (0.0076 g, 0.01 mmol, 1.0 equiv.).

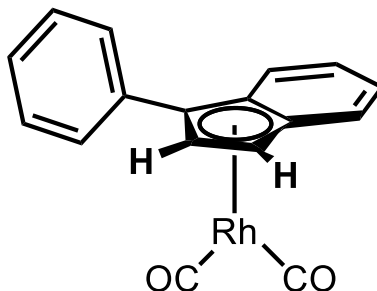
(significant amounts of impurities detected, so yield not found; ^1H shows a set of peaks that integrate 1:1 and another set that integrate 1:2, which we hypothesize to be the ligand **S2**)



S24 - (±)-dicarbonyl(η^5 -2,4,5,6,7-pentamethyl-3-phenylinden-1H-yl)rhodium(I)

Prepared according to *General Procedure B* using **S15** (0.0153 g, 0.04 mmol, 1.0 equiv.).

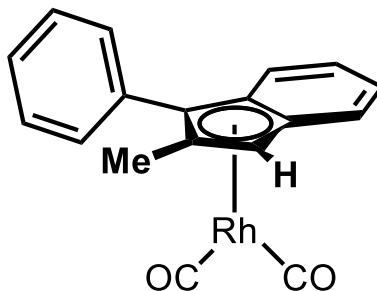
(0.0125 g, 92%) $^1\text{H NMR}$ (600 MHz, C_6D_6) δ 7.90 (dq, $J = 7.6, 1.3$ Hz, 1H), 7.21 (dddd, $J = 7.7, 5.1, 3.3, 1.6$ Hz, 1H), 7.14 – 7.09 (m, 3H), 5.30 (s, 1H), 2.15 (s, 3H), 1.96 (s, 3H), 1.90 (s, 3H), 1.89 (s, 3H), 1.82 (d, $J = 2.1$ Hz, 3H) ppm. $^{13}\text{C NMR}$ (151 MHz, C_6D_6) δ 192.40, 191.83, 135.95, 133.96, 133.25, 131.85, 131.00, 128.89, 123.72, 122.04, 115.31 (d, $J = 2.2$ Hz), 115.10 (d, $J = 6.2$ Hz), 114.87, 104.01 (d, $J = 3.9$ Hz), 72.61 (d, $J = 3.5$ Hz), 30.23, 16.88, 16.33 (d, $J = 5.3$ Hz), 15.49, 14.40 ppm. **HRMS** (+APCI) calculated for $\text{C}_{22}\text{H}_{22}\text{O}_2\text{Rh}$ $[\text{M}+\text{H}]^+$ 421.06748, mass to be taken.



S25 - (±)-dicarbonyl(η^5 -3-phenylinden-1H-yl)rhodium(I)

Prepared according to *General Procedure B* using **S16** (0.0101 g, 0.02 mmol, 1.0 equiv.).

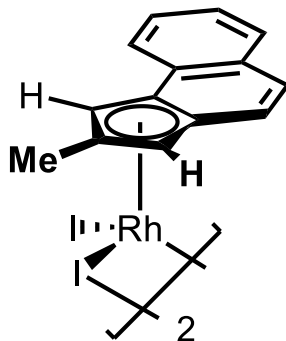
(0.0070 g, 79%) $^1\text{H NMR}$ (600 MHz, C_6D_6) δ 7.61 – 7.57 (m, 2H), 7.43 – 7.38 (m, 1H), 7.15 – 7.12 (m, 2H), 7.10 – 7.07 (m, 1H), 6.99 – 6.92 (m, 3H), 5.95 (dd, $J = 2.9, 2.4$ Hz, 1H), 5.17 (dd, $J = 2.9, 0.8$ Hz, 1H) ppm. $^{13}\text{C NMR}$ (151 MHz, C_6D_6) δ 190.77, 190.20, 134.60 (d, $J = 6.2$ Hz), 129.55, 129.47, 128.90, 125.54, 125.32, 119.54, 118.22, 117.49 (d, $J = 2.4$ Hz), 116.77, 99.92 (d, $J = 3.3$ Hz), 98.09 (d, $J = 6.1$ Hz), 72.34 (d, $J = 4.0$ Hz) ppm. **HRMS** (+APCI) calculated for $\text{C}_{17}\text{H}_{12}\text{O}_2\text{Rh}$ $[\text{M}+\text{H}]^+$ 350.98923, found 350.98869.



S26 - (±)-dicarbonyl(η^5 -2-methyl-3-phenylinden-1H-yl)rhodium(I)

Prepared according to *General Procedure B* using **S17** (0.0289 g, 0.08 mmol, 1.0 equiv.).

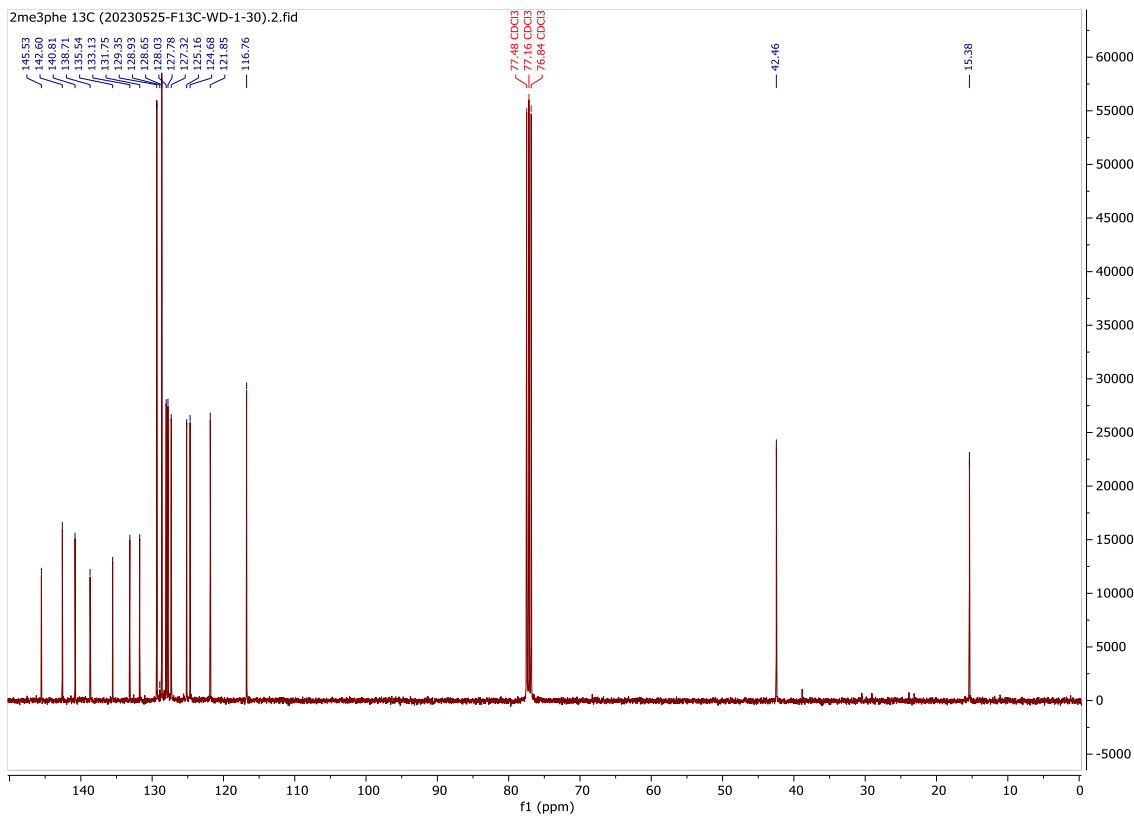
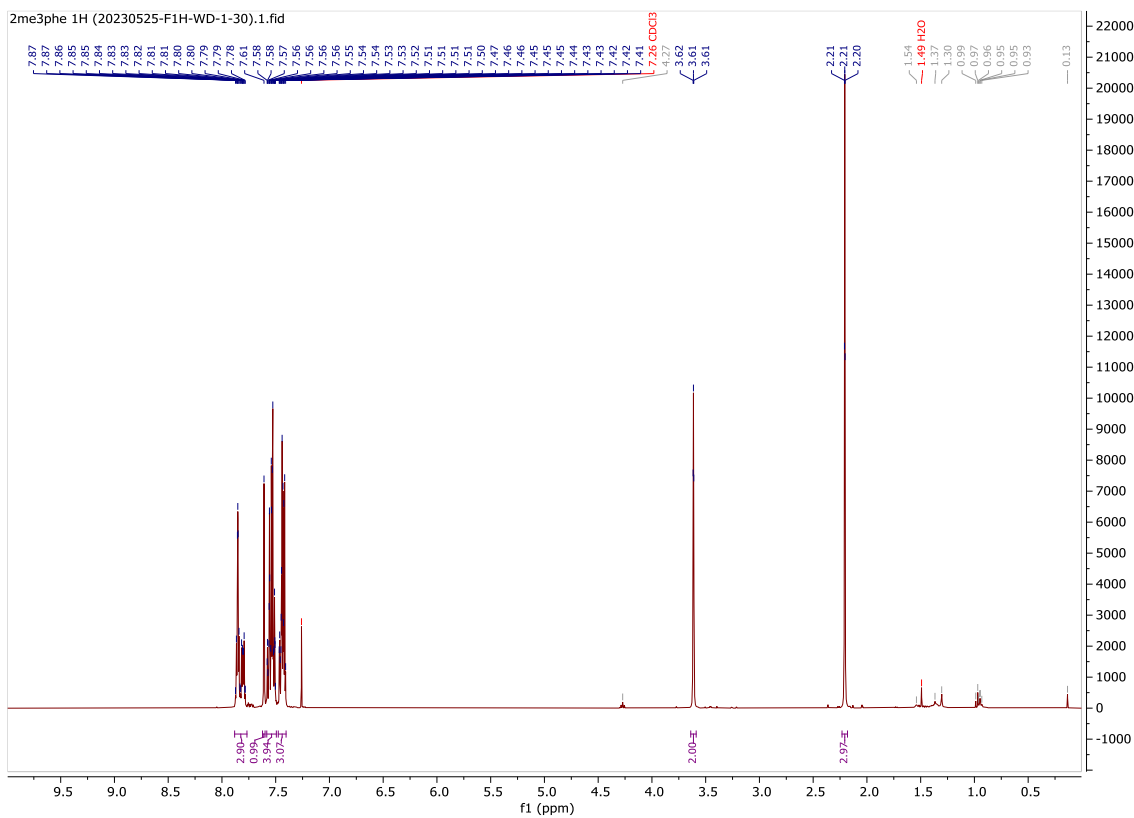
(0.0179 g, 70%) $^1\text{H NMR}$ (600 MHz, C_6D_6) δ 7.59 – 7.51 (m, 2H), 7.19 – 7.17 (m, 2H), 7.14 (t, $J = 0.9$ Hz, 1H), 7.13 – 7.07 (m, 1H), 6.95 (dd, $J = 3.6, 1.2$ Hz, 2H), 6.92 (ddd, $J = 8.1, 4.8, 3.4$ Hz, 1H), 5.11 (s, 1H), 1.95 (d, $J = 2.3$ Hz, 3H) ppm. $^{13}\text{C NMR}$ (151 MHz, C_6D_6) δ 191.24, 190.67, 133.45, 131.35, 128.81, 128.11, 125.10, 124.90, 118.61, 118.37 (d, $J = 2.0$ Hz), 117.74, 116.10 (d, $J = 2.2$ Hz), 115.86 (d, $J = 6.6$ Hz), 100.43 (d, $J = 3.5$ Hz), 73.34 (d, $J = 3.8$ Hz), 14.55. **HRMS** (+APCI) calculated for $\text{C}_{18}\text{H}_{14}\text{O}_2\text{Rh}$ $[\text{M}+\text{H}]^+$ 365.00488, found 365.00434.



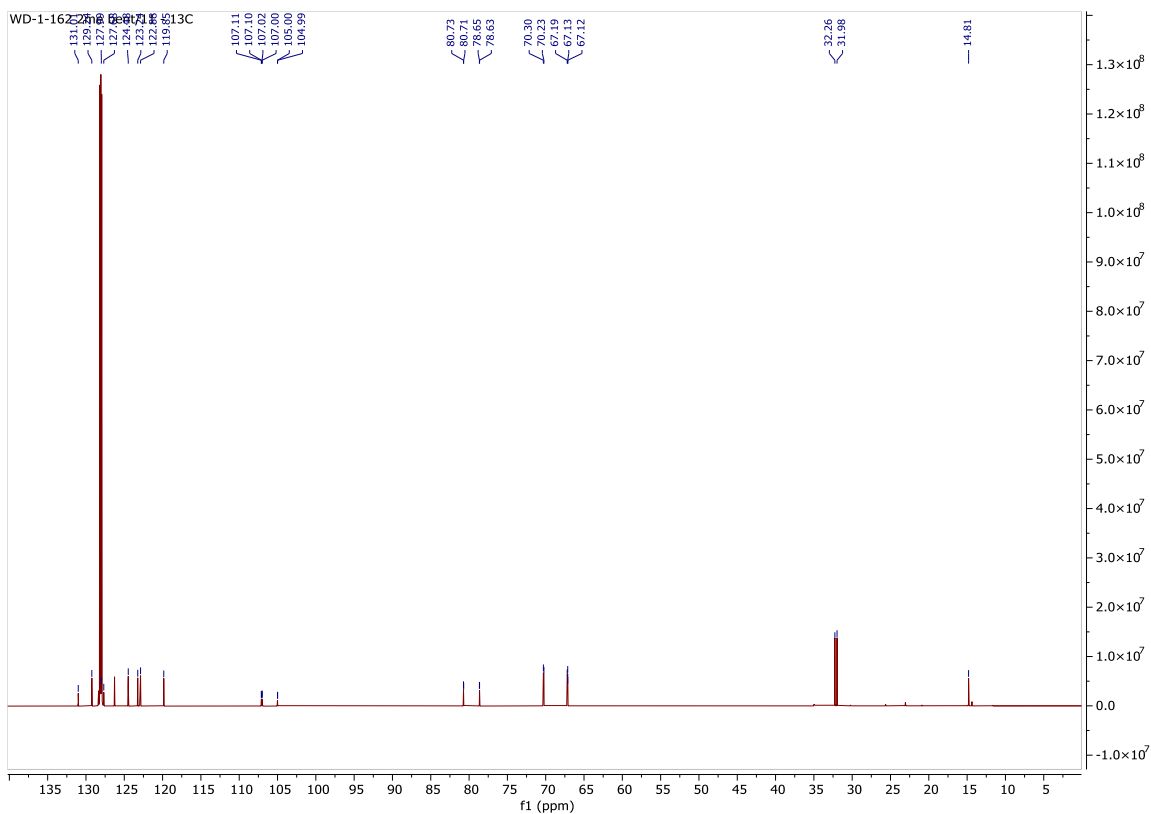
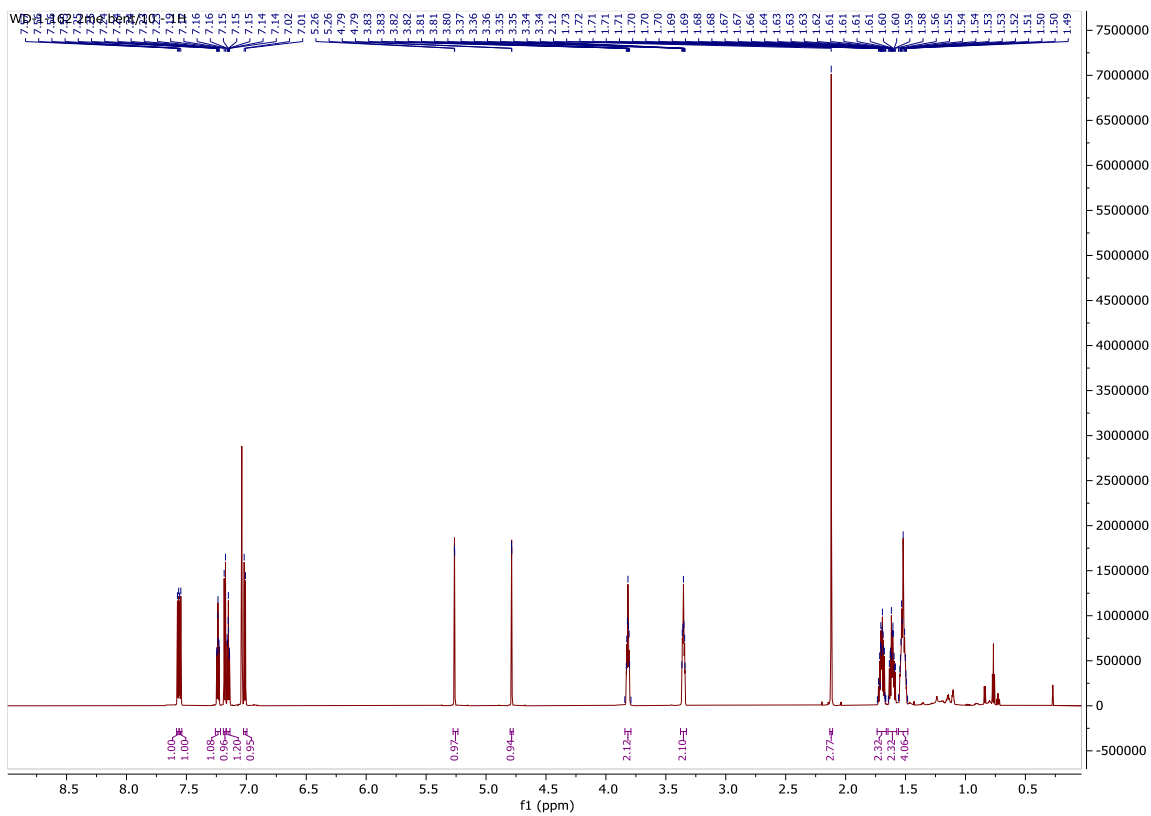
S27 - (±)-(η⁵-2-methyl-3H-cyclopenta[a]naphthalen-1H-yl)rhodium(III) diiodide dimer

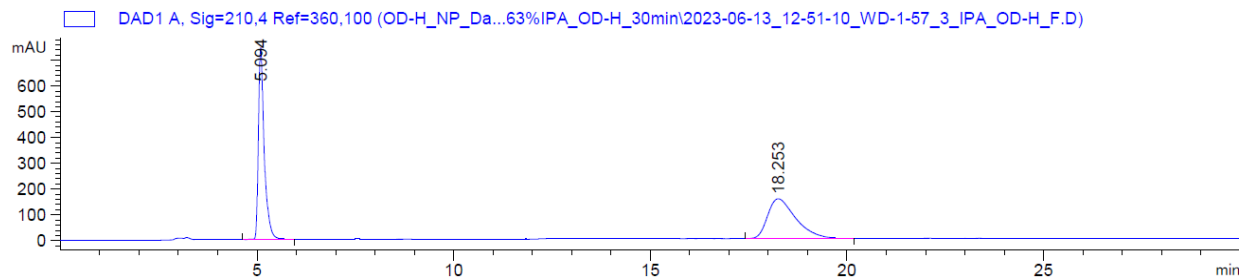
With no precautions against air or moisture exposure, I₂ crystals (0.1028 g, 0.38 mmol, 5.0 equiv.) were added to a 20 mL scintillation vial containing **S9** (0.0591 g, 0.15 mmol, 2.0 equiv.), 5.0 mL of Et₂O, and a stir bar. The vial was capped to prevent solvent evaporation and the black solution was stirred for 24 hours. The reaction was filtered through a Büchner funnel and washed with Et₂O (until the filtrate was clear). Purification by *non-flash* chromatography on silica using a 99:1 DCM:MeOH solvent system provided the desired complex, (±)-(η⁵-2-methyl-3H-cyclopenta[a]naphthalen-1H-yl)rhodium(III) diiodide dimer. No impurities were visible by TLC (imaged by light, iodine stain, and KMNO₄), but a bright pink band traveled down the column prior to the black, product band. (0.0764 g, 94% yield) ¹H NMR (600 MHz, DMSO) δ 8.26 – 8.21 (m, 2H), 7.97 (dd, *J* = 7.5, 1.6 Hz, 2H), 7.91 (d, *J* = 9.1 Hz, 2H), 7.78 – 7.70 (m, 4H), 7.36 (dd, *J* = 9.1, 0.7 Hz, 2H), 6.72 – 6.69 (m, 2H), 6.24 (d, *J* = 1.4 Hz, 2H), 2.40 (s, 6H) ppm. ¹³C NMR (151 MHz, DMSO) δ 135.54, 134.25, 130.34, 130.29, 128.85, 128.22, 127.13, 121.76, 111.89 (d, *J* = 6.1 Hz), 104.09 (d, *J* = 4.8 Hz), 103.12 (d, *J* = 4.9 Hz), 79.88 (d, *J* = 6.1 Hz), 78.04 (d, *J* = 6.3 Hz), 15.61 ppm. HRMS (+APCI) calculated for C₂₈H₂₃I₄Rh₂ [M+H]⁺ 1072.60888, mass to be taken.

S4



S9



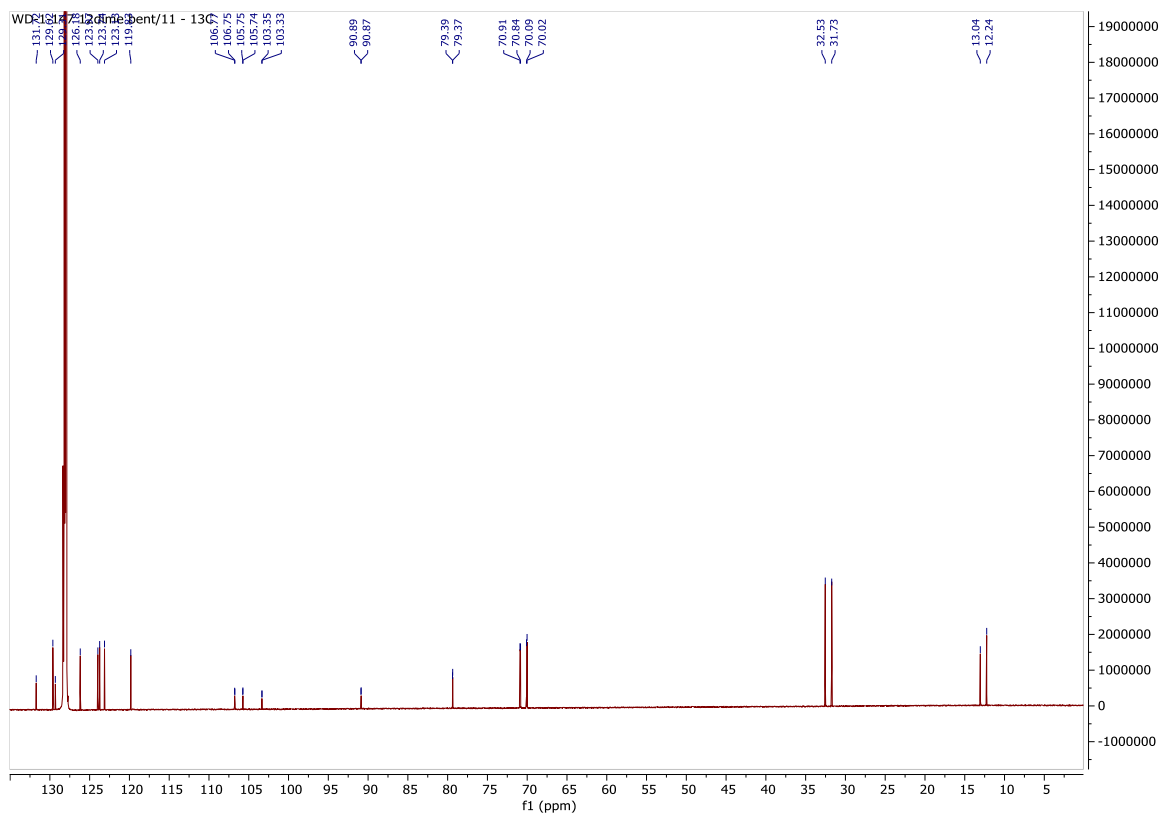
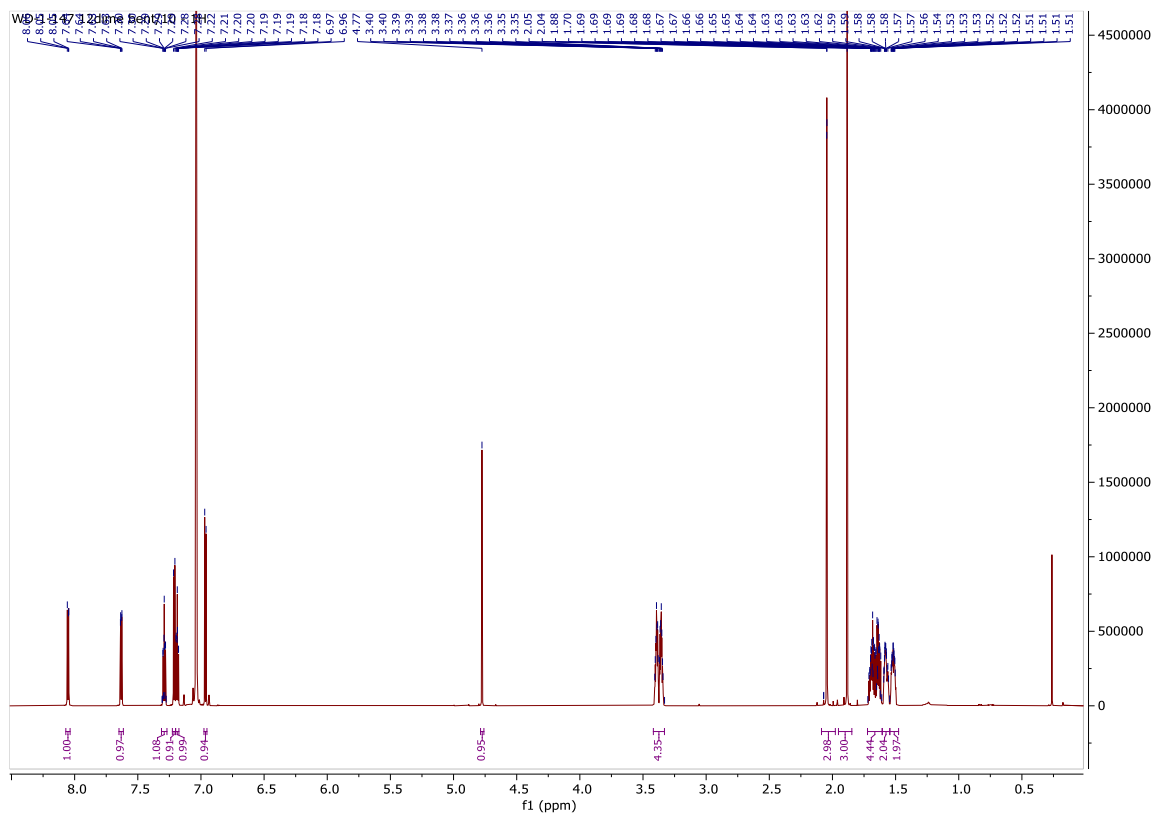


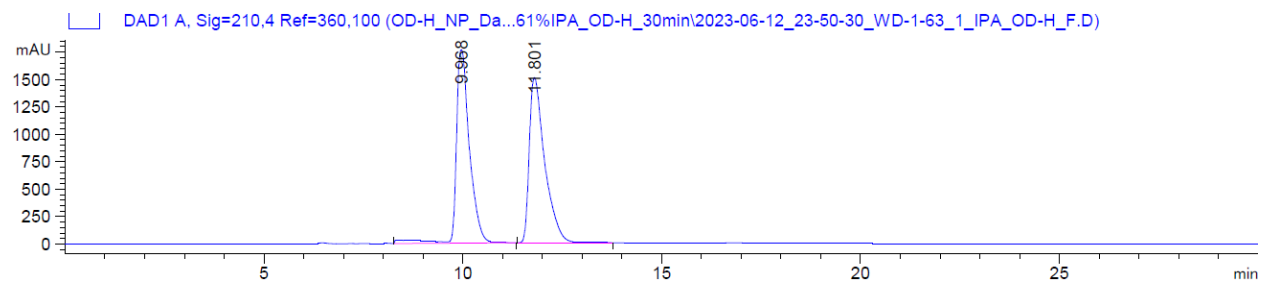
Signal 1: DAD1 A, Sig=210,4 Ref=360,100

Peak #	RetTime [min]	Type	Width [min]	Area [mAU*s]	Height [mAU]	Area %
1	5.094	VV R	0.1515	7715.59912	744.95117	50.1472
2	18.253	BV R	0.5813	7670.29053	154.21671	49.8528

Totals : 1.53859e4 899.16788

S10



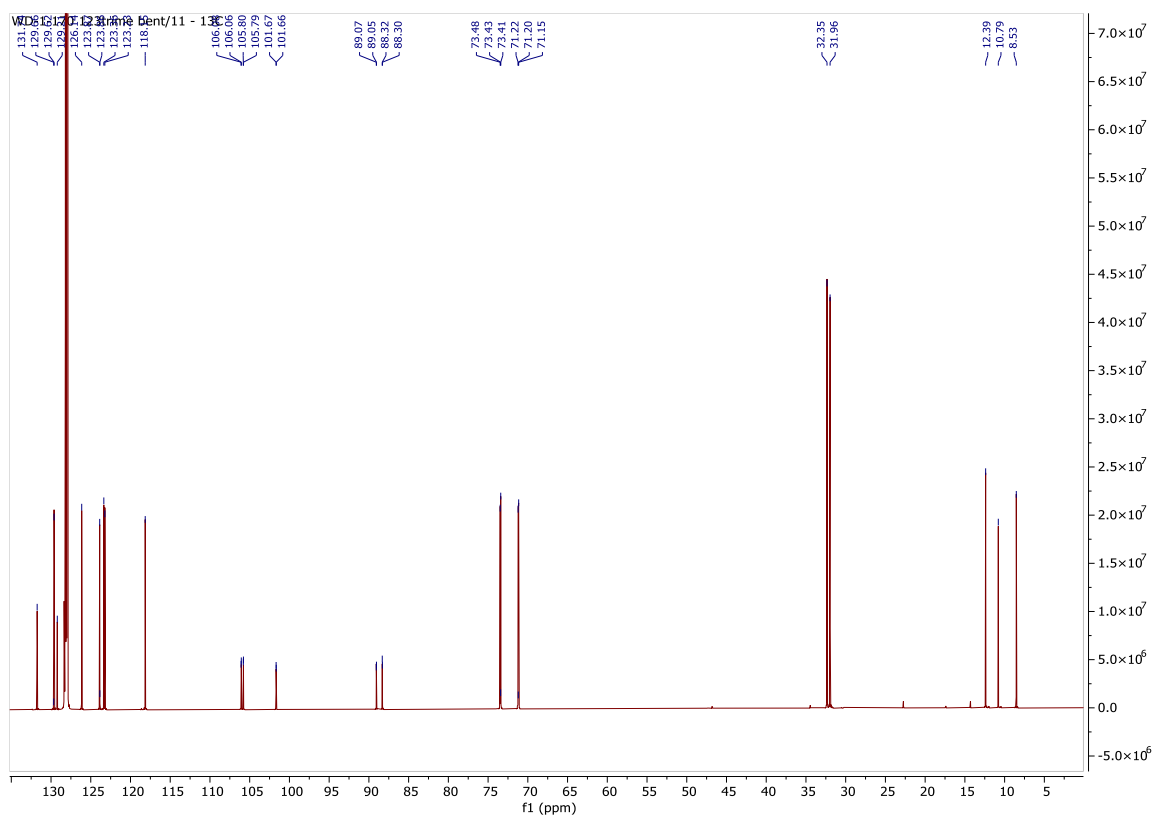
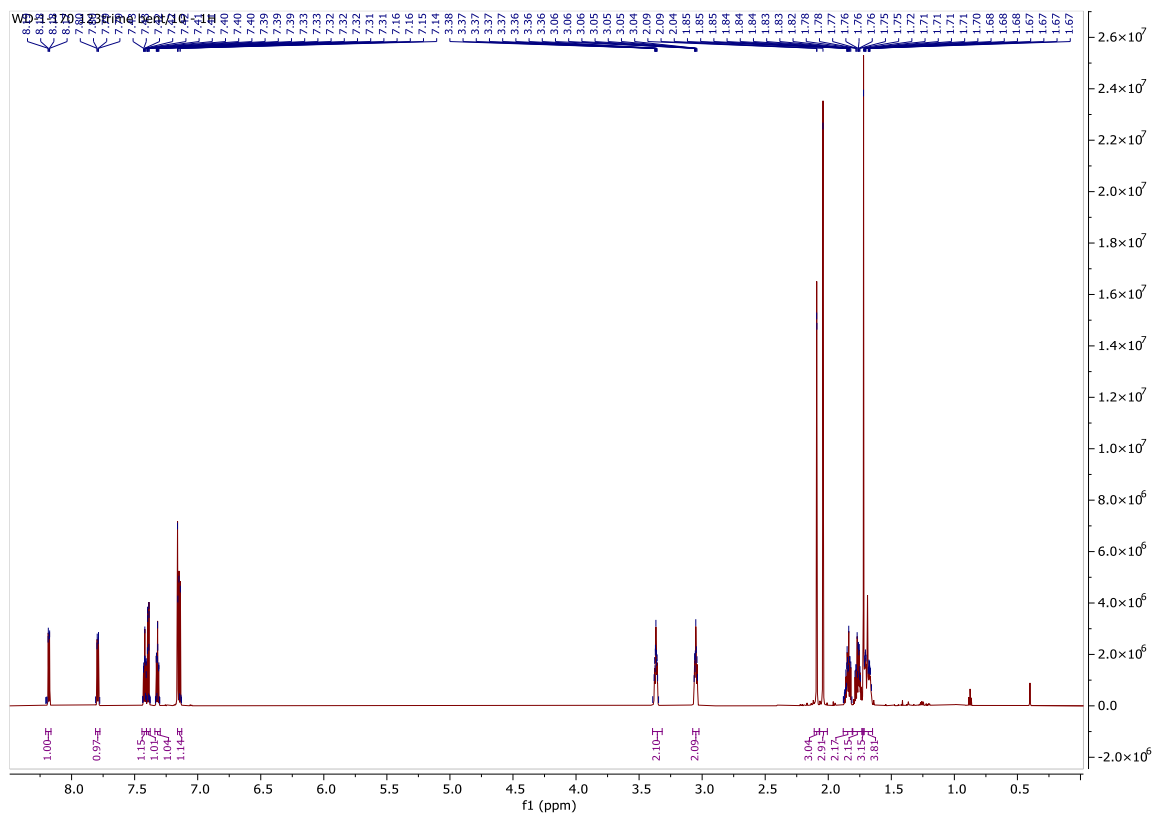


Signal 1: DAD1 A, Sig=210,4 Ref=360,100

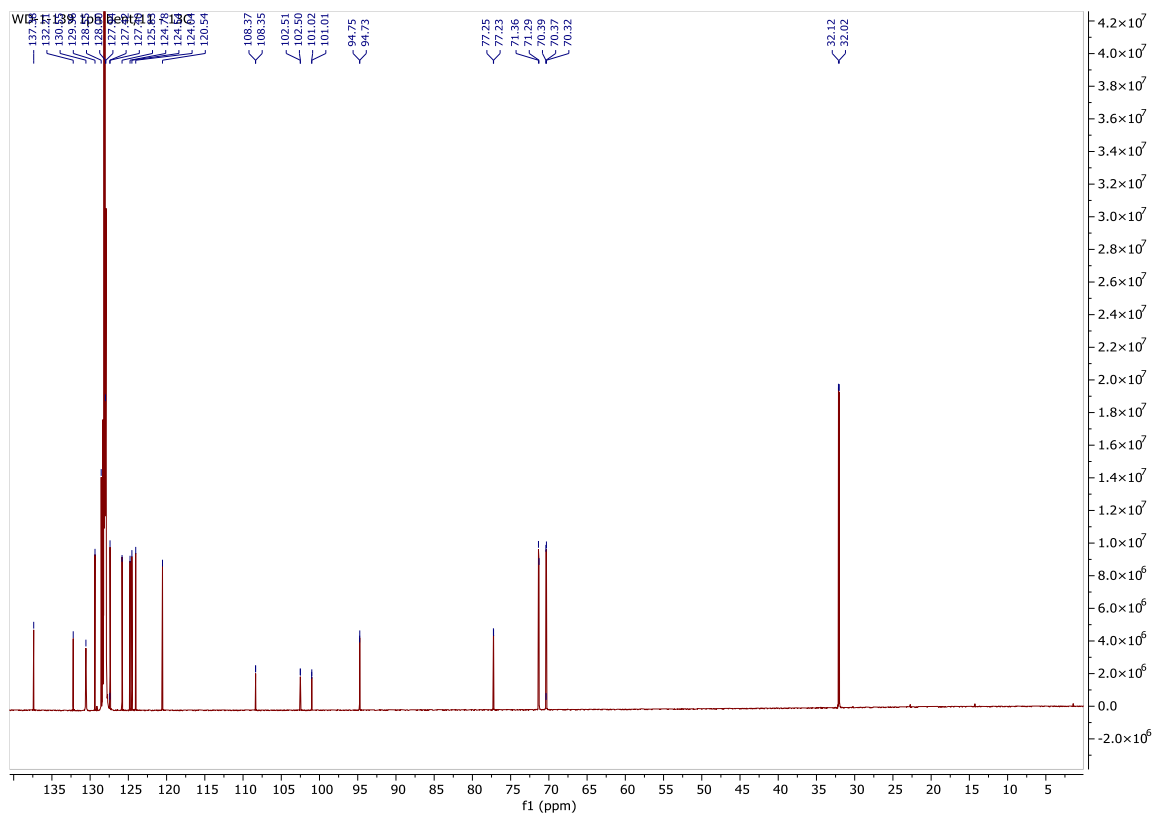
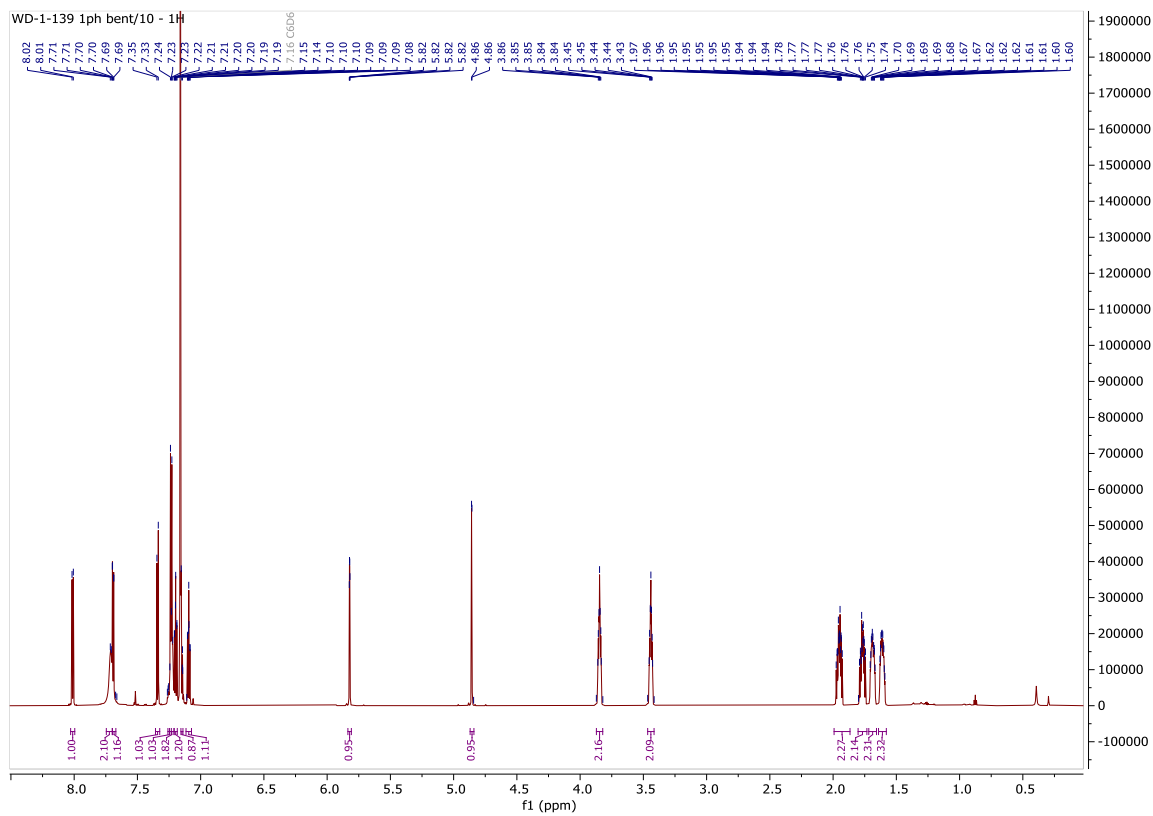
Peak #	RetTime [min]	Type	Width [min]	Area [mAU*s]	Height [mAU]	Area %
1	9.968	VB R	0.2622	4.07824e4	1762.93420	50.0867
2	11.801	BV R	0.3236	4.06412e4	1504.86633	49.9133

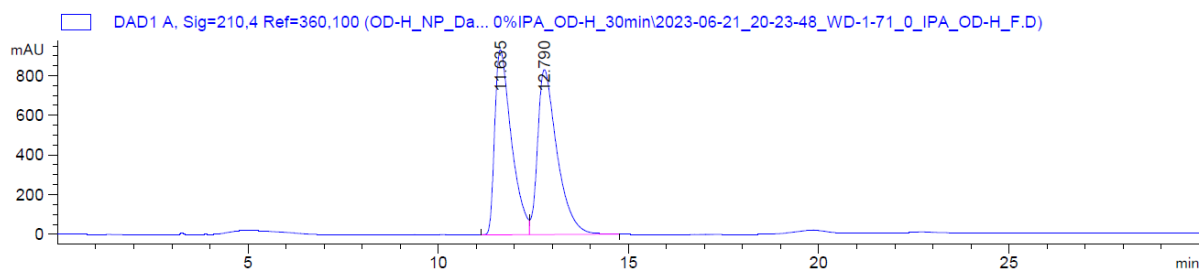
Totals : 8.14237e4 3267.80054

S11



S12

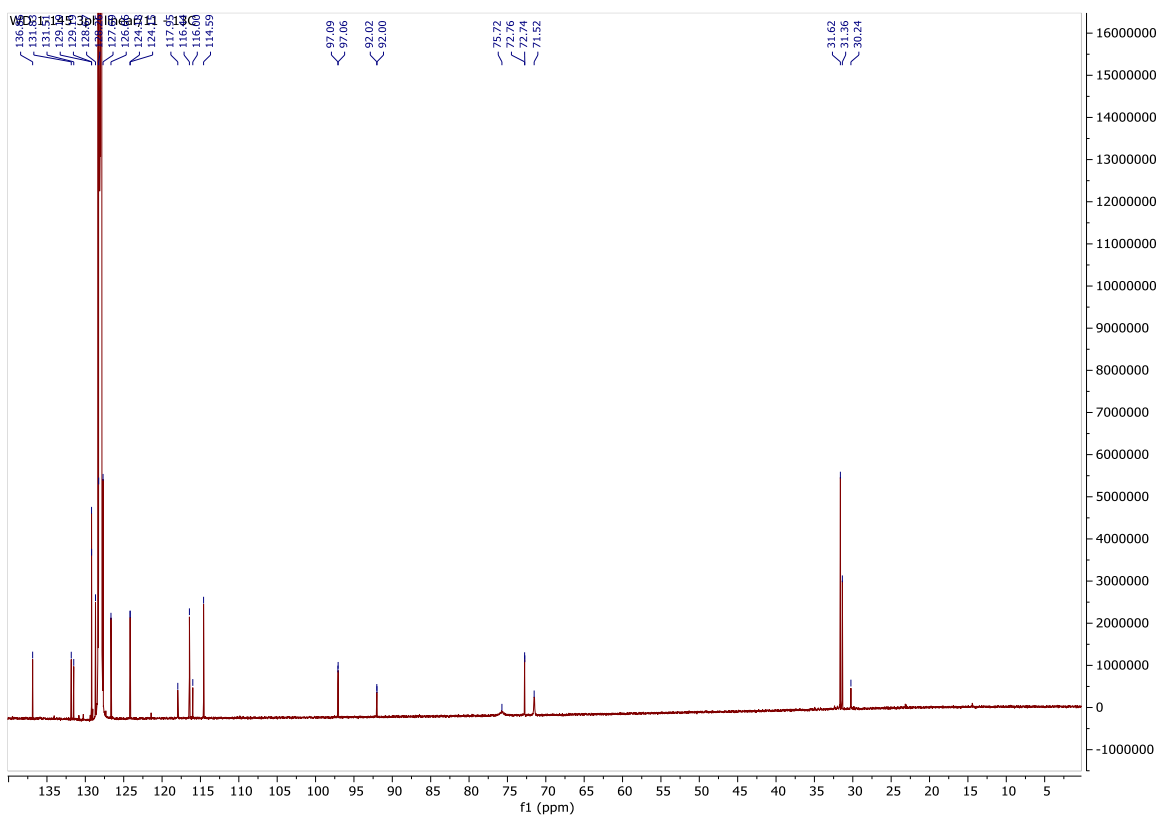
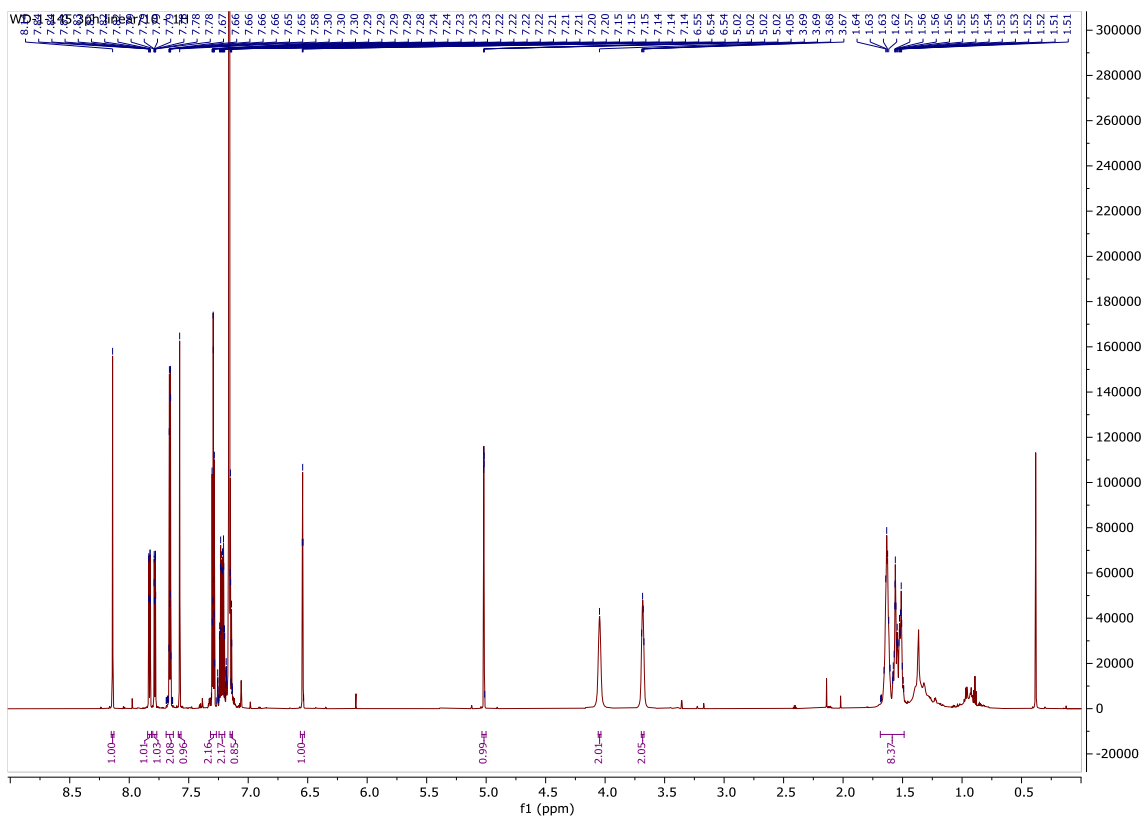


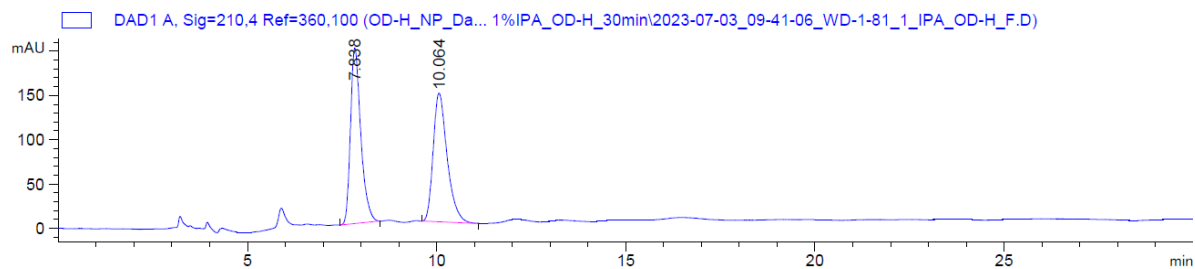


Signal 1: DAD1 A, Sig=210,4 Ref=360,100

Peak #	RetTime [min]	Type	Width [min]	Area [mAU*s]	Height [mAU]	Area %
1	11.635	BV	0.4185	2.83435e4	932.66235	48.8740
2	12.790	VV R	0.4668	2.96494e4	831.91412	51.1260

Totals : 5.79929e4 1764.57648



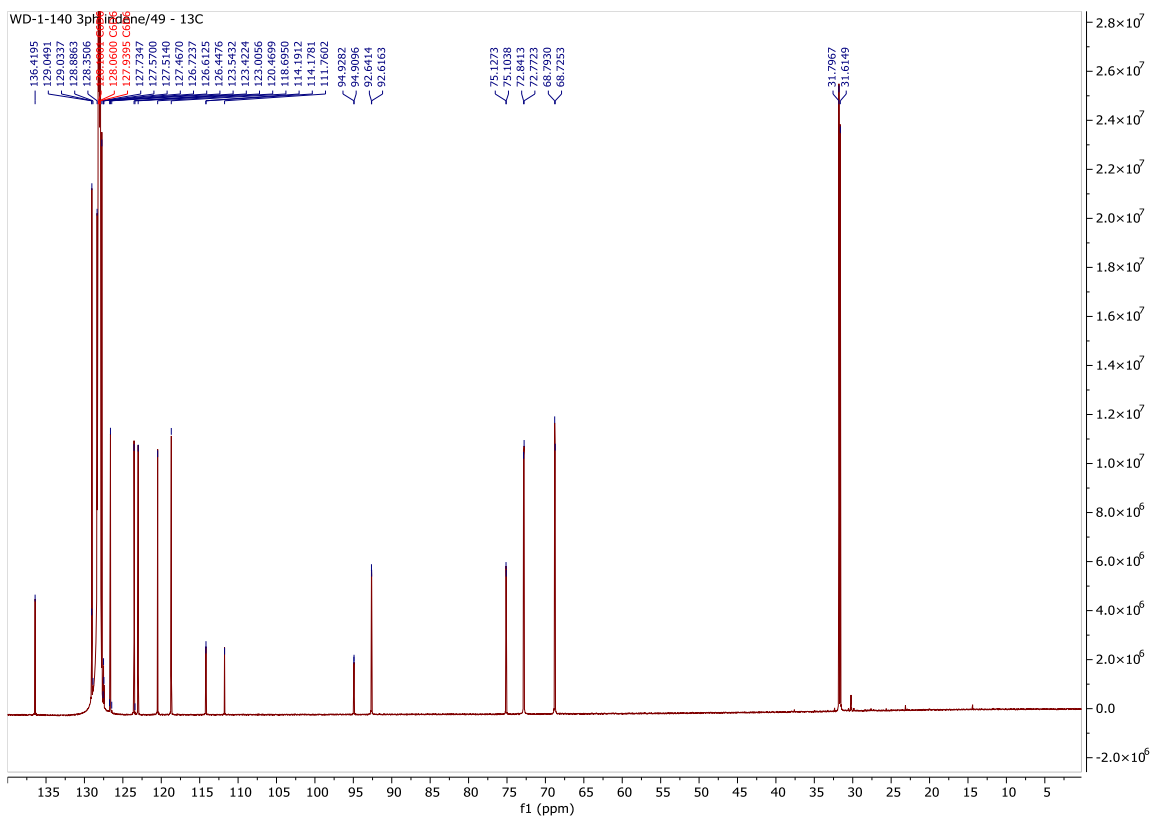
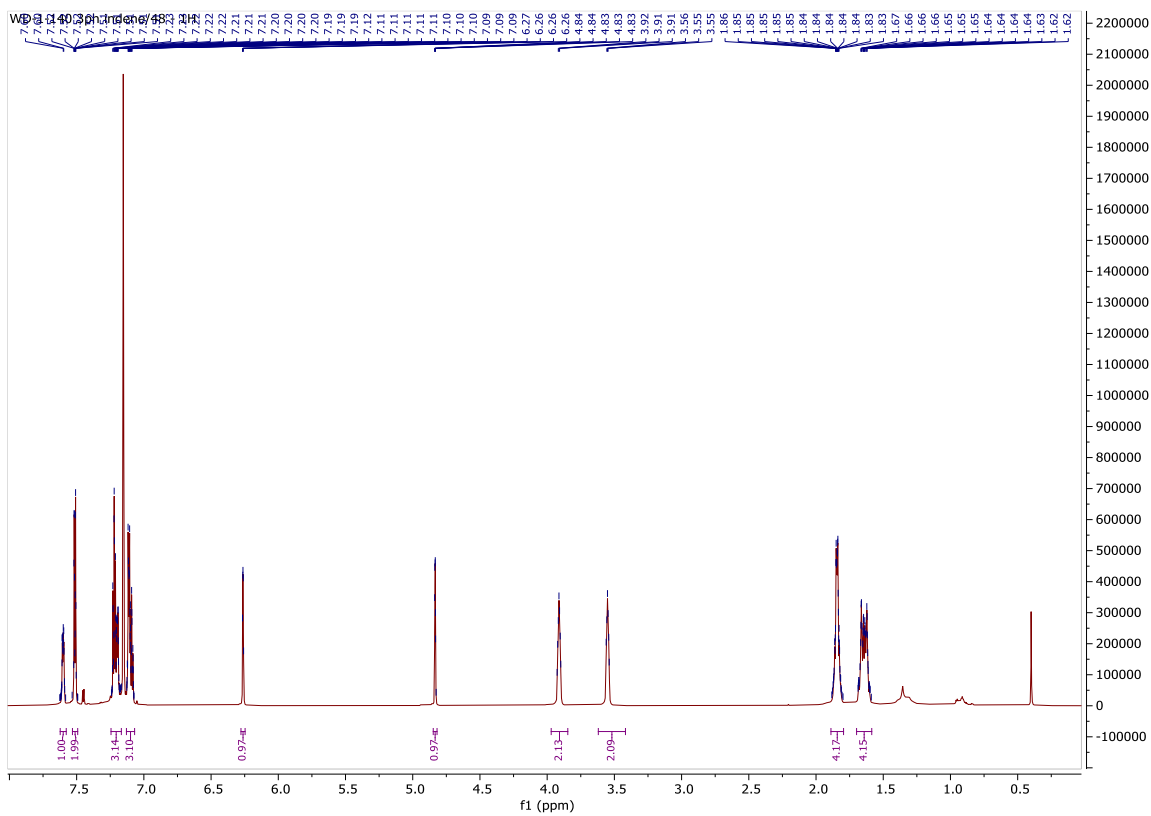


Signal 1: DAD1 A, Sig=210,4 Ref=360,100

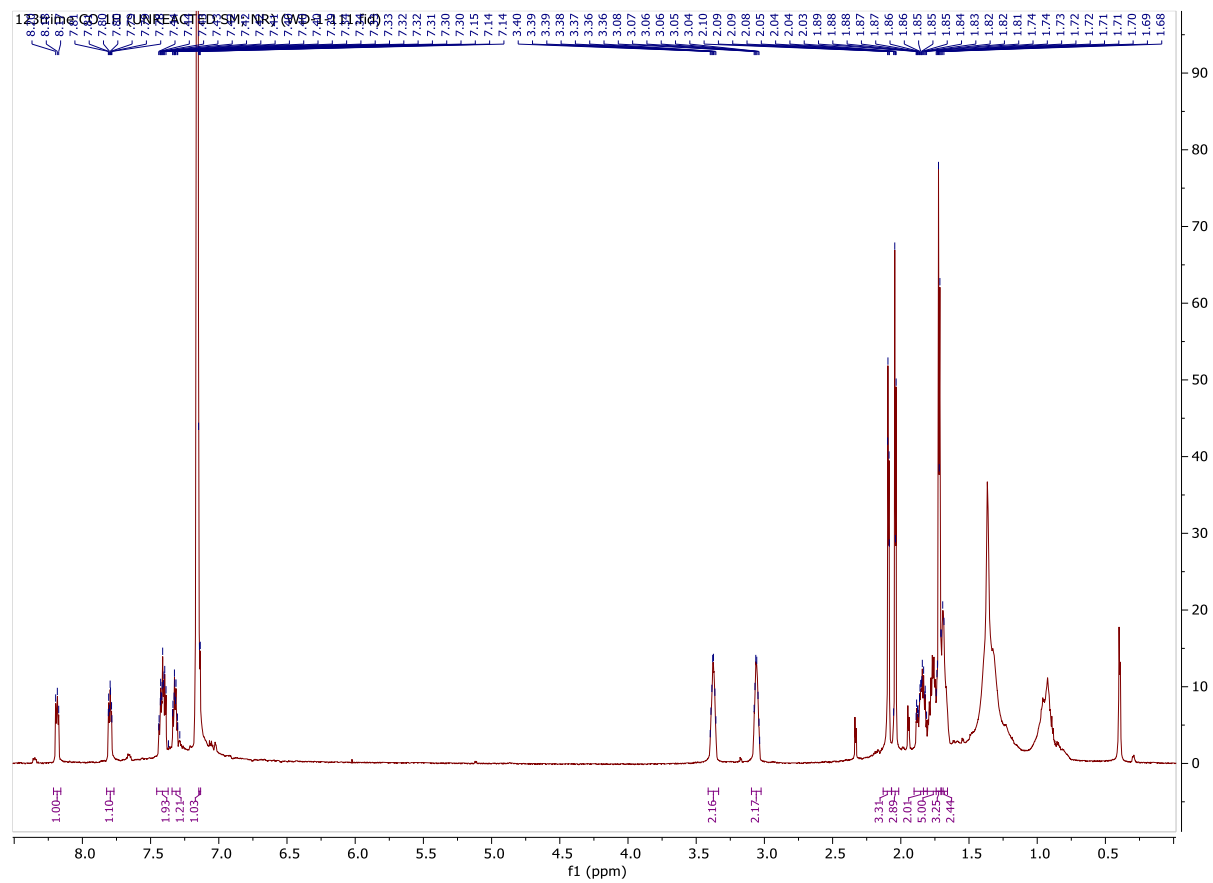
Peak #	RetTime [min]	Type	Width [min]	Area [mAU*s]	Height [mAU]	Area %
1	7.838	BB	0.2596	3764.58545	198.23906	50.2355
2	10.064	BB	0.3046	3729.28735	145.20604	49.7645

Totals : 7493.87280 343.44510

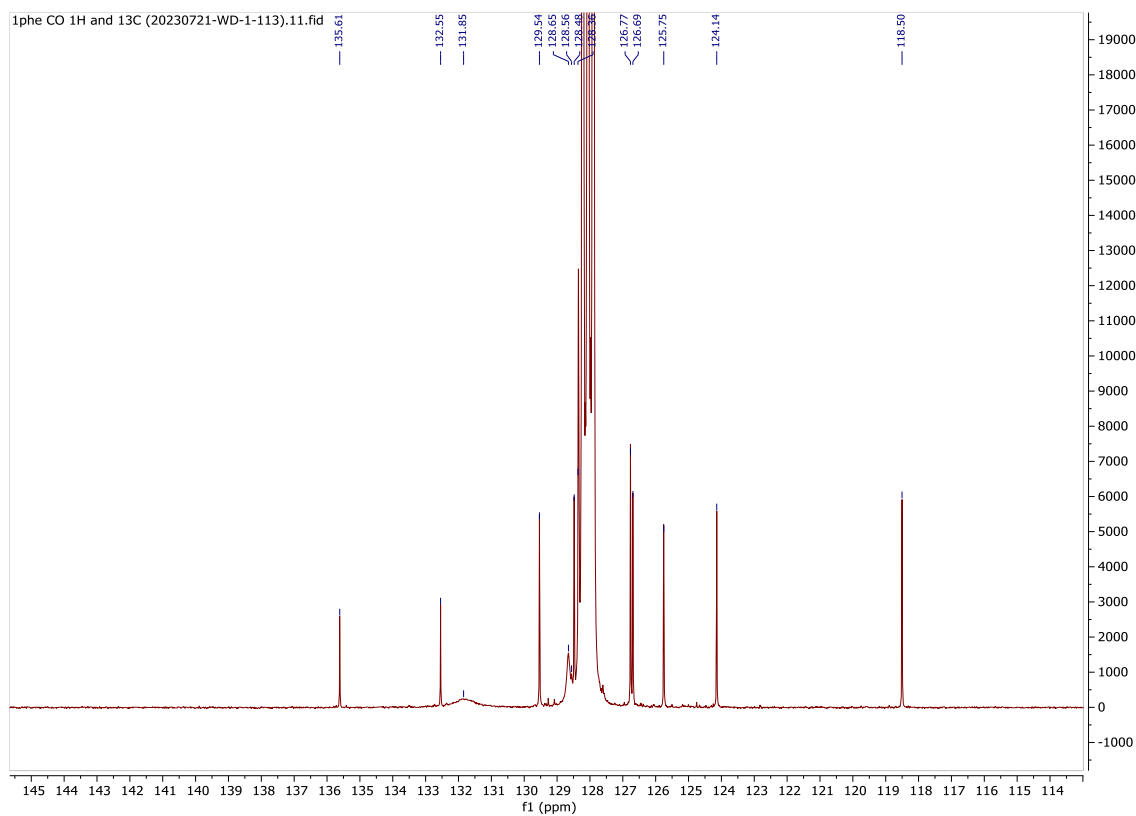
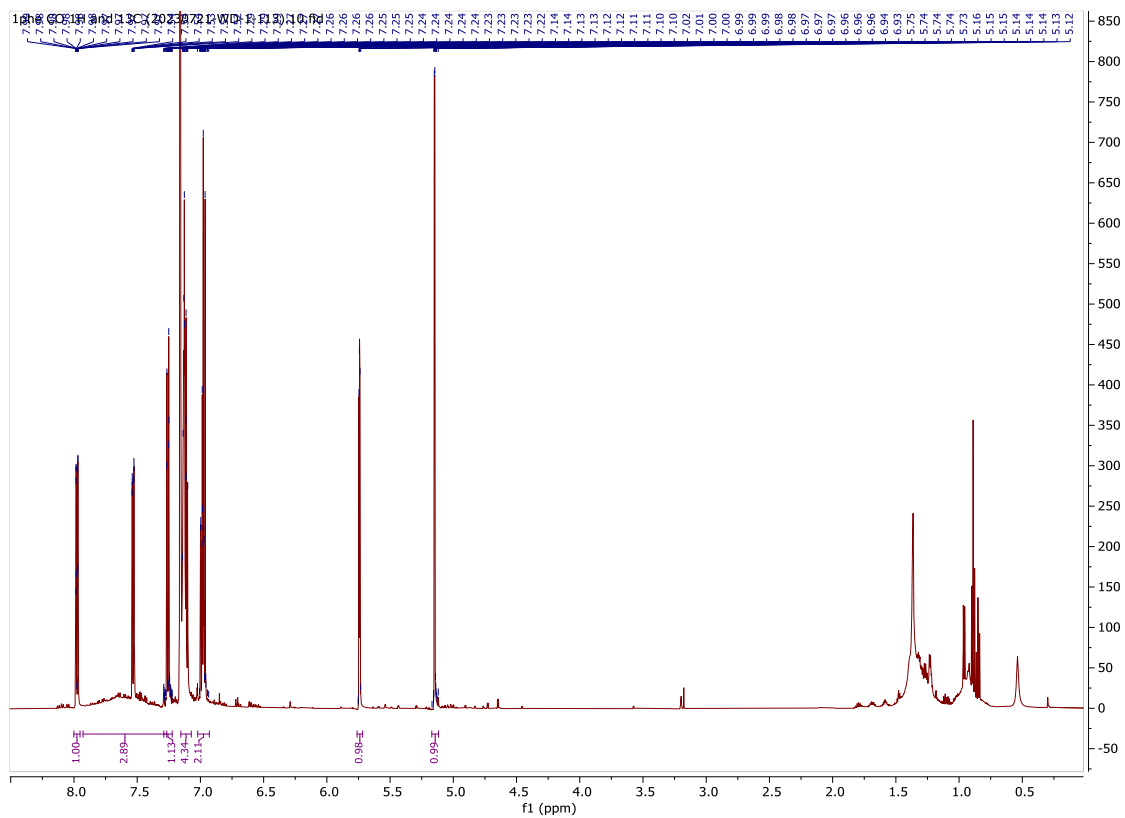
S16



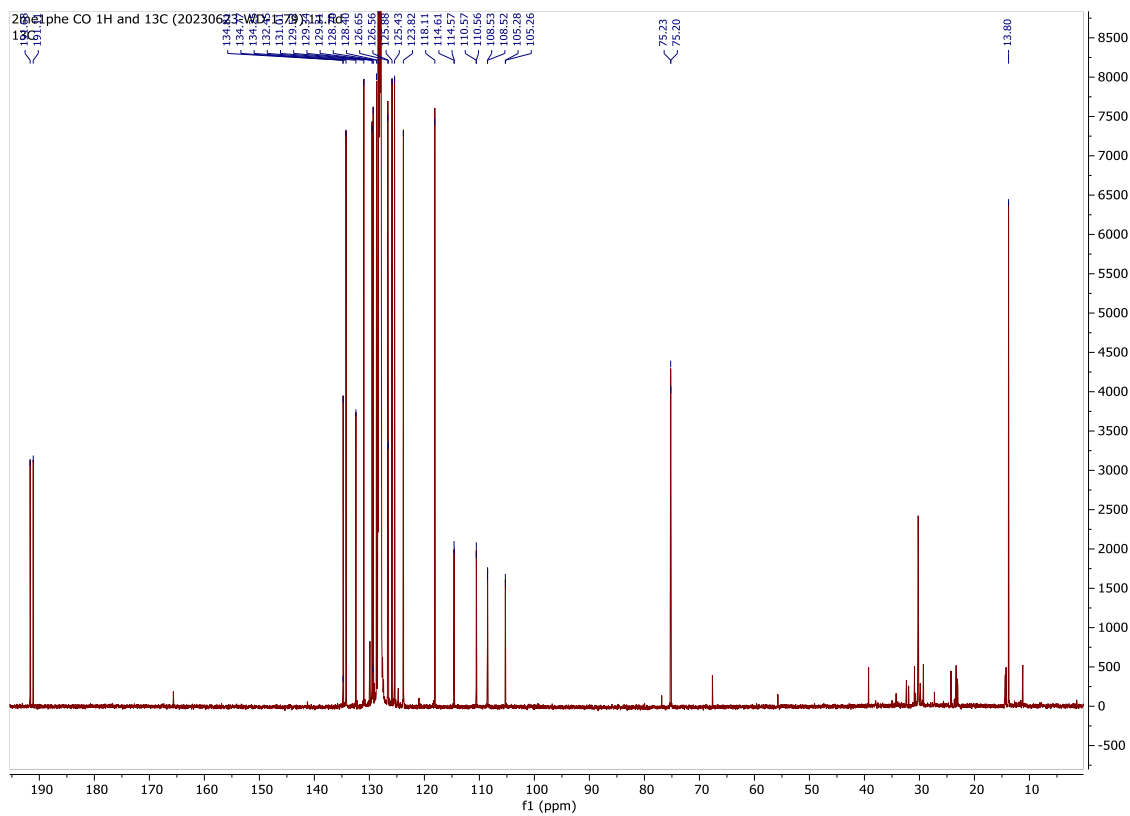
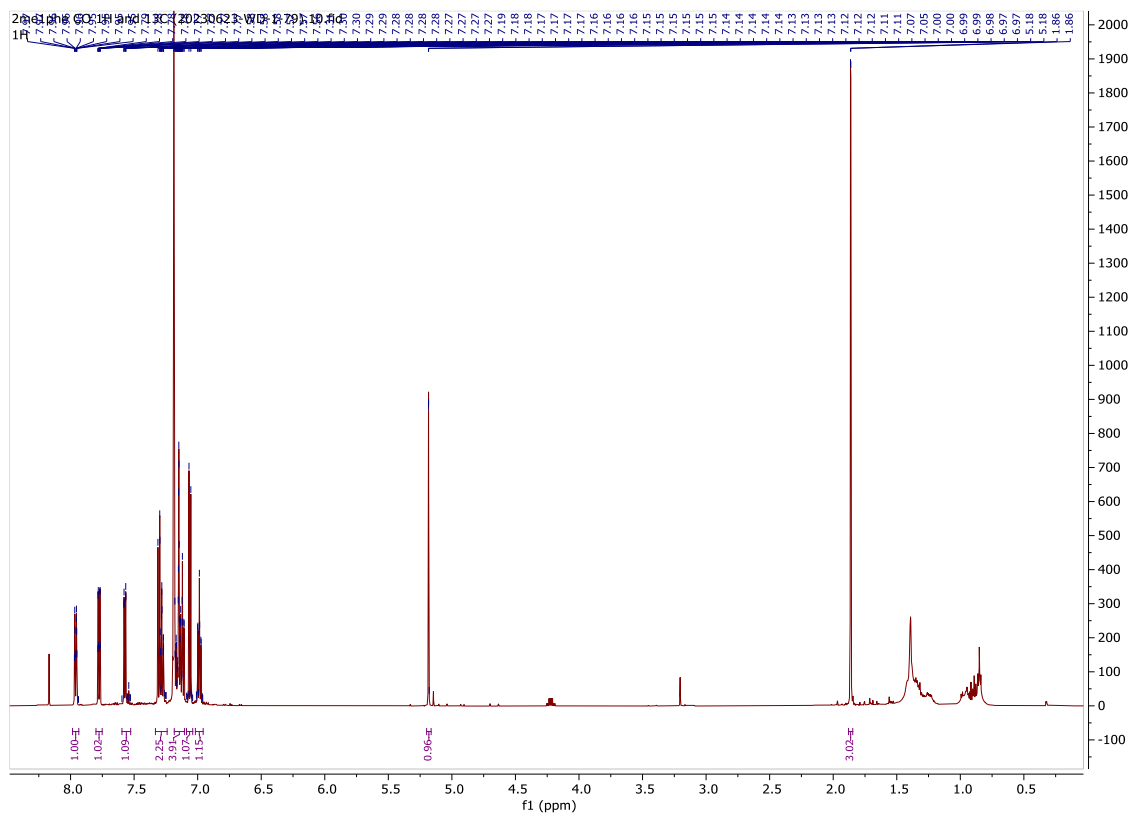
S20



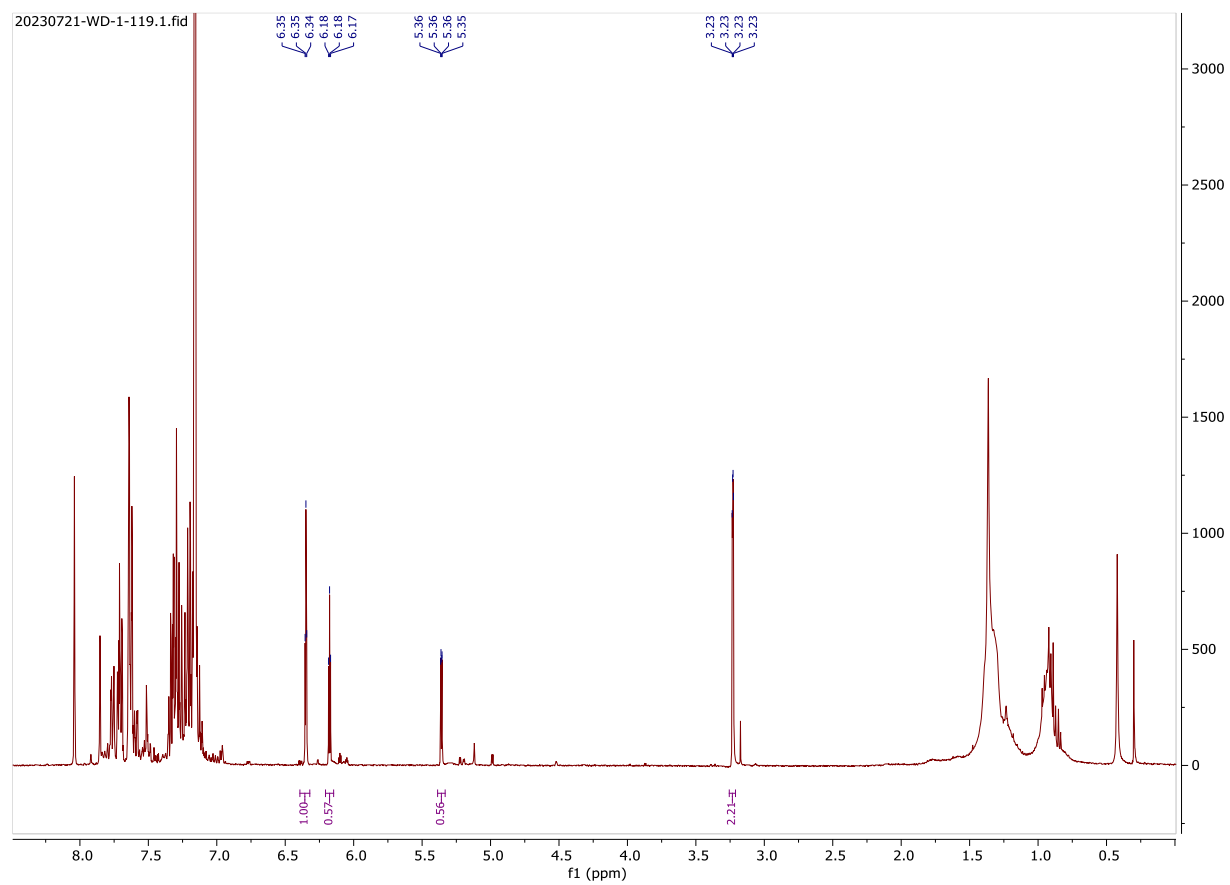
S21



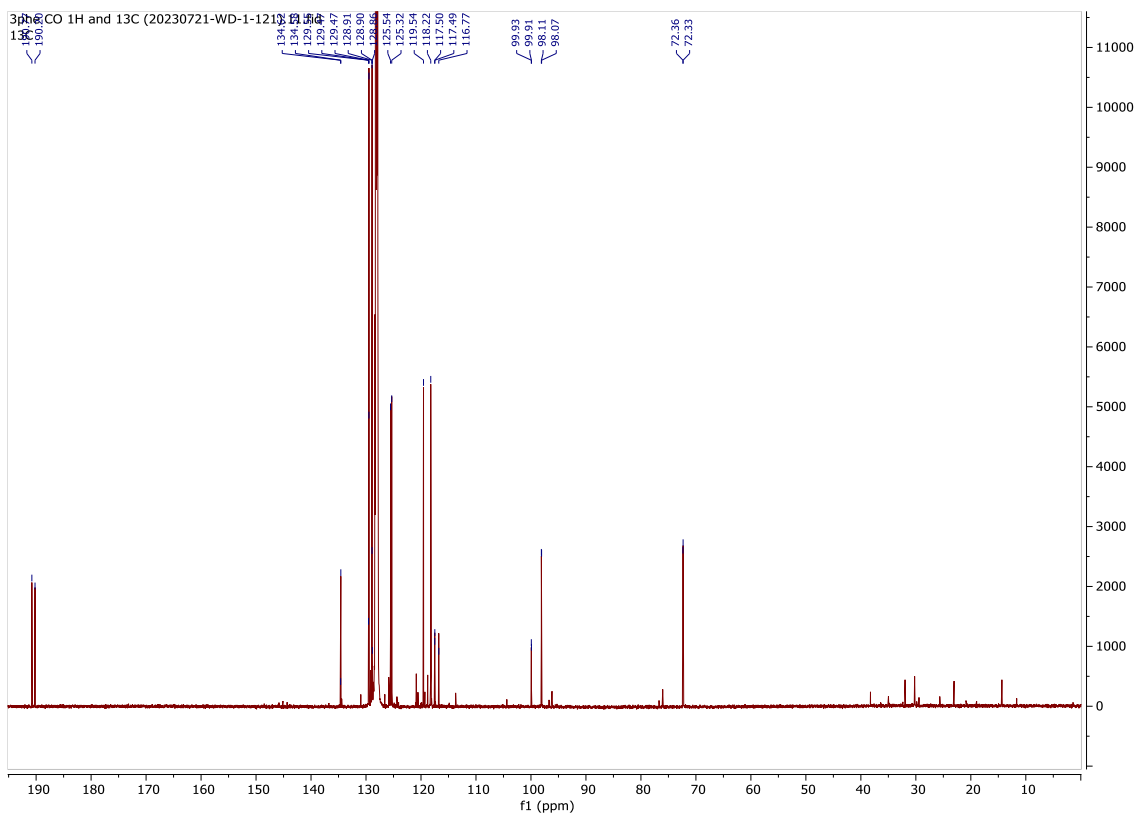
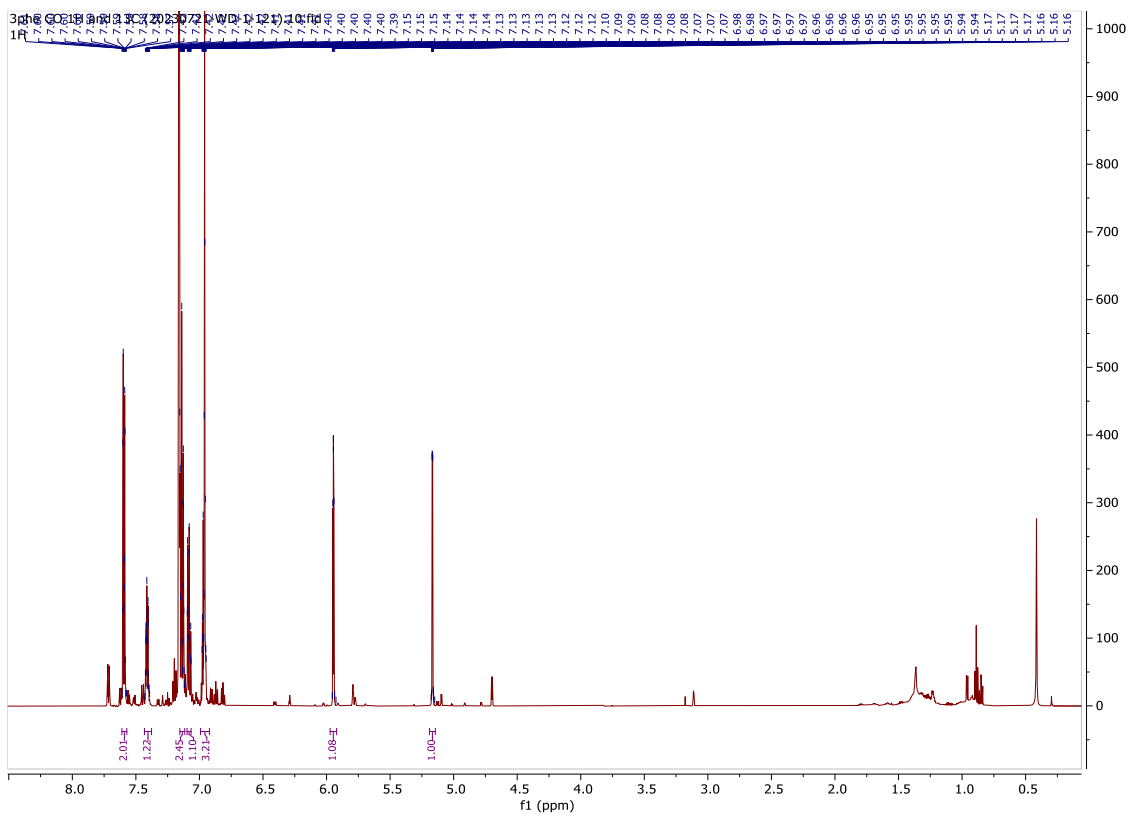
S22



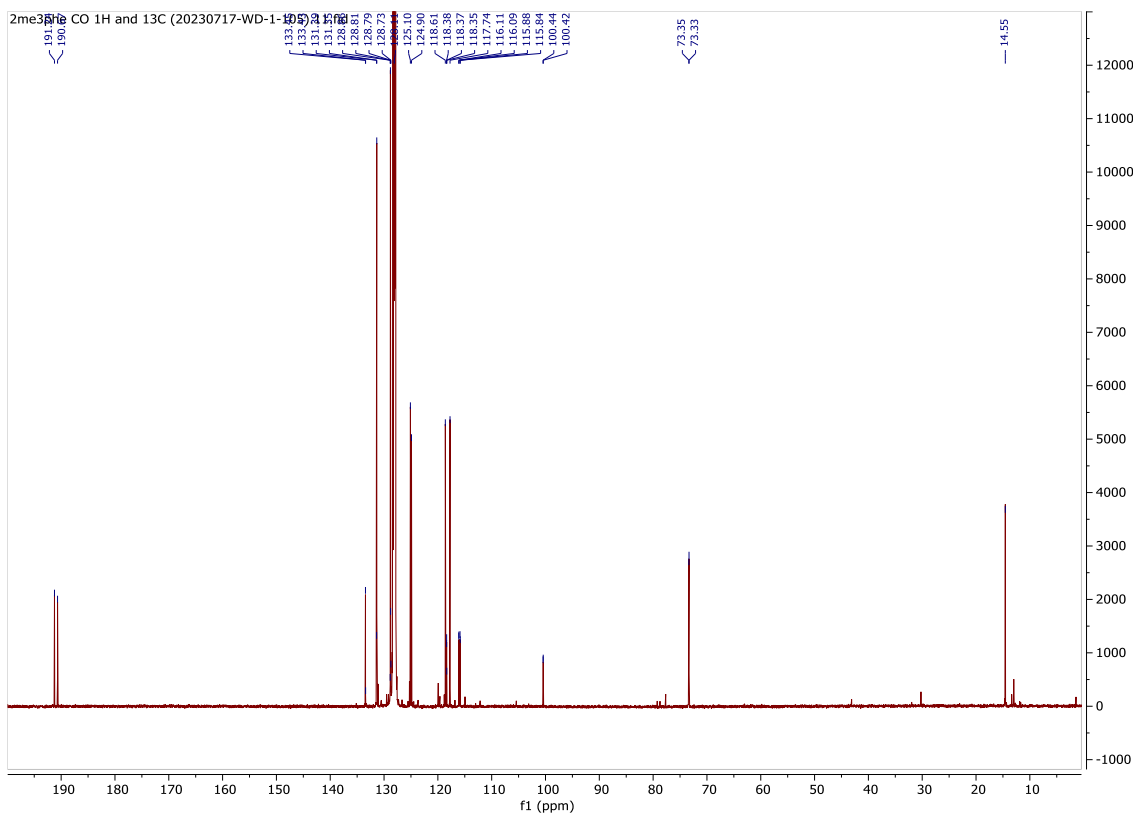
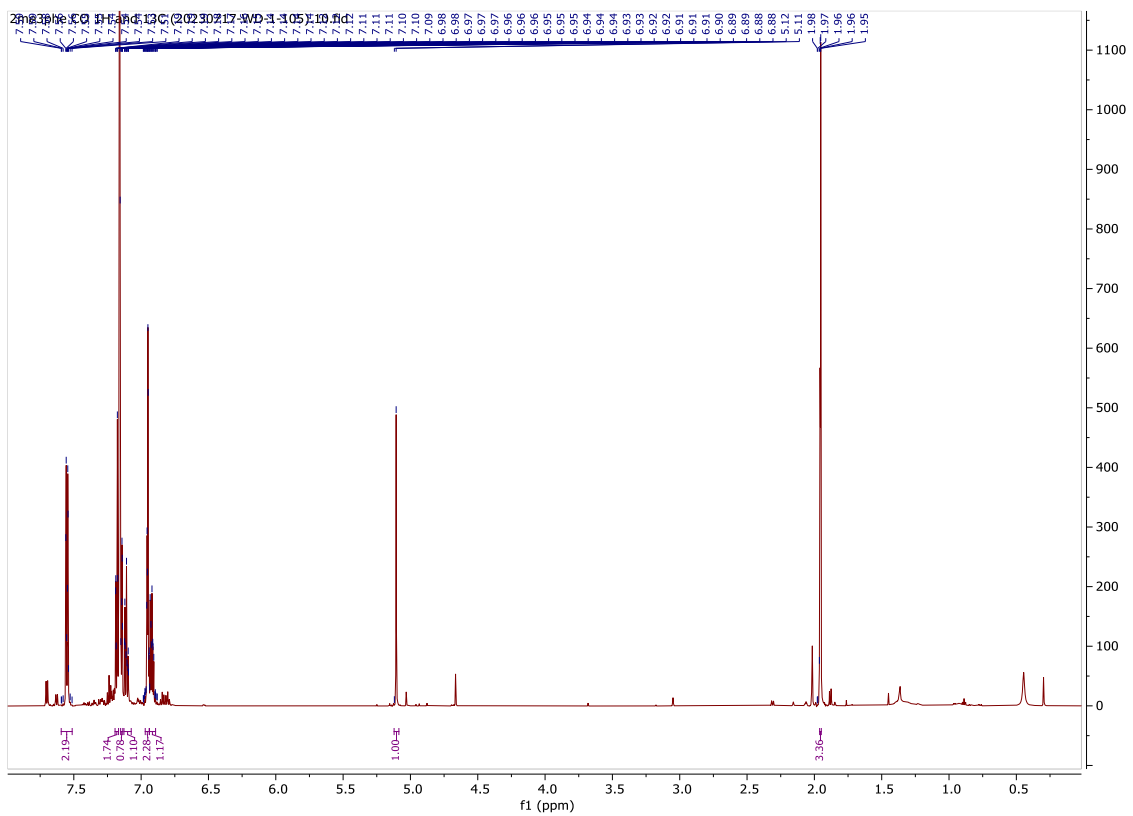
S23



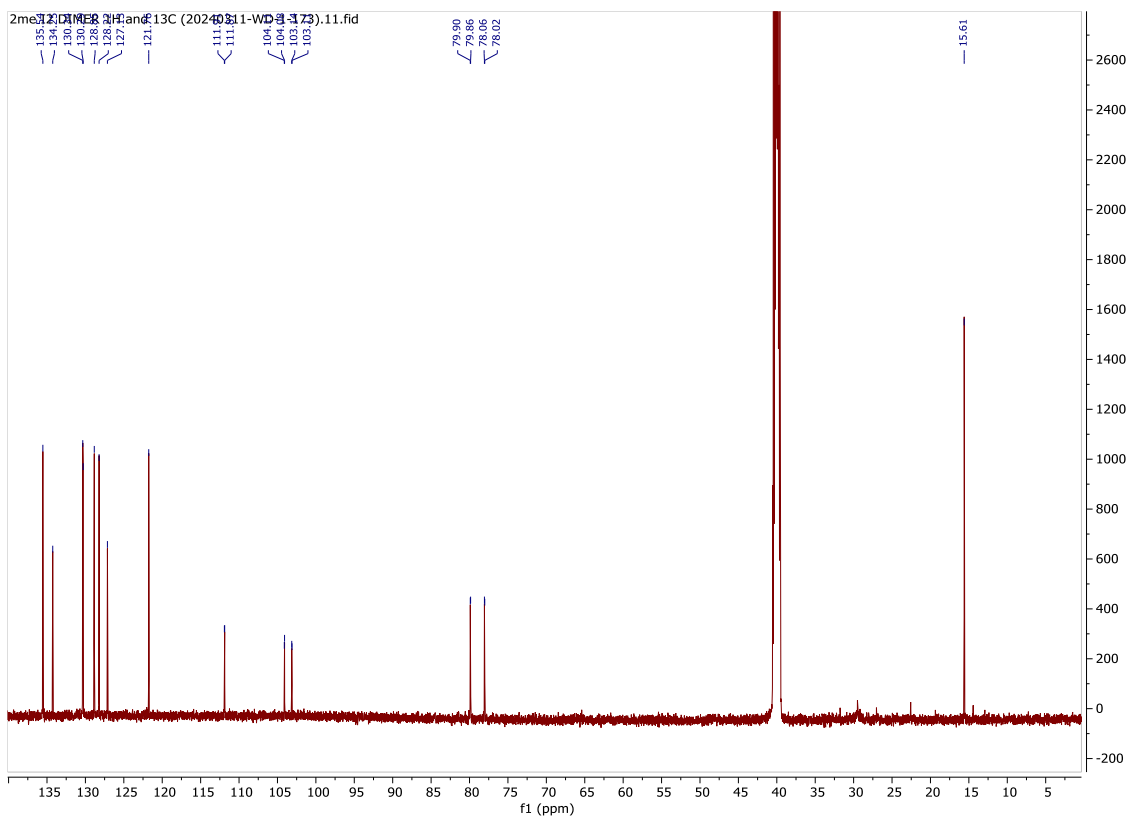
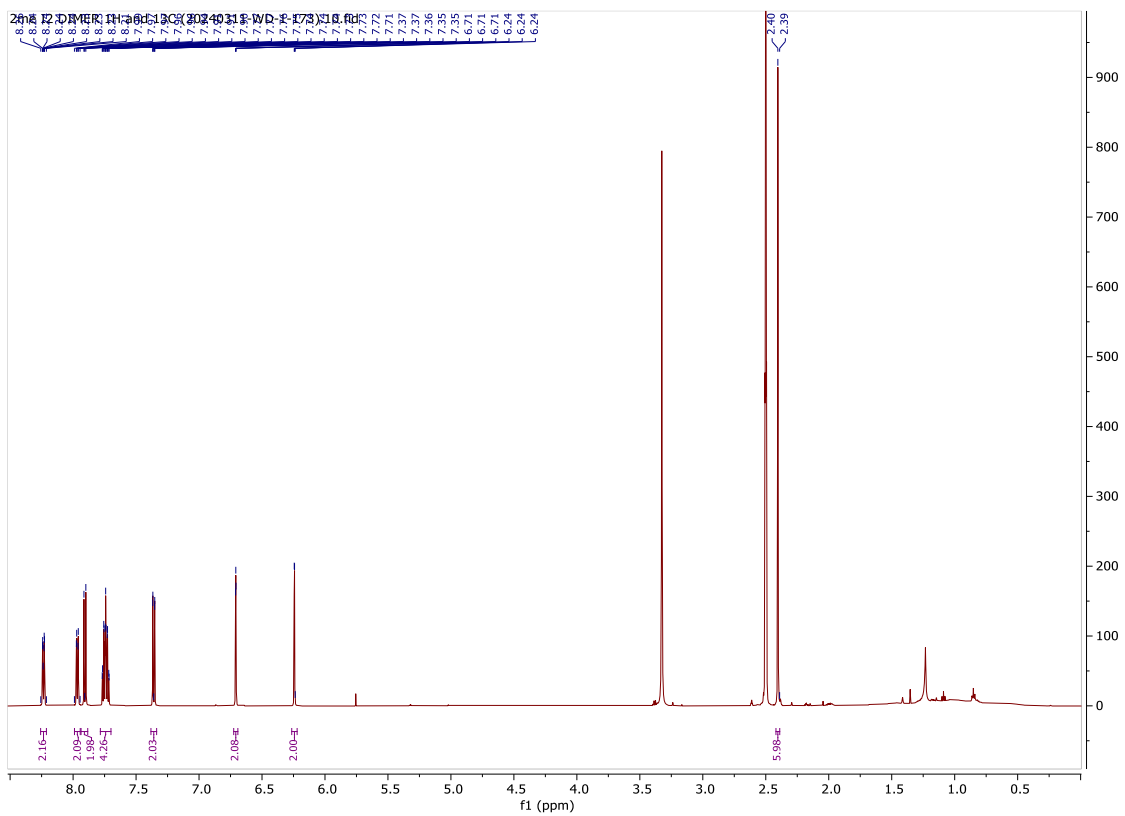
S25



S26



S27



5 – References

- (1) Davies, H. M. L.; Morton, D. Recent Advances in C–H Functionalization. *J. Org. Chem.* **2016**, *81* (2), 343–350. <https://doi.org/10.1021/acs.joc.5b02818>.
- (2) Guillemard, L.; Kaplaneris, N.; Ackermann, L.; Johansson, M. J. Late-Stage C–H Functionalization Offers New Opportunities in Drug Discovery. *Nat. Rev. Chem.* **2021**, *5* (8), 522–545. <https://doi.org/10.1038/s41570-021-00300-6>.
- (3) Gutekunst, W. R.; Baran, P. S. C–H Functionalization Logic in Total Synthesis. *Chem. Soc. Rev.* **2011**, *40* (4), 1976–1991. <https://doi.org/10.1039/C0CS00182A>.
- (4) Jana, R.; Begam, H. M.; Dinda, E. The Emergence of the C–H Functionalization Strategy in Medicinal Chemistry and Drug Discovery. *Chem. Commun.* **2021**, *57* (83), 10842–10866. <https://doi.org/10.1039/D1CC04083A>.
- (5) Murali, K.; Machado, L. A.; Carvalho, R. L.; Pedrosa, L. F.; Mukherjee, R.; Da Silva Júnior, E. N.; Maiti, D. Decoding Directing Groups and Their Pivotal Role in C–H Activation. *Chem. – Eur. J.* **2021**, *27* (49), 12453–12508. <https://doi.org/10.1002/chem.202101004>.
- (6) Yoshino, T.; Matsunaga, S. Chiral Carboxylic Acid Assisted Enantioselective C–H Activation with Achiral CpxMIII (M = Co, Rh, Ir) Catalysts. *ACS Catal.* **2021**, *11* (11), 6455–6466. <https://doi.org/10.1021/acscatal.1c01351>.
- (7) Carvalho, R. L. de; T. Diogo, E. B.; L. Homölle, S.; Dana, S.; Júnior, E. N. da S.; Ackermann, L. The Crucial Role of Silver(i)-Salts as Additives in C–H Activation Reactions: Overall Analysis of Their Versatility and Applicability. *Chem. Soc. Rev.* **2023**, *52* (18), 6359–6378. <https://doi.org/10.1039/D3CS00328K>.

- (8) Ghosh, S.; Shilpa, S.; Athira, C.; Sunoj, R. B. Role of Additives in Transition Metal Catalyzed C–H Bond Activation Reactions: A Computational Perspective. *Top. Catal.* **2022**, *65* (1), 141–164. <https://doi.org/10.1007/s11244-021-01527-9>.
- (9) Yu, C.; Sanjosé-Orduna, J.; Patureau, F. W.; Pérez-Temprano, M. H. Emerging Unconventional Organic Solvents for C–H Bond and Related Functionalization Reactions. *Chem. Soc. Rev.* **2020**, *49* (6), 1643–1652. <https://doi.org/10.1039/C8CS00883C>.
- (10) Mas-Roselló, J.; Herraiz, A. G.; Audic, B.; Laverny, A.; Cramer, N. Chiral Cyclopentadienyl Ligands: Design, Syntheses, and Applications in Asymmetric Catalysis. *Angew. Chem. Int. Ed.* **2021**, *60* (24), 13198–13224. <https://doi.org/10.1002/anie.202008166>.
- (11) Liu, C.-X.; Yin, S.-Y.; Zhao, F.; Yang, H.; Feng, Z.; Gu, Q.; You, S.-L. Rhodium-Catalyzed Asymmetric C–H Functionalization Reactions. *Chem. Rev.* **2023**, *123* (16), 10079–10134. <https://doi.org/10.1021/acs.chemrev.3c00149>.
- (12) Burman, J. S.; Blakey, S. B. Regioselective Intermolecular Allylic C–H Amination of Disubstituted Olefins via Rhodium/ π -Allyl Intermediates. *Angew. Chem. Int. Ed.* **2017**, *56* (44), 13666–13669. <https://doi.org/10.1002/anie.201707021>.
- (13) Burman, J. S.; Harris, R. J.; Farr, C. M. B.; Bacsa, J.; Blakey, S. B. Rh(III) and Ir(III)Cp* Complexes Provide Complementary Regioselectivity Profiles in Intermolecular Allylic C–H Amidation Reactions. *ACS Catal.* **2019**, *9* (6), 5474–5479. <https://doi.org/10.1021/acscatal.9b01338>.
- (14) Kazerouni, A. M.; Nelson, T. A. F.; Chen, S. W.; Sharp, K. R.; Blakey, S. B. Regioselective Cp*Ir(III)-Catalyzed Allylic C–H Sulfamidation of Allylbenzene Derivatives. *J. Org. Chem.* **2019**, *84* (20), 13179–13185. <https://doi.org/10.1021/acs.joc.9b01816>.

- (15) Harris, R. J.; Park, J.; Nelson, T. A. F.; Iqbal, N.; Salgueiro, D. C.; Bacsá, J.; MacBeth, C. E.; Baik, M.-H.; Blakey, S. B. The Mechanism of Rhodium-Catalyzed Allylic C–H Amination. *J. Am. Chem. Soc.* **2020**, *142* (12), 5842–5851.
<https://doi.org/10.1021/jacs.0c01069>.
- (16) Nelson, T. A. F.; Hollerbach, M. R.; Blakey, S. B. Allylic C–H Functionalization via Group 9 π -Allyl Intermediates. *Dalton Trans.* **2020**, *49* (40), 13928–13935.
<https://doi.org/10.1039/D0DT02313B>.
- (17) Trost, B. M.; Ryan, M. C. Indenylmetal Catalysis in Organic Synthesis. *Angew. Chem. Int. Ed.* **2017**, *56* (11), 2862–2879. <https://doi.org/10.1002/anie.201609054>.
- (18) Hart-Davis, A. J.; Mawby, R. J. Reactions of π -Indenyl Complexes of Transition Metals. Part I. Kinetics and Mechanisms of Reactions of Tricarbonyl- π -Indenylmethylmolybdenum with Phosphorus(III) Ligands. *J. Chem. Soc. Inorg. Phys. Theor.* **1969**, No. 0, 2403–2407.
<https://doi.org/10.1039/J19690002403>.
- (19) Rerek, M. E.; Basolo, F. Kinetics and Mechanism of Substitution Reactions of η^5 -Cyclopentadienyldicarbonylrhodium(I) Derivatives. Rate Enhancement of Associative Substitution in Cyclopentadienylmetal Compounds. *J. Am. Chem. Soc.* **1984**, *106* (20), 5908–5912. <https://doi.org/10.1021/ja00332a026>.
- (20) Cramer, R.; Seiwel, L. P. Nucleophilic Displacement of Ethylene from π -C₅H₅Rh(C₂H₄)₂. *J. Organomet. Chem.* **1975**, *92* (2), 245–252.
[https://doi.org/10.1016/S0022-328X\(00\)92096-5](https://doi.org/10.1016/S0022-328X(00)92096-5).
- (21) Hlatky, G. G. Metallocene Catalysts for Olefin Polymerization: Annual Review for 1996. *Coord. Chem. Rev.* **1999**, *181* (1), 243–296. [https://doi.org/10.1016/S0010-8545\(98\)00220-3](https://doi.org/10.1016/S0010-8545(98)00220-3).

- (22) Baker, R. W. Asymmetric Induction via the Structural Indenyl Effect. *Organometallics* **2018**, *37* (3), 433–440. <https://doi.org/10.1021/acs.organomet.7b00841>.
- (23) Farr, C. M. B.; Kazerouni, A. M.; Park, B.; Poff, C. D.; Won, J.; Sharp, K. R.; Baik, M.-H.; Blakey, S. B. Designing a Planar Chiral Rhodium Indenyl Catalyst for Regio- and Enantioselective Allylic C–H Amidation. *J. Am. Chem. Soc.* **2020**, *142* (32), 13996–14004. <https://doi.org/10.1021/jacs.0c07305>.
- (24) Laws, D.; Poff, C. D.; Heyboer, E. M.; Blakey, S. B. Synthesis, Stereochemical Assignment, and Enantioselective Catalytic Activity of Late Transition Metal Planar Chiral Complexes. *Chem. Soc. Rev.* **2023**, *52* (17), 6003–6030. <https://doi.org/10.1039/D3CS00325F>.
- (25) Gross, P.; Im, H.; Laws, D. I.; Park, B.; Baik, M.-H.; Blakey, S. B. Enantioselective Aziridination of Unactivated Terminal Alkenes Using a Planar Chiral Rh(III) Indenyl Catalyst. *J. Am. Chem. Soc.* **2024**, *146* (2), 1447–1454. <https://doi.org/10.1021/jacs.3c10637>.
- (26) Gutnov, A.; Heller, B.; Fischer, C.; Drexler, H.-J.; Spannenberg, A.; Sundermann, B.; Sundermann, C. Cobalt(I)-Catalyzed Asymmetric [2+2+2] Cycloaddition of Alkynes and Nitriles: Synthesis of Enantiomerically Enriched Atropoisomers of 2-Arylpyridines. *Angew. Chem. Int. Ed.* **2004**, *43* (29), 3795–3797. <https://doi.org/10.1002/anie.200454164>.
- (27) Heller, B.; Gutnov, A.; Fischer, C.; Drexler, H.-J.; Spannenberg, A.; Redkin, D.; Sundermann, C.; Sundermann, B. Phosphorus-Bearing Axially Chiral Biaryls by Catalytic Asymmetric Cross-Cyclotrimerization and a First Application in Asymmetric Hydrosilylation. *Chem. – Eur. J.* **2007**, *13* (4), 1117–1128. <https://doi.org/10.1002/chem.200600826>.

- (28) Hapke, M.; Kral, K.; Fischer, C.; Spannenberg, A.; Gutnov, A.; Redkin, D.; Heller, B. Asymmetric Synthesis of Axially Chiral 1-Aryl-5,6,7,8-Tetrahydroquinolines by Cobalt-Catalyzed [2 + 2 + 2] Cycloaddition Reaction of 1-Aryl-1,7-Octadiynes and Nitriles. *J. Org. Chem.* **2010**, 75 (12), 3993–4003. <https://doi.org/10.1021/jo100122d>.
- (29) Ernst, A. B.; Moore, E. J.; Myers, C. L.; Quan, R. W. Ligands and Catalysts for Producing Elastomeric Propylene Polymers. CA2355236A1, June 22, 2000. <https://patents.google.com/patent/CA2355236A1/en> (accessed 2024-04-08).
- (30) Sullivan, J.; Gately, D. Constrained Geometry Ligands and Complexes Derived Therefrom. US20020123639A1, September 5, 2002. <https://patents.google.com/patent/US20020123639A1/en> (accessed 2024-04-08).
- (31) KULANGARA, S. V.; Friederichs, N. H. Catalyst Comprising a Metallocene Complex and a Co-Catalyst. WO2015132346A1, September 11, 2015. <https://patents.google.com/patent/WO2015132346A1/en> (accessed 2024-04-08).
- (32) Crowther, D. J.; Brant, P.; Gracia, C. U. D.; Lovell, J. A. Catalysts and Methods of Use Thereof to Produce Vinyl Terminated Polymers. US8455597B2, June 4, 2013. <https://patents.google.com/patent/US8455597B2/en> (accessed 2024-04-08).
- (33) Kim, D. H.; Lee, J. A.; Lee, B. Y.; Chung, Y. K. Synthesis of Zirconocenes Bearing Benz[*f*]Indenyl Ligand and Their Use as a Catalyst in Ethylene Polymerization. *J. Organomet. Chem.* **2005**, 690 (7), 1822–1828. <https://doi.org/10.1016/j.jorganchem.2005.02.008>.
- (34) Foster, P.; Chien, J. C. W.; Rausch, M. D. Highly Stable Catalysts for the Stereospecific Polymerization of Styrene. *Organometallics* **1996**, 15 (9), 2404–2409. <https://doi.org/10.1021/om950990a>.

- (35) Zhao, X.; Luo, X.; Li, B.; Song, H.; Xu, S.; Wang, B. A New Ruthenium Complex with Benz[*f*]Indenyl Ligand for Living Radical Polymerization. *Eur. Polym. J.* **2008**, *44* (10), 3264–3270. <https://doi.org/10.1016/j.eurpolymj.2008.07.029>.
- (36) Piou, T.; Romanov-Michailidis, F.; Romanova-Michaelides, M.; Jackson, K. E.; Semakul, N.; Taggart, T. D.; Newell, B. S.; Rithner, C. D.; Paton, R. S.; Rovis, T. Correlating Reactivity and Selectivity to Cyclopentadienyl Ligand Properties in Rh(III)-Catalyzed C–H Activation Reactions: An Experimental and Computational Study. *J. Am. Chem. Soc.* **2017**, *139* (3), 1296–1310. <https://doi.org/10.1021/jacs.6b11670>.
- (37) Piou, T.; Rovis, T. Electronic and Steric Tuning of a Prototypical Piano Stool Complex: Rh(III) Catalysis for C–H Functionalization. *Acc. Chem. Res.* **2018**, *51* (1), 170–180. <https://doi.org/10.1021/acs.accounts.7b00444>.
- (38) Morris, J. L.; Becker, C. L.; Fronczek, F. R.; Daly, W. H.; McLaughlin, M. L. Synthesis of Extended Linear Aromatics Using Tandem Diels-Alder Aromatization Reactions. *J. Org. Chem.* **1994**, *59* (21), 6484–6486. <https://doi.org/10.1021/jo00100a065>.
- (39) Krasovskiy, A.; Knochel, P. A LiCl-Mediated Br/Mg Exchange Reaction for the Preparation of Functionalized Aryl- and Heteroarylmagnesium Compounds from Organic Bromides. *Angew. Chem. Int. Ed.* **2004**, *43* (25), 3333–3336. <https://doi.org/10.1002/anie.200454084>.
- (40) Zheng, Y.-L.; Newman, S. G. Nickel-Catalyzed Domino Heck-Type Reactions Using Methyl Esters as Cross-Coupling Electrophiles. *Angew. Chem. Int. Ed.* **2019**, *58* (50), 18159–18164. <https://doi.org/10.1002/anie.201911372>.
- (41) Zawisza, A. M.; Ganchegui, B.; González, I.; Bouquillon, S.; Roglans, A.; Hénin, F.; Muzart, J. Heck-Type Reactions of Allylic Alcohols: Part IV: (2-Substituted)-1-Indanones

- via 5-Endo-Trig Cyclizations. *J. Mol. Catal. Chem.* **2008**, 283 (1), 140–145.
<https://doi.org/10.1016/j.molcata.2007.12.021>.
- (42) Jones, D. W.; Marmon, R. J. 1,5-Sigmatropic Formyl Migration in 1,3-Dimethylbenz[*f*]Indene-1-Carbaldehyde; Evidence for Product-like Transition States. *J. Chem. Soc. Perkin I* **1990**, No. 12, 3271–3275. <https://doi.org/10.1039/P19900003271>.
- (43) Ge, Y.; Su, X.; Li, G.; Yang, Y.-F.; She, Y. Oxidative Functionalization of Naphthalene Derivatives Catalyzed by Mn(III)-Porphyrins. *Tetrahedron Lett.* **2023**, 123, 154535.
<https://doi.org/10.1016/j.tetlet.2023.154535>.
- (44) Jefford, C. W.; Sledeski, A. W.; Patrick, L.; Boukouvalas, J. The Alkylation of Silyl Enol Ethers with SN1-Unreactive Iodides in the Presence of Silver Trifluoroacetate. *Tetrahedron Lett.* **1992**, 33 (14), 1855–1858. [https://doi.org/10.1016/S0040-4039\(00\)74160-8](https://doi.org/10.1016/S0040-4039(00)74160-8).
- (45) Dayan, S.; Almog, J.; Khodzhaev, O.; Rozen, S. A Novel Synthesis of Indandiones Using the HOF·CH₃CN Complex. *J. Org. Chem.* **1998**, 63 (8), 2752–2754.
<https://doi.org/10.1021/jo972088d>.
- (46) van Leeuwen, T.; Danowski, W.; Otten, E.; Wezenberg, S. J.; Feringa, B. L. Asymmetric Synthesis of Second-Generation Light-Driven Molecular Motors. *J. Org. Chem.* **2017**, 82 (10), 5027–5033. <https://doi.org/10.1021/acs.joc.7b00852>.
- (47) H·普莱尼奥; C·弗莱肯施泰因; R·卡德罗夫; J·阿尔梅纳; A·蒙西斯; T·里尔迈尔. New Cyclopentadienyl, Indenyl or Fluorenyl Substituted Phosphine Compounds and Their Use in Catalytic Reactions. CN101622264A, January 6, 2010.
<https://patents.google.com/patent/CN101622264A/en> (accessed 2024-04-08).

- (48) Orlova, T.; Lancia, F.; Loussert, C.; Iamsaard, S.; Katsonis, N.; Brasselet, E. Revolving Supramolecular Chiral Structures Powered by Light in Nanomotor-Doped Liquid Crystals. *Nat. Nanotechnol.* **2018**, *13* (4), 304–308. <https://doi.org/10.1038/s41565-017-0059-x>.
- (49) Burckhalter, J. H.; Fuson, R. C. 2-Alkyl-1-Indanones. *J. Am. Chem. Soc.* **1948**, *70* (12), 4184–4186. <https://doi.org/10.1021/ja01192a061>.
- (50) Tolman, C. A. Steric Effects of Phosphorus Ligands in Organometallic Chemistry and Homogeneous Catalysis. *Chem. Rev.* **1977**, *77* (3), 313–348. <https://doi.org/10.1021/cr60307a002>.
- (51) du Plooy, K. E.; du Toit, J.; Levendis, D. C.; Coville, N. J. Multiply Substituted Cyclopentadienyl Metal Complexes: I. Solid-state and solution conformational studies on (η^5 -C₅Me₄R) Fe (CO)(L) I (R= H, tBu). *J. Organomet. Chem.* **1996**, *508* (1), 231–242. [https://doi.org/10.1016/0022-328X\(95\)05865-M](https://doi.org/10.1016/0022-328X(95)05865-M).
- (52) Kakkar, A. K.; Taylor, N. J.; Marder, T. B.; Shen, J. K.; Hallinan, N.; Basolo, F. Kinetics and Mechanism of CO Ligand Substitution in the Ring-Substituted Indenyl Rhodium Complexes [(H₅-C₉RnH_{7-n})Rh(CO)₂]. *Inorganica Chim. Acta* **1992**, *198–200*, 219–231. [https://doi.org/10.1016/S0020-1693\(00\)92364-8](https://doi.org/10.1016/S0020-1693(00)92364-8).
- (53) Bresler, L. S.; Buzina, N. A.; Varshavsky, Yu. S.; Kiseleva, N. V.; Cherkasova, T. G. Carbon-13 Nuclear Magnetic Resonance Spectra of Rhodium Carbonyl Complexes. *J. Organomet. Chem.* **1979**, *171* (2), 229–235. [https://doi.org/10.1016/S0022-328X\(00\)81544-2](https://doi.org/10.1016/S0022-328X(00)81544-2).
- (54) Köhler, F. H. ¹³C-NMR-Spektren von π -Komplexen Des Indens Zur Bestimmung Der Haptoeigenschaften von Liganden. *Chem. Ber.* **1974**, *107* (2), 570–574. <https://doi.org/10.1002/cber.19741070224>.

- (55) Marder, T. B.; Calabrese, J. C.; Roe, D. Christopher.; Tulip, T. H. The Slip-Fold Distortion of π -Bound Indenyl Ligands. Dynamic NMR and x-Ray Crystallographic Studies of (η -Indenyl)RhL₂ Complexes. *Organometallics* **1987**, *6* (9), 2012–2014.
<https://doi.org/10.1021/om00152a041>.
- (56) Westcott, S. A.; Kakkar, A. K.; Stringer, G.; Taylor, N. J.; Marder, T. B. Flexible Coordination of Indenyl Ligands in Sandwich Complexes of Transition Metals. Molecular Structures of [(η -C₉R₇)₂M] (M = Fe, R = H, Me; M = Co, Ni, R = H): Direct Measurement of the Degree of Slip-Fold Distortion as a Function of *d*-Electron Count. *J. Organomet. Chem.* **1990**, *394* (1), 777–794. [https://doi.org/10.1016/0022-328X\(90\)87268-I](https://doi.org/10.1016/0022-328X(90)87268-I).